Study of the Earth's Thermal History and Magnetic Field Evolution Using Geodynamical Models and Geochemical Constraints

A Thesis Submitted to the

College of Graduate Studies and Research

in Partial Fulfillment of the Requirements

for the degree of Doctor of Philosophy

in the Department of Geological Sciences

University of Saskatchewan

Saskatoon

By

Simona E. O. Costin

Permission to Use

In presenting this thesis in partial fulfilment of the requirements for a Doctor in Philosophy degree from the University of Saskatchewan, I agree that the Libraries of this University may make it freely available for inspection. I further agree that permission for copying of this thesis in any manner, in whole or in part, for scholarly purposes may be granted by the professor or professors who supervised my thesis work or, in their absence, by the Head of the Department or the Dean of the College in which my thesis work was done. It is understood that any copying or publication or use of this thesis or parts thereof for financial gain shall not be allowed without my written permission. It is also understood that due recognition shall be given to me and to the University of Saskatchewan in any scholarly use which may be made of any material in my thesis.

Requests for permission to copy or to make other use of material in this thesis in whole or part should be addressed to:

Head of the Department of Geological Sciences

114 Science Place

University of Saskatchewan

Saskatoon, Saskatchewan

Canada

S7N 5E2

Abstract

The thermal history of the Earth, from planetary accretion and core differentiation up to the present time, is of paramount importance for understanding our planet. The thermal evolution of the core and the mantle dictate the generation of the Earth's internal magnetic field and its evolution through time. In this dissertation, I study scenarios for the thermal and magnetic evolution of the Earth, using numerical simulations for mantle convection and implementing recent geochemical models for the mantle and core. The conditions for which a magnetic field can be generated in the Earth's core are studied using parameterized models for energy and entropy. The model devised in this project couples the results of the numerical simulations with the parameterized models for the core, to produce a global thermal and magnetic history, with feed-back between events happening in the mantle and the core.

The dissertation presents an analysis of the scenarios that can be constructed from implementing new constraints into the thermal models for the mantle and core and emphasizes the most relevant scenarios which can be applied to the Earth's evolution, consistent with physical parameters, and geochemical and magnetic constraints known to date. In addition, I discuss the relevance of some of the scenarios which appear incompatible with the Earth's evolution, but are reminiscent of the evolution of other terrestrial bodies.

The results of this work show that the most successful scenarios for the thermal and magnetic evolution require the presence of small amounts of core internal heating in the form of ^{40}K, or a slightly increased concentration of radioactive elements at the base of the mantle, due to isolated, primordial reservoirs. Successful scenarios are also obtained if the base of the mantle is less mobile and acts as a thermal insulator between the core and the overlying convective mantle. If the base of the mantle is less mobile and acts as a thermal insulator between the core and the overlying convective mantle, termed D$''$.

Acknowledgements

Uncountable and sincere thanks, beyond words, go to Prof. Sam Butler, the chief architect of this work, who was always generous in offering his time and advice, who has supported my many actions as a graduate student, and has encouraged me to make my work known in the scientific community. Many thanks go to my committee members, Prof. K. Ansdell, Prof. Y. Pan, Prof. J. Merriam, Prof. R. Kerrich, Prof. J. Tse and external examiner Prof. M. Jellinek for the insightful dialogues and constructive comments which helped improve the quality of this dissertation. Dr. J. Mound from the University of Leeds has kindly agreed to review the manuscript. His suggestions towards the general presentation of the thesis are here acknowledged. I also gratefully acknowledge the University of Saskatchewan and the Department of Geological Sciences for providing a great research environment, for giving me the opportunity to undertake graduate education, and for supporting this project. I am grateful for having spent five years of my life in Saskatoon, having made so many friends and having had so many pleasant moments while being here.

To my father who has seen a dream come true.

To everyone in my family, in the four corners of the world, for being supportive, incredibly understanding and patient, and having encouraged me throughout the years.

Contents

List of Tables

List of Figures

List of Abbreviations

CMB	Core Mantle Boundary
ICB	Inner-Core Boundary
IC	Inner Core
ULVZ	Ultra-low Velocity Zone
BSE	Bulk Silicate Earth
MORB	Mid-ocean Ridge Basalt
OIB	Ocean-Island Basalt
PSV	Paleo-Secular Variation
PREM	Preliminary Reference Earth Model
LOF	List of Figures
LOT	List of Tables

Chapter 1

Introduction

1.1 Motivation

The internal structure of the Earth, as inferred from seismic waves, consists of a series of concentric and interacting layers. Starting from the inside, there is the solid iron inner core, the liquid outer core composed of an iron-based alloy, the silicate mantle, and finally, the oceanic and continental crusts (Figure 1.1). At the surface, the Earth is covered by the oceans and the atmosphere. The constant motion of these interdependent layers generates the internal magnetic field, plate tectonics, mountain building and climate, to mention just a few. The way our planet has evolved through geological time has significant implications for all its systems and therefore understanding the dynamics of the Earth's evolution is a topic of great interest among geoscientists.

The convective processes in the Earth's interior play a fundamental role in the thermal and chemical evolution of the planet. Two giant heat engines have cooled the Earth from the inside since its accretion and differentiation. One gives us plate tectonics, volcanism and magmatism, the other generates and maintains the internal magnetic field of the Earth. Convection in the silicate mantle is the main mechanism through which heat is transported from the interior towards the surface since planetary formation about 4.55 billion years ago. Although solid, the mantle behaves like a fluid on geological timescales, transporting heat and mass by convection. At the same time, the cooling of the Earth's mantle implies the cooling of the Earth's core.

Secular cooling of the core occurs due to heat and mass transport through convection of the hot, iron-based fluid alloy which composes the core. When the temperature at the Earth's centre dropped sufficiently as to become equal to the liquidus temperature of the metallic alloy, a solid

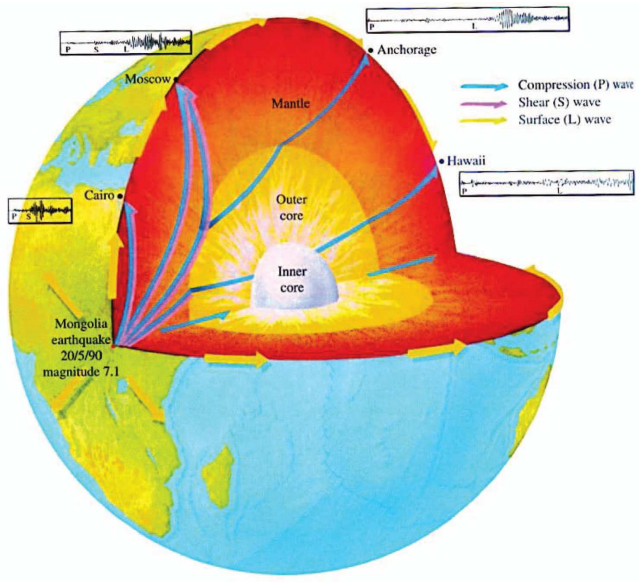

Figure 1.1: Internal structure of the Earth (from *Alfè*, 2007).

phase began to crystallize and the inner core (IC) started to grow. Solidification of the inner core releases latent heat of crystallization at the inner core boundary (ICB). In addition, gravitational energy is released into the core system, due to the expulsion from the solid phase of the lighter elements found in the core alloy. The thermal regime in the liquid core is largely dictated by the amount of heat exchanged at the core-mantle boundary (CMB) horizon. This in turn is controlled by the ability of the mantle to extract heat from the core and transport it towards the surface. Thus, the rate of cooling in the core and the growth of the inner core are intrinsically related to the motions of the more sluggish, overlying silicate mantle.

Our current understanding is that the internal magnetic field of our planet is generated in the metallic core by the geodynamo action. The mechanism is powered by the convection in the outer core, which supplies energy to compensate for the dissipative processes (ohmic and viscous). Convection in the core is driven by compositional and thermal buoyancy forces. In the presence of the core magnetic field, the motions of highly conductive fluid material continuously generate the magnetic field and replace the one that diffuses away (Figure 1.2). The most important forces that act in the core are the Coriolis force, the buoyancy force, the pressure and the magnetic (Lorentz) force. In the magnetogeostrophic approximation, to leading order, the balance of forces in the

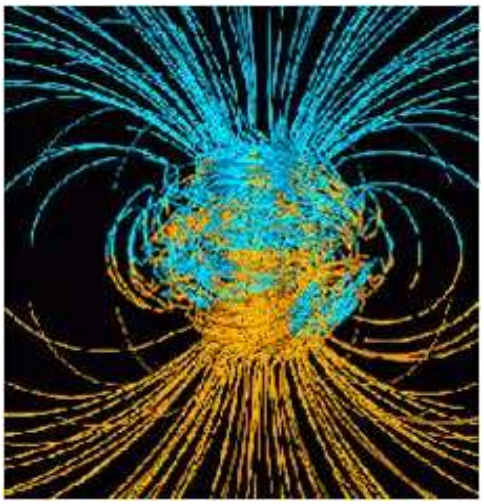

Figure 1.2: Distribution of magnetic field lines obtained from numerical geodynamo models in the core (from *Glatzmaier and Roberts*, 1995).

core is achieved by accounting for all these forces. On the other hand, if the pressure gradient is balanced only by the Coriolis and magnetic forces, the fluid core is said to be in magnetostrophic balance. The consequences of assuming one or the other momentum balance in the core reflect in the predicted magnitude of the magnetic field components.

Fluid motions in the core are ultimately controlled by the amount of heat which flows across the core-mantle boundary. If the amount of heat extracted from the core is large, vigorous convection takes place in the core and the generation of the magnetic field is maintained against dissipation. If the heat flow across the CMB is too low, the cooling of the core is done through conduction, as convection cannot be sustained by the low rate of cooling, and the geodynamo process shuts off. Release of latent heat and gravitational potential energy due to the inner core solidification has a positive effect on the magnetic field generation because it supplements the energy available to drive convection in the core, represented by the secular cooling of the core. It is commonly assumed that the principal driving mechanism for the present-day dynamo process is the release of light elements at the ICB due to the ongoing solidification of a pure metallic solid phase and rejection of most lighter elements from this phase [*Nimmo*, 2007]. Therefore, knowledge of the onset of crystallization of the IC, and its evolution in time, with possible melting episodes or variability in

the IC rate of growth are crucial information for modeling the magnetic history and understanding the contributing factors to the evolution of the Earth's magnetic field.

Though important for constraining the thermal and magnetic history of the core, the geological evidence for the age of the inner core is scarce and inconsistent. Evolutionary models [*e.g., Labrosse*, 2003; *Nimmo et al.*, 2004; *Butler et al.*, 2005] suggest that the IC is $\sim$ 0.5 - 2 Gyr old, much less than the age of the Earth, while some prefer an older age, with a high CMB heat flux originating from radioactive heating [*e.g., Gubbins et al.*, 2004]. The experimental work of *Aurnou et al.* [2003] and geodynamo models of *Aubert* [2005], have also shown that rapid growth of the inner core, or a young inner core, is consistent with the buoyancy flux at the CMB required to drive polar vortex motions at the CMB, similar in magnitude with those inferred from present-day secular variation of the magnetic field [*e.g., Olson and Aurnou*, 1999].

In contrast, geochemical arguments based on isotopic ratios ^{186}Os/^{188}Os and ^{187}Os/^{188}Os derived from surface lavas have been used to argue for an early onset of the core solidification process and suggest a 3.5 Gyr old inner core [*e.g., Brandon et al.*, 2003]. The rationale for the geochemical model [*e.g., Walker et al.*, 1995] assumes that both Re and Pt partition preferentially into the outer core relative to Os, as solidification proceeds. ^{187}Re and ^{190}Pt decay to ^{187}Os and ^{186}Os, respectively, so as the solidification advances, the outer core will become progressively enriched in these Os isotopes relative to stable ^{188}Os, assuming chondritic ratios in the bulk core. The amount of enrichment is proportional to the time elapsed from the initiation of solidification, and both radiogenic isotopic enrichments should be coupled, as they occur due to the same process (solidification of the IC). Elevated Os isotopic ratios, compared to chondritic values, have been observed in ancient komatiites (2.7-2.8 Gyr ago), and in more recent lavas from Hawaii, Siberia, and Gorgona Island [e.g., *Brandon et al.*, 1998, 2003]; therefore, it has been argued [*Brandon et al.*, 2003] that the onset of inner core crystallization must have been prior to 3.5 Gyr ago to explain the komatiite Os isotopic values. The core-mantle interaction and the core origin for the Os anomalous isotopic signal in Hawaiian lavas is also supported by the Fe/Mn analysis of hot spot lavas [*Humayun et al.*, 2004]. These geochemical arguments have lead to a currently unresolved disagreement between the

geophysical and geochemical models on the age of the IC.

More recent studies, however, have contested the origin of the Os isotopic anomalies [*Lassiter*, 2006], on the grounds that the absence of tungsten anomalies does not support the core origins of material in lavas. The study of *Luguet et al.* [2008] on Beni Bousera pyroxenites and eclogites brings strong evidence that the Os signal in plume lavas is due to metasomatism of abyssal sulfides, and hence does not represent a signature of core-mantle interactions. The study of *Luguet et al.* [2008] does not explain the Os signal in Siberian and Gorgona komatiites or Hawaiian lavas, and some arguments that have been invoked to support the metasomatic origin of the Os anomalies in the study of *Luguet et al.* [2008] come exactly from the results obtained by geophysical studies which conclude that the inner core is a recent geological feature. Theoretical studies however are very sensitive to not sufficiently constrained parameters (e.g., heat flow across the core-mantle boundary, present-day temperatures in the core, etc). Thus it seems quite possible that the last word on the core-mantle interactions and the origin of the isotopic anomalies has not been said. Undoubtedly, more scientific work on the age of the IC will be generated in the future and geochemical modeling will contribute to this unresolved issue.

Constraints on the age of the inner core may come from magnetic paleointensity measurements in single silicate crystals or whole rocks. Consistency in paleointensities from the Late Archean to Early Proterozoic with the field of the last 5 million years, has prompted *Tarduno et al.* [2006] to suggest that the inner core had started to grow by 2.5 Gyr ago (Early Proterozoic). In addition, the inferred internal field strengths from Archean rocks ($\sim$ 3.2 Gyr ago) are roughly 50 % lower than the present day values [e.g., *Tarduno et al.*, 2007], indicating perhaps a purely thermally driven, but still active dynamo, at that time (Figure 1.3).

Paleomagnetic data is also used to reconstruct the evolution of the Earth's main magnetic field. Present-day records show that a mainly dipolar, occasionally reversing magnetic field has existed at least intermittently for the past 3.5 Gyr [*e.g., Mc Elhinny and Senanayake*, 1980; *Hale and Dunlop*, 1984], however, observations are sparse before the oldest surviving oceanic floor ($\sim$150 Myr) and there is not enough evidence for reconstructing trends in the field amplitude from observations.

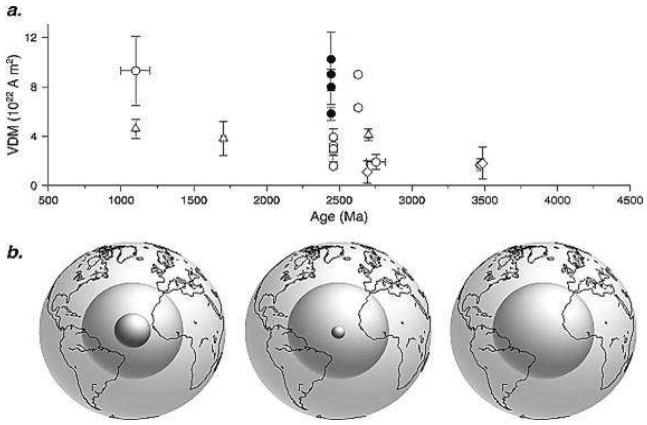

Figure 1.3: Hypothetical evolution of the inner core as inferred from single crystal paleointensities measurements (from *Tarduno et al.*, 2006).

Therefore, a direct constraint for the functioning of the dynamo from observations is difficult to obtain, or difficult to model, or both. A number of analytical studies show a discrepancy between the time-integrated energy available to drive the geodynamo in the outer core and its persistence for the past 3.5 Gyr. Several analyses [*e.g., Buffett*, 2002; *Nimmo et al.*, 2004] have shown that a core cooling history compatible with a continuous dynamo action and a magnetic field that was not much weaker in the past implies sufficiently high initial core temperatures as to cause pervasive lower mantle melting. These models predict a late onset of the inner core, requiring a purely thermally driven dynamo for a long period of time and suggest that a continuous 3.5 Gyr magnetic history in the core is more readily predicted if additional heat sources, such as ^{40}K in the core are present in the system. Radiogenic heat due to the radioactive decay supplements the energy available in the system and may help explain how the geodynamo was sustained for times prior to the formation of the inner core.

It is widely believed that the Earth's core is formed by an iron-rich alloy, with up to $5 - 10\%$ of nickel. The core also must contain a significant fraction of light impurities, roughly $2 - 3\%$ in the solid part and $6 - 7\%$ in the liquid, though the exact nature of these light impurities is unknown [*Alfè*, 2007]. The behavior of the Earth's liquid core is difficult to establish in laboratory experiments, given the high pressures and temperatures found at the core horizon. On the other hand, *ab initio* calculations are time-consuming and rely on the use of a set of assumptions to ensure

computational speed-up [*e.g., Alfè et al.*, 2007]. Recent results from first principles calculations predict modern temperatures at the CMB around 4100 K [*Vočadlo et al.*, 2003], in good agreement with the experimental work of *Ma et al.* [2004] and *Boehler* [2000], but not with earlier studies which predict CMB temperatures around 3500 K [*e.g., Boehler*, 1995].

The requirement of high present-day temperatures at the CMB in conjunction with the continuity of magnetic field generation in the core, brings a further complication in modeling the thermal history in the core, as it inevitably leads to initial temperatures above the solidus temperature of the mantle material above the CMB. This contradicts the concept that upon complete accretion, the Earth was hot and fully differentiated into a mantle and a core. The core started to cool from superliquidus temperatures, whereas the mantle started from near solidus temperatures [*e.g., Stevenson et al.*, 1983; *Schubert et al.*, 2001]. On the other hand, recent studies based on geochemical arguments have advocated that the Earth's mantle started to cool from a molten state [*e.g., Labrosse et al.*, 2007], hence a high present-day CMB temperature would be much easier to attain in a thermal evolution which assumes this scenario.

As mentioned earlier, the presence of radioactive potassium in the core may alleviate the difficulties of modeling a thermal history in the core that is compatible with the magnetic constraints and mineral physics studies on the present-day core temperatures. Recently, the ability of potassium to combine with the core fluid at high temperatures and pressures has been documented in laboratory experiments, but the chemical reactions depend in a complex fashion on a number of factors, such as temperature and the amounts of sulphur and oxygen present in the core [*Murthy et al.*, 2003, *Lee and Jeanloz*, 2003]. Cosmochemical considerations, however, do not allow for significant quantities of potassium in the core (Fig. 1.4). The presence of significant amounts of potassium in the core in addition to the known abundance in the Earth is not consistent with the chemical composition as a function of condensation temperatures. The trend of the planetary volatility at 1 AU is shown Figure 1.4. The total potassium abundance on Earth is estimated to be from 120 to 300 ppm, whereas in chondrites, it is one order of magnitude higher [*Lassiter*, 2004]. Adding 400 ppm in the core, would increase the total abundance to around 300 ppm and would place potassium

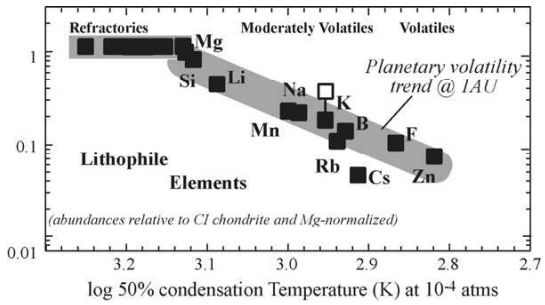

Figure 1.4: Diagram of chondrite-normalized abundances in lithophile elements. Open square indicates a content of 400 ppm K in the core (from *Davies*, 2007).

distinctly off the trend in Figure 1.4 [*McDonough*, 2004]; however, reduced concentrations ($\sim$ 60 ppm) could be envisaged [*Lassiter*, 2004]. The presence of radioactive elements in the core remains a disputed issue, even though it would mitigate the energy requirements for a continuous magnetic history. The next decades or so could possibly provide a better understanding of the Earth engine by looking at the lateral and vertical distribution of the radioactive elements through the detection of geo-neutrinos. At that time, unparalleled constraints on the thermal evolution of the Earth will be provided [*McDonough*, 2007], which will possibly elucidate the issue of radioactivity in the core.

Although experimental evidence may lead to supporting a certain geochemical or cosmochemical model for the composition of the core, the isolation of the core from the mantle means that the chemistry of the core is not amenable to direct investigation. The composition of the core must be inferred from a global mass balance between a model for the composition of the whole Earth (built from cosmochemical evidence) and a model for the Bulk Silicate Earth (BSE).

The BSE is composed of a number of geochemical reservoirs [*Jackson*, 1998], including the continental crust; the oceanic crust; the depleted, well-stirred upper mantle, which is the source region for mid-ocean ridge basalt (MORB); the enriched, heterogeneous, source regions for ocean-island basalt (OIB); and lastly, possibly primitive mantle that has never been differentiated. The depleted mantle source for the MORB is in its depleted state probably by extraction of continental crust from it, as a net result of several successive melt-extraction processes. In contrast, the OIB source has an isotopically different signature, more enriched in moderately-incompatible elements.

Whereas the MOR basalts sample the top of the mantle, it is believed that plume-related basalts (OIBs and flood basalts) sample the bottom thermal boundary layer of the mantle. The mass balance for the major elements and compatible and moderately-incompatible elements can be resolved accounting for the MORB source in the mantle. However, for highly-incompatible elements, this balance is much more difficult to explain. For instance, the concentration of radioactive elements (such as U, Th and K) is much more depleted in MORBs, compared to chondritic concentrations, even if accounting for the enriched continental crust. Consequently, geochemical models based on highly-incompatible elements such as noble gases and radioactive elements [*e.g., Tolstikhin and Hofmann*, 2005], have suggested the presence of a physically-distinct, primitive, isolated mantle reservoir, enriched in incompatible and radioactive elements. The absence of geophysical evidence for such a distinctive reservoir in the mantle leads to an unresolved hiatus between geochemical and geophysical modeling.

The Earth's mantle, and particularly the region above the core mantle boundary, dubbed D$''$, plays a crucial role in the thermal history of the core and the fate of the magnetic field generated within. This region is the scene of sudden changes from core conditions in temperature, density, conductivity, chemical composition and seismic wave velocities. Enhanced imaging methods using seismic waves unveil high complexity in the D$''$ region (Figure 1.5). Suggestions for the origin of the heterogeneities in D$''$ include the presence of mineral phase transitions [*Hernlund et al.*, 2005], partial melt [*e.g., Lay et al.*, 2004], or relics of primordial melt [*e.g., Labrosse et al.*, 2007]. The anomalous signature of the seismic waves may also be caused by geochemical heterogeneities, due to isolated, primeval mantle reservoirs, complementary to the rock forming element-incompatible source, which remain stagnant due to a density contrast with the mantle above [*e.g., Boyet and Carlson*, 2005]. Additionally, geochemical complexity in the lowermost mantle may be given by accumulations of dense oceanic crust [*e.g., McNamara and Zhong*, 2004].

Analytical studies have suggested mechanical interactions between the mantle and core [*e.g., Buffett et al.*, 2000], whereas the possibility of iron enrichment in D$''$ owing to chemical reactions with the liquid core has been documented in the laboratory [*e.g., Knittle and Jeanloz*, 1991;

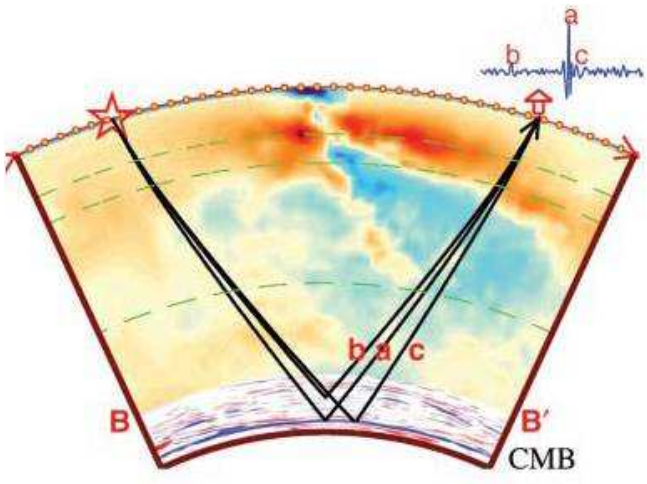

Figure 1.5: Tomography techniques showing P-wave velocity variations in the mantle and variations in P-wave reflectivity in D″, demonstrating the high complexity above the CMB (from *van der Hilst et al.*, 2007).

Dubrovinsky et al., 2003; *Sakai et al.*, 2006]. These experimental studies have shown that mantle perovskites react with liquid iron at high pressures to produce metallic alloys such as FeO, FeSi and nonmetallic silicates (e.g., stishovite). The density of the FeSi compounds can reach 9.0 g cm^{-3}, in contrast with the lower mantle density of 5.5 g cm^{-3} [*Dubrovinsky et al.*, 2003]. Furthermore, experiments performed above 106 GPa and 1740 K find solubility in excess of 75 mol% of FeO in mantle perovskite, stabilizing this phase [*Tateno et al.*, 2007], while *Mao et al.* [2005] report 80 mol% FeO solubility in post-perovskite. These two phases are thought to occur in the lowermost mantle. The iron enrichment of these minerals may increase the density of the lowermost mantle by up to 20 % and cause a drop in seismic velocities in D″ [*Mao et al.*, 2004].

All of the above demonstrate that the evolution of the Earth, may it be thermal, magnetic or geochemical, is insufficiently constrained from geological evidence and there are a number of unanswered questions, such as the timing for the inner core inception, the onset of the magnetic field or the existence of isolated geochemical mantle reservoirs. Nevertheless, although few, the constraints we now have on the evolution of the core, are surprisingly strong. Finding successful scenarios for the evolution of the planet, that can be brought forward to explain the riddles still surrounding the evolution of the core, is an interdisciplinary task. Moreover, the evolution of the

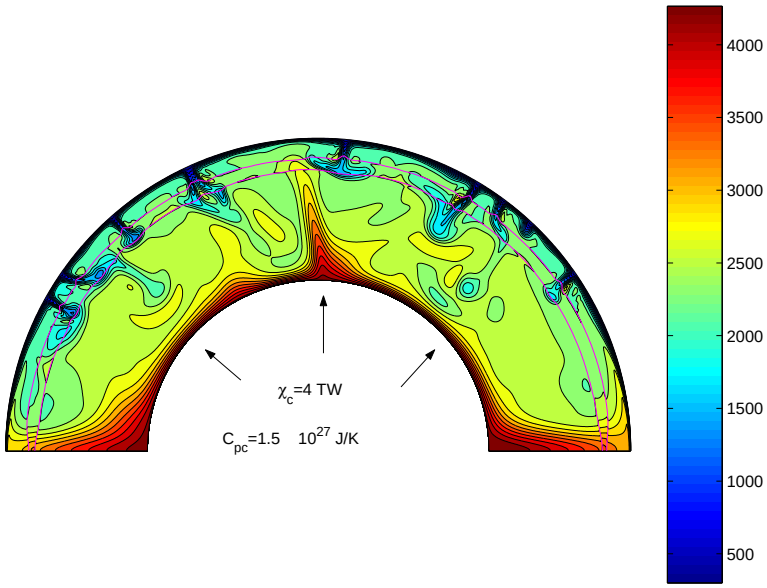

Figure 1.6: Snapshot of temperature distribution in the mantle obtained from the numerical model, showing phase transitions and lateral heterogeneities in mantle. The mantle model is coupled to a heat reservoir represented by the core.

magnetic field of the Earth, the time of its onset and the factors that affect its generation, are of unique interest, as it is well known that long-standing magnetic field is a key element in protecting the Earth's atmosphere against interaction with solar-wind and cosmic particles [*e.g., Ozima et al.*, 2005; *Atreya et al.*, 2007; *Lammer et al.*, 2008]. Thus, the presence of magnetic field may contribute directly to the presence of life on our planet, even though on shorter timescales, such as magnetic reversals or dipole lows, when the magnetic field intensity decreases severely, the effect on biota is less obvious [*e.g., Courtillot et al.*, 2007]. Last but not least, the light shed on various phenomena associated with Earth's evolution may give new perspectives on the thermal and magnetic field evolution of other bodies in our solar system and beyond, and could provide insights on the origin of our own planet.

1.2 Scope and Method

The main goal of this project is to analyze the global thermal evolution by incorporating some recent advances in geochemistry, mineralogy and mantle dynamics, which may affect the Earth's thermal

evolution. The study is performed by coupling 2D axi-symmetric mantle convection simulations with parameterized thermal models in the Earth's core, and provides successful scenarios that meet the known constraints for the thermal and magnetic evolution of the Earth. In addition, some scenarios which are not realistic for the Earth's evolution, prove to be reminiscent of the evolution of other planets, although a thorough analysis could only be completed with the correct scaling of parameters.

Investigations of the Earth's thermal history have largely been carried out using parameterized models of convection in the Earth's mantle. The earliest parameterized and numerical analyses include those of *McKenzie et al.* [1974], *Richter* [1978], *Sharpe and Peltier* [1978], *Schubert et al.* [1980], and *Davies* [1980]. Parameterized mantle convection models, coupled to a core heat balance that includes the inner core growth, have also been used to calculate the heat flux across the CMB [*e.g., Stevenson et al.*, 1983; *Breuer and Spohn*, 1993; *Buffett et al.*, 1996; *Labrosse*, 2003]. Modeling mantle convection with parameterized schemes is however not suitable for a system that includes lateral variability in physical parameters. In addition, the effects of phase transitions, plate tectonics and temperature-dependent viscosity are poorly captured in those models. Therefore, using a fully-dynamical mantle convection model coupled to a parameterized thermal evolution in the core gives us a better understanding of the thermal evolution of the Earth. A parameterized convection scheme is sufficient to realistically model the core evolution, as the motions due to convection in the core are orders of magnitude faster than motions in the mantle. Due to the vigorous convection in the core and the short characteristic timescales, the core is assumed to be well-mixed, isentropic and adiabatic. A coupling between fully dynamical models for the core and the mantle, in spite of bringing new insights into the global dynamics, would pose serious computational problems due to the different characteristic timescales in the core and the mantle.

Among the first studies employing a fully dynamical approach simulating mantle convection with core-cooling was the work by *Steinbach et al.* [1993], but their model did not explicitly discuss the thermal evolution of the core and inner core growth. *Stegman et al.* [2003] developed such an approach to study the thermal and magnetic evolution of the Moon. Other studies of the thermal

history in the mantle using a fully dynamical model for convection coupled to parameterized models for the core include *Tackley and Xie* [2002] and *Nakagawa and Tackley* [2004],[2005]. These papers have focused on studying the effects of chemical heterogeneities, chemical layering and the presence of core potassium on the mantle dynamics.

In this work, the thermal history in the mantle is studied in the framework of numerical simulations with phase transitions at 400 and 660-km depth, temperature-dependent viscosity and decaying radioactive sources in the mantle (Fig. 1.6). In order to study the thermal and magnetic evolution of the core concomitantly with the thermal history in the mantle, I have devised an energy model for the core which couples with the thermal evolution in the mantle through the numerical output for temperature and the heat flow at the core-mantle boundary. These quantities enter the equations for energy conservation and entropy production in the core and therefore control the cooling history of the core, inner core growth and magnetic field generation. The core equations are updated at each time step in the numerical model, therefore allowing for a complete feed-back between the cooling histories of the mantle and core.

The evolution of the magnetic field is modeled by computing the entropy available for Ohmic dissipation from the entropy production in the core and then scaling the electric current responsible for the Ohmic loss to the intensity of a magnetic field. Thus, although motions in the core and mantle have different characteristic timescales, the thermal histories in the mantle and core are coupled, permitting us to analyze the effects of short timescale and lateral thermal variations in the mantle on the thermal and magnetic evolution in the core. These effects cannot be studied in parameterized models for thermal evolution of the Earth, therefore coupling the mantle numerical model is a better approach.

In general, criteria for successful thermal histories for the mantle and core are the correct size of the inner core, initial temperatures at or below the mantle solidus point, CMB modern temperatures around 4000 K, a modern core heat flow ranging from 3 to 14 TW, and a magnetic history compatible with the paleomagnetic evidence, using geochemical constraints on the internal heating rates.

The next chapter of the thesis describes the theoretical framework for mantle and core models. The results from thermal history models with radioactive heating in the core, and from models with increased radioactivity at the base of the mantle are presented in Chapter 3. Additionally, I analyze the effects of initial CMB temperatures on the core and mantle thermal histories. Chapter 4 presents models which assume a denser layer in D″, represented by an iron-enriched, or long-standing, isolated, incompatible-element and radioactive enriched reservoir. Laboratory experiments show that such a stagnant layer can eventually become entrained in the convection of the overlying mantle after a few billion years of planetary evolution, due to thermal instabilities arising in the layer. This scenario will be also discussed in Chapter 4. The last chapter comprises a discussion on the results obtained.

Chapter 2

Theoretical Background and Model Description

2.1 Mantle Convection Theoretical Equations

Convective processes in the Earth's interior play a fundamental role in the thermal and geochemical evolution of the planet. Understanding convection in the mantle is one of the most important goals of geophysics. Disciplines that contribute toward advancing our understanding of mantle processes include seismology, high pressure and high temperature mineral physics, geodynamics, geomagnetism, geodesy, global gravimetry and geochemistry. Laboratory and numerical experiments are useful methods for understanding the complex processes that occur in the Earth's mantle.

Although the crystalline mantle is a solid from the standpoint of the passage of the rapid seismic waves, the mantle acts as a viscous fluid over long intervals of time. The interior is sufficiently liquid that the gravitational energy released by the upwelling of hot (low-density) material and downwelling of cold (high-density) material can overcome the energy lost by dissipation, making possible the onset of convection. In the following subsections I describe the relevant equations for convection in the mantle [*Schubert et al.*, 2001].

2.1.1 Conservation of mass

The continuity equation in a fluid parcel states,

$$\frac{\partial \rho}{\partial t} + \nabla \cdot (\rho \mathbf{u}) = 0\,, \tag{2.1}$$

where ρ is density, t is time and $\mathbf{u}$ is the velocity of a fluid particle. Equation (2.1) can be written as

$$\frac{1}{\rho}\frac{D\rho}{Dt} + \nabla \cdot \mathbf{u} = 0\,, \tag{2.2}$$

where $D/Dt = \partial/\partial t + \mathbf{u} \cdot \nabla$ is the material derivative. In tensor notation, 2.2 takes the form,

$$\frac{1}{\rho}\frac{D\rho}{Dt} + \frac{\partial u_i}{\partial x_i} = 0\,. \tag{2.3}$$

Depending on the media for which the general equations are applied, several assumptions can be made to simplify the calculations required. For instance, for the case of an incompressible fluid, $D\rho/Dt \equiv 0$, (2.2) becomes $\nabla \cdot \mathbf{u} = 0$, stating that the velocity of an incompressible fluid is solenoidal, or has zero divergence. Equation 2.1 is general enough to include sound waves. In the case of modeling convection in the mantle, the Mach number (representing the characteristic velocity flow divided by the velocity of sound) is of order 10^{-15}. Since seismic phenomena and mantle convection occur on vastly different time scales, we can set $\partial\rho/\partial t \approx 0$. Therefore, the anelastic mass conservation equation is

$$\nabla \cdot (\rho\,\mathbf{u}) = 0\,. \tag{2.4}$$

2.1.2 Conservation of momentum (Navier-Stokes equations)

Newton's second law states that the acceleration of an elemental parcel is given by the balance of forces that act upon the parcel, *i.e.,* $m\,\mathbf{a} = \sum \mathbf{F}$. The forces that act upon a parcel of fluid are the net surface forces and body forces. The net surface force can be divided in two parts, an isotropic part associated with the fluid pressure (p), and the deviatoric part, given by the contribution of the deviatoric stress tensor, τ_{ij}. In the mantle, the only important body force that acts upon a parcel of fluid is gravity (due to the gravitational acceleration $\mathbf{g}$), whereas in the core other body forces such as the Coriolis and the Lorentz force are important too. In tensor notation, Newton's second law of motion for a parcel of fluid in the mantle can be written as,

$$\rho\frac{Du_i}{Dt} = -\frac{\partial}{\partial x_i}p + \frac{\partial \tau_{ij}}{\partial x_j} + \rho g_i\,. \tag{2.5}$$

To simplify the equations, further assumptions can be made. Firstly, we assume that the bulk of the mantle behaves as a Newtonian fluid, meaning that there is linear dependence between the stress tensor (τ_{ij}) and the strain rate tensor (e_{ij}),

$$\tau_{ij} = 2\mu\, e_{ij} + \lambda\, e_{kk}\delta_{ij}\,, \tag{2.6}$$

where μ is dynamic viscosity and λ is the second viscosity, and the strain rate tensor is defined as

$$e_{ij} = \frac{1}{2}\left(\frac{\partial u_i}{\partial x_j} + \frac{\partial u_j}{\partial x_i}\right). \tag{2.7}$$

Stokes' assumption concerns the 'bulk viscosity' of the fluid ($\kappa_B = 2\mu/3 + \lambda$), which is very small, and therefore assumes this quantity to be zero. Thus, we can express τ_{ij} as,

$$\tau_{ij} = \mu\left(\frac{\partial u_i}{\partial x_j} + \frac{\partial u_j}{\partial x_j} - \frac{2}{3}\,\delta_{ij}\frac{\partial u_k}{\partial x_k}\right) = \mu\left(\frac{\partial u_i}{\partial x_j} + \frac{\partial u_j}{\partial x_j}\right) - \frac{2}{3}\,\mu\,\nabla\cdot\mathbf{u}\,. \tag{2.8}$$

To model mantle convection, a very useful assumption for computational speed-up is the Boussinesq approximation, which neglects changes in density, except in calculation of buoyancy forces where it assumes that the buoyancy force arises only from density variations due to temperature variations. In the anelastic approximation there is also a buoyancy force associated with pressure-induced density variations. In the Boussinesq formulation, the momentum equation may take the form,

$$\rho\frac{D\mathbf{u}}{Dt} = -\nabla p + \frac{\partial \tau_{ij}}{\partial x_j} + \rho g\,[1 - \alpha(T - T_0)]\hat{\mathbf{r}}\,, \tag{2.9}$$

where T is temperature, T_0 is a reference temperature, α is the coefficient of thermal expansion and $\hat{\mathbf{r}}$ is the radial coordinate. The Boussinesq approximation for free convection neglects all variable-property effects in the equations, except for density departures from the reference density state in the momentum equation; the material is otherwise deemed incompressible. This approximation is good for gravity-induced flows.

The left-had side of (2.9) represents the inertia terms, which are very small for mantle convection. These terms may be omitted, meaning if we stopped driving the mantle convection, the motion would stop instantaneously. Ignoring the inertia terms is also known as the infinite Prandtl number (Pr) assumption, as by grouping terms and performing a dimensional analysis, the inertia terms are scaled by the Pr^{-1}. For the mantle, $Pr \approx 2.5 \times 10^{23}$. Therefore, for an infinite Pr, anelastic mantle, the Navier-Stokes equations take the form [*Jarvis and McKenzie*, 1980],

$$0 = -\nabla p + \rho g_i + \frac{\partial\,\tau_{ij}}{\partial x_j}\,, \tag{2.10}$$

where τ_{ij} is expressed by (2.8).

2.1.3 Conservation of energy

The first law of thermodynamics states that the incremental change in internal energy, δe, is equal to the difference between the incremental heat added to the system, δq and the incremental work done by the system, δw,

$$\delta e = \delta q - \delta w \,. \tag{2.11}$$

The mechanical work is carried out by compression. If the process is reversible, *i.e.*, the change is carried out so slowly that the material passes through a succession of equilibrium states, the incremental quantity δw can be replaced by the mathematical derivative dw, and thus write

$$d\,w = p\,dv, \tag{2.12}$$

where v is volume. Therefore, the specific heat of a material is defined as the ratio of the increment of heat added to the material, δq, to the change in temperature δT. The specific heat at constant volume and constant temperature are defined by the following expressions,

$$C_v = \left(\frac{\delta q}{\delta T}\right)_v \text{ and } C_p = \left(\frac{\delta q}{\delta T}\right)_p . \tag{2.13}$$

The second law of thermodynamics states that for a reversible process,

$$d\,q = T\,ds. \tag{2.14}$$

where s is entropy. A process without heat addition is an adiabatic process. If an adiabatic process is also reversible, it is also isentropic, *i.e.*, the entropy is constant. If the adiabatic process is irreversible, the entropy increases. Using (2.14), the specific heat expressions for reversible processes are written as,

$$C_v = \left(\frac{T\delta s}{\delta T}\right)_v \text{ and } C_p = \left(\frac{T\delta s}{\delta T}\right)_p . \tag{2.15}$$

Applying the second law of thermodynamics (2.14), the change in entropy of an elemental volume of fluid, $\rho\, Ds/Dt$ must equal the heat added to the system. For the mantle, we account for the heat produced by radioactive heating, viscous heating and thermal conduction. Thus, we get the thermal energy equation,

$$\rho T \frac{Ds}{Dt} = \Phi + \frac{\partial}{\partial x_i}\left(k\frac{\partial}{\partial x_i}T\right) + \rho\,\mathcal{H}\,, \tag{2.16}$$

where k is the thermal conductivity and $\mathcal{H}$ is the internal heat production per unit mass. The terms in the right-hand side of (2.16) represent the volumetric heating due to viscous dissipation (Φ), thermal conduction and internal heat production. The thermal conduction term is derived assuming that Fourier's law for an isotropic medium is applicable,

$$q_i = -k\frac{\delta T}{\delta x_i}\,, \tag{2.17}$$

and hence

$$\frac{\delta q_i}{\delta x_i} = -\frac{\delta}{\delta x_i}\left(k\frac{\delta T}{\delta x_i}\right)\,. \tag{2.18}$$

For a Newtonian and incompressible fluid , the term $\Phi \equiv \tau_{ij}\frac{\partial u_i}{\partial x_j}$ simplifies to

$$\Phi = \frac{\mu}{2}\left(\frac{\partial u_i}{\partial x_j} + \frac{\partial u_j}{\partial x_i}\right)^2\,. \tag{2.19}$$

An alternate expression for the heat equation (2.16) can be obtained by substituting,

$$\frac{Ds}{Dt} = \frac{C_p}{T}\frac{DT}{Dt} - \frac{\alpha}{\rho}\frac{Dp}{Dt}T\,. \tag{2.20}$$

in the left-hand side of (2.16), and thus obtaining,

$$\rho C_p\frac{DT}{Dt} - \alpha\,T\frac{Dp}{Dt} = \Phi + \frac{\partial}{\partial x_i}\left(k\frac{\partial}{\partial x_i}T\right) + \rho\,\mathcal{H}\,, \tag{2.21}$$

or equivalently,

$$\rho C_p\left[\frac{DT}{Dt} - \frac{\alpha\,T}{\rho C_p}\frac{Dp}{Dt}\right] = \Phi + \frac{\partial}{\partial x_i}\left(k\frac{\partial}{\partial x_i}T\right) + \rho\,\mathcal{H}\,. \tag{2.22}$$

Further, the term $\alpha\,T/\rho C_p$ can be developed using (2.15), the definition of the thermal expansivity,

$$\alpha = \frac{1}{v}\left(\frac{\partial v}{\partial T}\right)_p\,, \tag{2.23}$$

and the identity

$$\left(\frac{\partial s}{\partial v}\right)_T = \left(\frac{\partial p}{\partial T}\right)_v\,, \tag{2.24}$$

to obtain

$$\frac{\alpha\,T}{\rho C_p} = \left(\frac{\partial T}{\partial p}\right)_s\,. \tag{2.25}$$

The thermal energy equation (2.21) can be rewritten as,

$$\rho C_p\left[\frac{DT}{Dt} - \left(\frac{\partial T}{\partial p}\right)_s\frac{Dp}{Dt}\right] = \Phi + \frac{\partial}{\partial x_i}\left(k\frac{\partial}{\partial x_i}T\right) + \rho\,\mathcal{H}\,. \tag{2.26}$$

The quantity $(\partial T/\partial p)_s$ is the adiabatic derivative of temperature with respect to pressure, and the term in square brackets in the left-hand side of (2.26) is the change in temperature in excess of that which comes from adiabatic compression. Expanding the material derivatives in the left-hand side, leads to [*Jarvis and McKenzie*, 1980],

$$\rho C_p \left\{ \frac{\partial T}{\partial t} - \frac{\alpha\, T}{\rho C_p} \frac{\partial p}{\partial t} + \mathbf{u} \cdot [\nabla T - (\nabla T)_s] \right\} = \Phi + \frac{\partial}{\partial x_i} \left(k \frac{\partial}{\partial x_i} T \right) + \rho\, \mathcal{H}\,. \tag{2.27}$$

2.2 Convection in the Mantle

To characterize the nature of transport in the mantle, and in other media, it is customary to compute the Ra number, which is a dimensionless parameter indicating the vigor of convection. For a fluid heated from below and cooled from above, the Ra number can have the following form,

$$Ra = \frac{C_p \alpha\, g\, \rho^2\, \delta T\, h^3}{k\, \eta}\,, \tag{2.28}$$

where δT represents the temperature difference in the mantle, h is the depth of the mantle, and η is dynamic viscosity. The critical value Ra_{crit} marks the onset of convection. The minimum Ra_{crit}, for which convection occurs in a horizontally-infinite layer, with free-slip boundaries, is 657.5 [*Turcotte and Schubert*, 2002]. The critical Ra number is dependent on the geometry of the convective region and is around 1000 for any given geometry. If $Ra > Ra_{crit}$, a perturbation will grow in time, whereas if $Ra < Ra_{crit}$, a disturbance will decay with time. The requirement that Ra_{crit} is exceeded in order that convection sets in, can be interpreted in a number of physical ways. For instance, one can think of a certain temperature difference across the layer, or a certain minimum viscosity of the fluid before convection can occur. Using $\eta = 10^{21}$ Pas from rebound studies [e.g. *Peltier and Jiang*, 1996], and other characteristic mantle physical properties, the Ra mantle value is $\sim 10^7$, which is much larger than the critical value. Detailed non-linear stability analyses, show that for $Ra >\sim 5 \times 10^6$, convection becomes time-dependent and chaotic, through boundary layer instabilities that generate thermal plumes [*Schubert et al.*, 2001].

The analysis for the onset of convection can be also computed for a fluid that is heated from within and cooled from above, whereas the lower boundary is assumed to be insulating. For this

case, the Ra number takes on the form,

$$Ra_H = \frac{\alpha\, g\, \rho^5\, \mathcal{H}\, h^5}{k\, \eta\, \kappa}\,, \tag{2.29}$$

where $\mathcal{H}$ and κ are the rate of internal heat generation per unit mass and thermal diffusivity, respectively. The critical Ra_H for a horizontally-infinite layer, with free-slip boundaries, is 867.8 [*Turcotte and Schubert*, 2002]. If the calculation for Ra_H is applied for the entire mantle, the value obtained is $\sim 2 \times 10^9$, far greater than the critical value [*Turcotte and Schubert*, 2002].

For specific topics related to convection in the Earth's mantle, such as the presence of insulating layers in the form of the continents, or the presence of compositionally-distinct layers, such as isolated mantle reservoirs, other dimensionless numbers and parameters are useful.

Despite the nearly homogeneous chemical mantle composition, chemically distinct layers may be present in the mantle, at the top or the bottom of the mantle [*Jaupart et al.*, 2007]. A relevant parameter to characterize the dynamics of a layered convection system, where the layers may have different physical properties is the buoyancy number, B. The buoyancy number represents the ratio between the intrinsic chemical density difference between the layers and the density difference due to thermal expansion, *i.e.*,

$$B = \frac{\Delta\rho/\rho_0}{\alpha\, \Delta T}\,, \tag{2.30}$$

where $\Delta\rho$ and ρ_0 represent the chemical density and the reference density, whereas α and ΔT represent the thermal expansion of the fluid and the temperature difference (across the layer or across the entire region).

The Biot number, Bi, is used to analyze the dynamics of a system where a resistive lid is placed over the surface of a fluid [*e.g., Grigné et al.*, 2007]. This number describes the insulating effect of the lid, and has the form,

$$Bi = \frac{k_{lid}}{k}\frac{d}{d_{lid}}\,, \tag{2.31}$$

where k_{lid} and k are the thermal conductivities of the lid and the fluid, respectively, and d_{lid} and d are their respective thicknesses. If the lid is very thick or has a low thermal conductivity, then the lid is very insulating ($Bi \to 0$). For instance, for a continental lithosphere in a whole-mantle convection, the value for Bi is 10 [*Grigné et al.*, 2007].

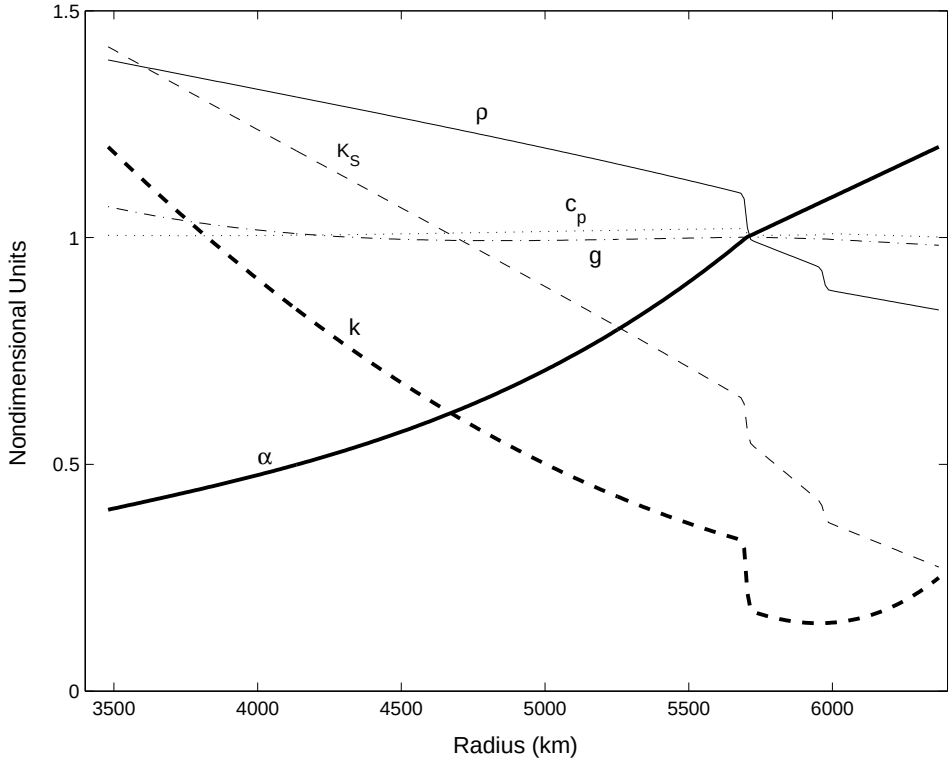

Figure 2.1: Depth-dependent physical parameters for the mantle convection model. Coefficient of thermal expansion (α, thick, solid line). Density (ρ, solid line). Thermal conductivity (k, thick, dashed line). Adiabatic bulk modulus (K_S, dash line). Gravitational acceleration (g, dash-dot line). Heat capacity (C_p, dotted line)(from Butler and Peltier, 2000).

2.3 Numerical Model for Mantle Convection

The numerical model employed in this study is derived from the version employed by *Butler and Peltier* [2000] and an older version of *Solheim and Peltier* [1994a,b]. The assumptions and dimensionless governing equations of the model are given below [*Butler and Peltier*, 2000].

The continuity equation is solved for an anelastic mantle,

$$\nabla \cdot (\rho_r \, \mathbf{u}) = 0 \,, \tag{2.32}$$

where the subscript r assumes depth-dependent (*i.e.*, radial) variation. The equation for linear momentum conservation in the convection model assuming an infinite Pr number is expressed by,

$$0 = -\nabla p - \rho \, g \, \hat{\mathbf{r}} + \alpha_0 \Delta T [-\nabla \times (\eta \nabla \times \mathbf{u}) + 4/3 \nabla (\eta \nabla \cdot \mathbf{u}) + 2\nabla(\mathbf{u} \cdot \nabla \eta) - 2(\mathbf{u} \cdot \nabla)\nabla\eta - 2\nabla\eta\nabla\cdot\mathbf{u}], \tag{2.33}$$

where α_0 denotes a constant reference value of thermal expansivity. The energy conservation solved in the numerical model has the following form,

$$\frac{DT}{Dt} - \frac{\tau_0}{\alpha_0 T_c C_p}\frac{D(l_1\Gamma_1 + l_2\Gamma_2)}{Dt} = \frac{\kappa}{Ra}\left[\nabla^2 T + \frac{1}{k}\frac{\partial k}{\partial r}\frac{\partial T}{\partial t}\right] + \frac{h}{C_p Ra} + \frac{\tau_0}{\rho_r C_p}\Phi - \tau_r u_r (T - T_S). \quad (2.34)$$

Lastly, the equation of state for the convection model states,

$$\rho = \rho_r\{1 - \alpha_0 T_c \alpha(T - T_r) + 1/K_S(p - p_r)\} + \Delta_1(\Gamma_1 - \Gamma_{r1}) + \Delta_2(\Gamma_2 - \Gamma_{r2})\,. \quad (2.35)$$

In the above formulations, subscript 0 is employed for constant reference values used for non-dimensionalization purposes. The non-dimensional parameters in the equations above include the Rayleigh number,

$$Ra = \alpha_0 \Delta T g_0 d^3 \rho_0 / \kappa_0 \eta_0\,, \quad (2.36)$$

and the dissipation numbers,

$$\tau_0 = g_0 \alpha_0 d / C_{p0}\,; \;\; \tau_r = g\tau_0 \alpha / C_p\,. \quad (2.37)$$

The non-dimensional internal heating per unit mass is

$$h = \frac{\rho_0 \mathcal{H} d^2}{k_0}\Delta T\,. \quad (2.38)$$

The parameter d in these formulations represents the depth of the mantle. The effects of phase transitions are included through the phase density functions Γ_1 and Γ_2. In (2.34) and (2.35), l_1 and l_2 represent latent heat per unit mass, while Δ_1 and Δ_2 are the differences in density at the phase boundaries.

The numerical code uses a finite-difference method to solve the anelastic and infinite Prandtl number convection equations. The physical properties density, thermal expansivity, thermal conductivity, adiabatic bulk modulus, heat capacity and gravity are depth dependent, and are fit to be as Earth-like as possible (Figure 2.1).

The mantle viscosity varies radially and depends on the temperature in the mantle and hence on time. This model uses a simplification compared to the azimuthally-dependent viscosity models, but allows for significant computational speed-up. In addition, *Brunet and Machetel* [1998] have shown

that the heat flow in calculations with laterally-varying, temperature-dependent viscosity is quite similar to the heat flow calculated with only radially-varying temperature dependence, where the radial dependence was the same as the azimuthally-averaged viscosity in the temperature dependent case.

The radial dependence is assumed to consist of two linear segments, one in the lower mantle and one in the upper mantle and transition zone, as follows [*Butler et al.*, 2005],

$$\begin{aligned} \eta(r) &= \frac{\eta_e - \eta_l}{R_{660} - R_{cmb}}\, r + \frac{\eta_l R_{660} - \eta_e R_{cmb}}{R_{660} - R_{cmb}}, \text{ for } r < 5500\,\text{km}\,, \\ \eta(r) &= \frac{\eta_u - \eta_e}{R_s - R_{660}}\, r + \frac{\eta_e R_s - \eta_u R_{660}}{R_s - R_{660}}, \quad \text{for } r > 5900\,\text{km}\,. \end{aligned} \tag{2.39}$$

For the region $5500\,\text{km} < r < 5900\,\text{km}$ the profile is that of a cubic that is chosen so that the viscosity and its first derivative are continuous at $r = 5500$ km and $r = 5900$ km. The viscosity at the base of the lower mantle, η_l, at 660-km depth, η_e, and in the upper mantle, η_u, are calculated from

$$\begin{aligned} \eta_l &= \eta_{l0}\, \exp T_A \left[\frac{1}{T_l} - \frac{1}{T_{lf}}\right], \\ \eta_e &= \eta_{e0}\, \exp 2\, T_A \left[\frac{1}{T_u + T_l \phi_{le}} - \frac{1}{T_{uf} + T_{lf}\phi_{le}}\right], \\ \eta_u &= \eta_{u0}\, \exp T_A \left[\frac{1}{T_u \phi_{eu}} - \frac{1}{T_{uf}}\right]. \end{aligned} \tag{2.40}$$

Here T_l and T_u represent the average temperature at each time step in the lower mantle and in the transition zone and upper mantle, respectively. The value for the constants T_{uf}, T_{lf}, T_A (used to model the activation energy of material creep processes in the mantle), η_{l0}, η_{e0}, η_{u0} and ϕ_{le} and ϕ_{eu} (used to describe the adiabatic drop in temperature from the core-mantle boundary to 660 km-depth and from 660 km depth to the surface) are given in Table 2.1. The viscosity used in the model is higher than values inferred on the basis of post-glacial rebound [e.g. *Peltier and Jiang*, 1996]. As well as increasing computational efficiency, these high values are necessary in order that the calculated surface heat flow is similar in magnitude to the observed surface heat flow [*Butler and Peltier*, 2000]. The viscosity in the lower mantle is also higher than the viscosity in the upper mantle and transition zone as is evidenced in Figure 1.6 by the significantly larger spatial wavelength of rising plumes in the lower mantle compared with the sinking boundary layer

instabilities in the upper mantle. The CMB and surface are assumed to be free-slip.

The internal heating rate in the mantle is also made time-dependent with the same intensity used in the parameterized calculations of *Butler and Peltier* [2002]. The uranium/thorium/potassium ratios used are 1/4/10000 following *Hart and Zindler* [1986] and a bulk silicate Earth uranium concentration of 21 parts per billion is assumed, which gives a total modern-day heating power of 19.4 TW for the mantle and crust. The distribution of internal heating is assumed such that 6.4 TW are stored in the continental crust and 13 TW are used in the model mantle. The heat sources are fixed in position and 11 TW and 2 TW of heat sources are uniformly distributed in the regions above and below the 660-km depth horizon, respectively. The low heating rate in the upper mantle is used in order that the upper mantle internal heating rate matches the observed heating power in MORB source material.

The model also includes the effects of the 400 and 660 km depth phase transitions with Clapeyron slopes of 3 MPa/K and -2.8 MPa/K, respectively. The phase boundaries are indicated in Figure 1.6 by colored lines and it can be seen that the 660-km depth phase transition is providing a partial barrier to mantle flow. In most of the simulations, the initial condition is taken from a previous simulation run with a similar Rayleigh number but without time varying viscosity, core-mantle boundary temperature and internal heat sources. The initial average temperature as a function of depth was chosen to lie on an adiabat with temperature at the mantle solidus for the upper mantle and the initial core temperature was chosen to be 4300 K; these initial temperature conditions are identical to the ones employed in parameterized investigations of *Butler and Peltier* [2002] and numerical models for thermal evolution of *Nakagawa and Tackley* [2004, 2005]. In contrast, a value of 4800 K is employed in the analysis of *Nimmo et al.* [2004].

2.4 Core Thermal History Model

The global energy balance in the core is obtained by integrating the local energy conservation equation over the volume of the core. The global heat conservation states that the heat loss of the core, which equals the total heat flux at the core-mantle boundary (Q_{cmb}), is balanced by the sum

of the heat sources in the core [*Buffett et al.*, 1992; *Lister and Buffett*, 1995; *Buffett*, 2002; *Labrosse*, 2003; *Gubbins et al.*, 2003; *Nimmo et al.*, 2004],

$$Q_{cmb} = \chi_{IC} + \chi_{OC} + \chi_L + \chi_G + \chi_R \,, \tag{2.41}$$

where $\chi_{IC}, \chi_{OC}, \chi_L, \chi_G, \chi_R$ represent the rates of secular cooling of the inner and outer core, latent heat and gravitational energy releases due to the growth of the inner core, and internal heating in the core respectively. To a good approximation, the core can be assumed adiabatic [*Buffett et al.*, 1992], therefore both secular cooling terms can be combined in a single term, χ_C. The cooling of the core is given by

$$\chi_C \equiv -\frac{\partial}{\partial t} \int_{\mathcal{V}_c} \rho_c \, c_{pc} \, T_C \, d\,V \cong -M_C \, c_{pc} \, \frac{d < T_C >}{dt}, \tag{2.42}$$

where ρ_c, T_C, M_c, c_{pc}, represent the density, temperature, mass of the core, and specific heat capacity per unit mass, and $< T_C >$ represents the mean temperature in the core.

The latent heat released due to the crystallization of the inner core [*Lister and Buffett*, 1995] is integrated over the volume of the inner core,

$$L \equiv \int_{\mathcal{V}_{ic}} \mathcal{L} \, \rho_{ic} \, dV_{ic} \cong \frac{4}{3} \, \pi \, R_{ic}^3 \, \mathcal{L} \, \rho_{ic} \,, \tag{2.43}$$

assuming that the latent heat of melting of the iron-rich material at inner core conditions, $\mathcal{L}$, and ρ_{ic} are constant. Differentiating with respect to time gives the rate of latent heat release

$$\chi_L = 4 \, \pi \, \mathcal{L} \, R_{ic}^2 \, \frac{d \, R_{ic}}{dt} \,. \tag{2.44}$$

As expected, the release of latent heat of solidification depends on the rate of growth of the inner core radius, dR_{ic}/dt.

In equation (2.41), χ_G defines the release of gravitational energy due to the inner core solidification and expelling of a lighter fraction of core material. Detailed analyses show that the gravitational energy released by thermal contraction and adiabatic compression are balanced by the work of the pressure forces on the CMB during contraction [*e.g. Gubbins et al.*, 1979]. These terms are not directly available to drive the dynamo action and do not have an important contribution to the global heat budget [*Stacey*, 1992], hence they are omitted from further calculations.

The part of gravitational energy which contributes to the dynamo action is associated with the buoyancy fluxes which drive convection in the outer core, due to the density contrast at the inner core boundary associated with light element, $\Delta\rho_{icb}$ [*Buffett et al*, 1996]. To calculate the gravitational energy released by inner core solidification we assume that the inner core has grown to the radius R_{ic} and that an increment dR_{ic} is formed [*Stacey*, 1992]. By this increase in the radius, the mass fraction withdrawn from the outer core can be written as

$$\delta m \;=\; 4\pi R_{ic}^2 \Delta\rho_{icb}\, dR_{ic}\,. \tag{2.45}$$

The mass fraction that comes from the range r to $r+dr$ can be expressed as

$$dM = \delta M/M \;=\; \frac{4\,\pi\rho_c\; r^2\, dr}{\frac{4\pi}{3}\,\rho_c\,(R_{cmb}^3 \;-\; R_{ic}^3)},, \tag{2.46}$$

where R_{cmb} represents the radius of the outer core. Assuming constant density throughout the outer core, the gravity at the radius r is given by,

$$g(r) \;=\; \frac{G\,m(r)}{r^2} = \frac{4\pi}{3}\,G\,\rho_c\,r\,. \tag{2.47}$$

At the CMB horizon, the gravity is then $g_c = 4\pi/3\,G\,\rho_c\,R_{cmb}$. We can express the gravity at any radius inside the core (2.47) as a function of the gravity at the CMB, g_c,

$$g(r) \;=\; g_c\,\frac{r}{R_{cmb}}\,. \tag{2.48}$$

The gravitational potential difference between an arbitrary r and R_{ic} is computed from the integral,

$$\Delta V_g \;=\; \int_{r'=R_{ic}}^{r} g(r')dr' \;=\; \int_{R_{ic}}^{r} g_c\,\frac{r'}{R_{cmb}}dr' \;=\; \frac{g_c}{2\,R_{cmb}}\left(r^2 - R_{ic}^2\right). \tag{2.49}$$

The result in (2.49) is subsequently used to compute the gravitational energy released by accumulation of the mass δm at the inner core,

$$dE_{grav} \;=\; \int_{r=R_{ic}}^{R_{cmb}} \delta m\,\Delta V_g\, dM. \tag{2.50}$$

Substituting (2.45) and (2.46) and (2.49) in (2.50) gives the final expression for the energy release,

$$dE_{grav} = \frac{6\,\pi\,\Delta\rho_{icb}\;R_{ic}^2\,g_c}{R_{cmb}\,(R_{cmb}^3 - R_{ic}^3)}\;\left(\frac{R_{cmb}^5}{5} - \frac{R_{cmb}^3\,R_{ic}^2}{3}\right)\,dR_{ic}\,. \tag{2.51}$$

The result in (2.51) is integrated from zero to the radius R_{ic}, to obtain the total energy released as a result of the growth of the inner core,

$$E_{grav} = \frac{8\,\pi^2}{15}\,G\,\Delta\rho_{icb}\,\rho_c\,R_{ic}^3\,\left(R_{cmb}^2 - R_{ic}^2\right). \tag{2.52}$$

This expression is similar to the one used by *Labrosse et al.* [2001]. The rate of gravitational energy release is given by

$$\chi_G = \frac{8\,\pi^2}{15}\,G\,\Delta\rho_{icb}\,\rho_c\,\left(3\,R_{cmb}^2\,R_{ic}^2 - 5\,R_{ic}^4\right)\frac{dR_{ic}}{dt}. \tag{2.53}$$

The gravitational energy released by the formation of the inner core depends on the density contrast between the inner and outer core and on the rate of growth of the IC (which by conservation of matter relates to the rate at which the light elements are released at the ICB).

Finally, the last term in (2.41) represents the internal heating due to radioactive sources in the core. As mentioned before, the presence of radioactive sources in the core is still not well established, however, recent calculations of energy required to drive the geodynamo [*e.g., Buffett*, 2002; *Nimmo*, 2004; *Butler et al.*, 2005] clearly show that assuming radioactive heat sources in the core can explain continuous generation of magnetic field prior to the inner core formation. To compute the radioactive heating, we assume that the core convects vigorously and therefore the radioactive elements, if present, are uniformly mixed throughout the core. The internal heating rate is expressed by

$$\chi_R = \sum_i Q_0(i) e^{-\lambda(i)t}, \tag{2.54}$$

where Q_0 and λ represent the total heat 4.55 billion years ago and the decay constant for each isotope. Experimental work has demonstrated that potassium can be included in the geochemistry of the iron melt at core temperature and pressure conditions, as it enters Fe^{2+} sulphide (FeS) in a strongly temperature-dependent fashion [*Murthy et al.*, 2003], although there is no consensus on the estimated possible concentrations of potassium in the core [*e.g., Corgne et al.*, 2007]. Hence, the presence of radioactive potassium in the core could be incorporated in a thermal evolution model. In all subsequent calculations where radioactivity in the core is assumed, I only account for the presence of ^{40}K, but small fractions of other isotopes could also be considered. The isotope ^{40}K

has a half-life of 1250 Myr [*Stacey*, 1992] and represents 0.012 % of naturally-occurring potassium at the present-day [*Nimmo*, 2007].

The thermal history in the core can be computed from the energy conservation equation stated in (2.41). The terms of the equation can be re-arranged to obtain the evolution of the CMB temperature (on the core side)

$$\frac{d}{dt}\,T_{cmb} = \frac{1}{C_{pE}}\,\left(\chi_R - Q_{cmb} + \chi_L + \chi_G\right), \tag{2.55}$$

where T_{cmb} is the temperature at the CMB and the quantity C_{pE} represents an effective heat capacity at the CMB, computed from a Gaussian-averaged adiabatic profile for the heat capacity in the core [*e.g., Labrosse et al.*, 2001],

$$C_{pE} = \int_0^{R_{cmb}} \rho_{cen}\,\exp\left[-\frac{r^2}{L^2}\right]\,c_{pc} \times \exp\left[\frac{R_{cmb}^2 - r^2}{D^2}\right] r^2 dr\,. \tag{2.56}$$

Here, r is radius, ρ_{cen} is the density at the centre of the Earth, L and D are characteristic length scales for the density variation variation within the core and adiabatic temperature profile in the core, respectively [*Labrosse et al.*, 2001]. C_{pE} is not the true total heat capacity of the core, but rather an effective heat capacity, since it is multiplied by the change in temperature at the CMB rather than the average of temperature in the core. Since the choice of specific heat capacity value varies from one author to another, and D falls in the range 6000-8300 km, C_{pE} ranges from 1.4×10^{27} to 2.1×10^{27} J/K. The value adopted for all the calculations shown in this work is 1.5×10^{27} J/K [*Butler et al.*, 2005].

The evolution of the temperature in the core is influenced by the history of the inner core formation, since the last two terms in (2.55) depend on the rate of growth of the IC radius (see (2.44) and (2.53)). It is expected that the effect of the inner core will be small at the beginning of the growth process, due to the small size of the inner core, however, in the later stages, the heat sources associated with the solidification of the inner core can have a significant influence on the thermal and magnetic evolution of the core.

2.5 Inner Core Growth

The rate of growth for the IC is determined from the analytical model of *Buffett et al.* [1992]. The model assumes that at $t = 0$, the whole core is initially superliquidus. Once the planet cools and the adiabatic temperature reaches the liquidus temperature of the core alloy at the Earth's centre, the nucleation of the inner core begins (Figure 2.2). As the inner core solidifies, and $R_{ic} > 0$, lighter elements are released into the alloy.

The analytical model for inner core solidification assumes that buoyancy forces drive vigorous convection in the outer core which yields a well-mixed alloy with an adiabatic temperature profile. It is also assumed that the surface of the inner core is in thermodynamic equilibrium with the liquid outer core. Within a certain range of pressure, the solidification temperature can be approximated using a Taylor series expansion about the temperature of solidification at the centre of the Earth. If the state of the core is hydrostatic, isentropic and well mixed, to first order, the variations in temperature due to changes in pressure (P) and composition (C) are described by [*Buffett et al.*, 1992],

$$T_L(R_{ic}) = T_L(0) + \frac{\partial T_L}{\partial P}(P - P_0) + \frac{\partial T_L}{\partial C}(C - C_0), \tag{2.57}$$

where P_0 and C_0 represent the reference pressure and composition at the centre of the Earth, and $T_L(0)$ represents the solidification temperature of core material at the pressure of the centre of the Earth. In subsequent calculations, I assume $T_L(0) = 5700$ K [*Stacey*, 1992, *Steinle-Neumann et al.*, 2001]. The liquidus value at the centre of the Earth is estimated by extrapolating the melting temperatures of pure iron at the inner core/outer core boundary obtained from *ab initio* calculations. Thus, the estimates for the liquidus temperature $T_L(0)$ are model and assumptions dependent, and they also vary with the content of light elements assumed in the outer core. The melting temperature of the iron at the pressures corresponding to the ICB are ranging from *e.g.*, 5400 ± 400 K in the study of *Laio et al.* [2000] to a much more higher value, 6450 ± 100 K in a recent study of Alfè [2009]. Accordingly, the melting temperatures at the centre of the Earth, will span a wide range. The choice for $T_L(0)$ is also in agreement with the analysis of *Nimmo et al.*

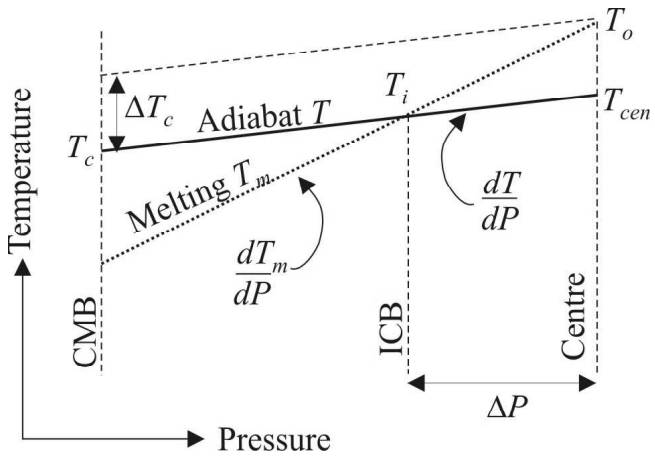

Figure 2.2: Diagram of temperature structure in the core (from *Nimmo*, 2007).

[2004], where a value of 5500 ± 300 K is suggested. A different approach used in thermal history models is to express the liquidus temperature of the core as a quadratic function of pressure, where the constants that enter the quadratic are guided by Lindemann's law [*e.g., Stevenson et al.*, 1983].

The phase diagram of the iron alloy constituting the core is poorly constrained at present. At the same time, theoretical models [*Loper*, 1991] suggest that in the case of the Earth, the influence of the compositional variations are small, therefore, the compositional dependence of T_L is neglected. Assuming constant density and hydrostatic pressure in the core, the pressure at the inner core boundary is given by

$$P(R_{ic}) \;=\; P_0 - \frac{2\pi}{3}\, G\, \rho_c^2\, R_{ic}^2 \,. \tag{2.58}$$

Substituting the expression derived for pressure in (2.58) into (2.57), the solidification temperature becomes

$$T_L(R_{ic}) = T_L(0) - \frac{2\pi}{3}\, G\, \rho_c^2\, R_{ic}^2\, \frac{\partial T_L}{\partial P} \,. \tag{2.59}$$

The solidification temperature in (2.59) decreases with the increase in the size of the inner core R_{ic}. Therefore, the evolution of the solidification temperature, *i.e.*, $T_L(R_{ic}(t))$, shows a slow decrease with time, due to core cooling and the growth of the inner core.

The growth of the inner core can be determined from (2.59), if the temperature at the ICB

and the rate of change in the solidification temperature with pressure ($\partial T_L/\partial P$) are known. The temperature at the ICB must lie at the intersection of the solidification temperature with the adiabatic profile (Figure 2.2). The ICB temperature $T_{icb} \equiv T_L(R_{ic}(t))$ can be expressed as a function of the temperature at the CMB, assuming a relation of the form

$$T_L(R_{ic}(t)) = \Gamma\, T_{cmb}(t), \tag{2.60}$$

where the parameter Γ represents the fractional increase in the adiabatic temperature from the CMB radius to the IC radius. Using 2.59, the radius of the inner core is given by

$$R_{ic} = \left(\frac{T_L(0) - T_L(R_{ic})}{\Lambda}\right)^{1/2}, \tag{2.61}$$

where I have defined the liquidus parameter $\Lambda = 2\pi/3\, G\rho_c^2\, \partial T_L/\partial P$ and $\partial T_L/\partial P = 7\times 10^{-9}$ K/Pa [*Buffett*, 1992]. Substitution of (2.60) into (2.61) leads to

$$R_{ic}(t) = \left(\frac{T_L(0) - \Gamma\, T_{cmb}(t)}{\Lambda}\right)^{1/2}, \tag{2.62}$$

thus relating the evolution of the radius of the inner core to the history of the CMB temperature. The rate of growth of the inner core is

$$\frac{dR_{ic}}{dt} = -\frac{1}{2\,\Lambda^{1/2}} \frac{\Gamma\,(d\,T_{cmb}(t)/dt)}{(T_L(0) - \Gamma\, T_{cmb}(t))^{1/2}}\,. \tag{2.63}$$

Solving (2.55) and (2.63) simultaneously yields the thermal history in the core and the inner core growth through geological time.

2.6 Entropy in the Core

The energy balance (2.41) relates the heat flux across the CMB to the sum of heat sources in the core, however it does not account for the magnetic energy, because, physically, the magnetic energy is both generated and dissipated internally in the core and therefore does not affect the heat balance [*Gubbins et al.*, 2003]. Since the magnetic energy can be related to the dissipative processes (via Ohmic losses), one way to estimate the energy available for regeneration of magnetic field is to examine the entropy production in the core and assess the contribution given by dissipation. This

in turn will clue us into the available energy to drive the geodynamo and allow investigation of circumstances under which the dynamo will operate.

The dissipative processes in the core include the ohmic dissipation (Joule heating) and viscous dissipation (shear heating). In the outer core, the dissipation is dominated by the Joule heating [*e.g. Labrosse*, 2003], and only a small percent ($\sim 2\%$ to 5% of the total dissipation) occurs through viscous dissipation, because electrical resistance dominates viscosity in its dissipative effects in a highly conductive material such as the iron alloy [*Gubbins et al.*, 2003]. To calculate the entropy produced by ohmic dissipation from the known energy sources in the core, we need the entropy production of the system. The sources that enter the heat budget are stated in equation (2.41). The entropy sources are determined by dividing each of the heat sources by the temperature at which they are supplied.

The energy generated by radioactive decay, if present, is assumed to yield uniform heating within the core, because convection in the core keeps a uniform concentration of radioactive elements. The heating due to radioactive isotopes gives the following local entropy term

$$E_{R\,,local} \;=\; \frac{\chi_{R\,,local}}{T_{local}}, \tag{2.64}$$

which can be integrated over the volume of the core to obtain the entropy in the core due to internal heating,

$$E_R \;=\int_{\mathcal{V}} \frac{\chi_{R\,,local}}{T_{local}} dV \cong\; \frac{\chi_R}{< T_C >}, \tag{2.65}$$

where χ_R represents the amount of internal heating throughout the entire core and $< T_C >$ is the mean temperature in the core. Similarly, we compute the entropy due to specific heat, which is the largest term in the energy balance. The local entropy produced by the secular cooling is integrated over the volume of the core to give the total entropy due to the secular cooling of the core (includes both inner and outer core)

$$E_C \;=\int_{\mathcal{V}} \frac{\chi_{C\,,local}}{T_{local}} dV \cong\; \frac{\chi_S}{< T_C >}\,. \tag{2.66}$$

The internal heating and the secular cooling are mathematically equivalent [*Labrosse and Macouin*, 2003], since these two energy sources are uniformly distributed within the core.

The heat sources at the inner core boundary are the specific heat due to the secular cooling of the inner core (which is included in the total secular cooling term) and the latent heat released by the crystallization of the inner core material. The latent heat depends on the rate of growth of the inner core, which in turn depends on the thermal history in the core. The latent heat is similar to the specific heat, in that when the core cools by a small amount, the IC solidification releases heat concentrated at the inner core boundary [*Gubbins et al.*, 2003]. The entropy of latent heat at the inner core boundary is

$$E_L \;=\; \frac{\chi_L}{T_{icb}}\,, \tag{2.67}$$

where T_{icb} represents the temperature at the ICB.

For an isentropic (and isochemical) outer core, the temperature gradient is adiabatic and obeys $\nabla T_{adb} \;=\; \alpha_c\, g_c\, T/c_{pc}$, where α_c represents the thermal expansivity in the core, c_{pc} is the heat capacity of the core per unit mass, and g_c is the gravitational acceleration in the core. The entropy gain from thermal diffusion is estimated using the adiabatic temperature [*Gubbins et al.*, 2003],

$$\int_{\mathcal{V}} E_{adb}(t)\, dV \;=\; \int_{\mathcal{V}} k_c \left(\frac{\nabla T_{adb}}{T}\right)^2 dV \;=\; 4\pi \int_{R_{ic}(t)}^{R_{cmb}} k_c \left(\frac{\alpha_c\, g_c}{c_{pc}}\right)^2 r^2\, dr\,, \tag{2.68}$$

where k_c is the thermal conductivity of the core, and r is the radius. Following *Labrosse et al.* [2001] and *Nimmo et al.* [2004], the adiabatic temperature can be expressed as $T(r) = T_{cen} \exp(-r^2/D^2)$, where T_{cen} is the temperature at the centre of the Earth, and $D^2 = 3\, c_{pc}\,/(2\,\pi\,\alpha_c\,\rho_{cen}\,G)$. Therefore (2.68) can be written as [*Nimmo et al.*, 2004],

$$E_{adb} = \frac{16\,\pi\,k_c\,R_{cmb}^5}{5\,D^4}\,. \tag{2.69}$$

At last, the equivalence between the CMB temperatures using the adiabatic parameter Γ and the formulation of *Nimmo et al.* [2004], *i.e.*,

$$\begin{aligned} T_{cen} &= \Gamma\, T_{cmb} \\ T_{cmb} &= T_{cen} \exp\left(\frac{-R_{cmb}^2}{D^2}\right)\,, \end{aligned} \tag{2.70}$$

is used to express $\Gamma = \exp(R_{cmb}^2/D^2)$, and hence (2.69) becomes,

$$E_{adb} = \frac{16\,\pi\,k_c\,R_{cmb}}{5}\,(\ln\Gamma)^2\,. \tag{2.71}$$

The local entropy of the dissipation processes (assumed to be due solely to the Joule heating effect) is given by

$$E_\Omega \,=\, \frac{\Phi_\Omega}{T_D}\,. \tag{2.72}$$

where Φ_Ω represents the local ohmic dissipation and T_D is the typical temperature at which this dissipation occurs. Similar to the secular cooling term, we make the assumption that the entropy given by dissipation is effectively produced at the mean temperature in the core, since it ultimately reflects the production of magnetic energy, which is the work done by the heat engine. An additional argument follows from the fact that the 'ideal efficiency' of the engine cannot be exceeded. In other words, for a heat engine working in an 'ideal' Carnot-cycle, if the temperature at which the input heat is provided (say, $\mathcal{T}_+$) is higher that the temperature at which heat is extracted ($\mathcal{T}_-$), the efficiency of the engine to do useful work is computed as $\eta = 1 - \frac{\mathcal{T}_-}{\mathcal{T}_+}$, therefore dissipation must occur at such a temperature T_D, that $T_{cmb} \leq T_D \leq T_{icb}$ [*Braginsky and Roberts*, 1995].

The entropy production in the core is evaluated by integrating the local entropy equation over the volume of the core. The entropy equation [*Labrosse*, 2003] integrated over the volume of the outer core $\mathcal{V}$, states that the entropy at the CMB is given by the sum of entropy sources within the core

$$\frac{Q_{cmb}}{T_{cmb}} \,=\, E_L \,+\, \int_{\mathcal{V}} E_{adb}\, dV \,+\, \int_{\mathcal{V}} E_\Omega\, dV \,+\, (E_R + E_C)\,. \tag{2.73}$$

Re-arranging the terms yields the entropy production in the core

$$\int_{\mathcal{V}} E_\Omega\, dV \,+\, \int_{\mathcal{V}} E_{adb}\, dV \,=\, \frac{Q_{cmb}}{T_{cmb}} \,-\, (E_R + E_C) \,-\, E_L\,. \tag{2.74}$$

The physical meaning of (2.74) is better revealed by substituting Q_{cmb} from the energy balance (2.41) into (2.74), and using the definitions (2.65) - (2.72) for the entropy terms, which yields

$$\begin{aligned}\int_{\mathcal{V}} \frac{\Phi_\Omega}{T_D}\, dV \,+\, \int_{\mathcal{V}} k \left(\frac{\nabla T}{T}\right)^2 dV \,=\, \\ (\chi_R + \chi_C)\left(\frac{1}{T_{cmb}} - \frac{1}{< T_C >}\right) \,+\, \chi_L \left(\frac{1}{T_{cmb}} - \frac{1}{T_{icb}}\right) \,+\, \\ \chi_G \left(\frac{1}{T_{cmb}}\right).\end{aligned} \tag{2.75}$$

The changes in entropy arising from having heat sources and sinks at different temperatures appear in left-hand side of (2.75). The right-hand side contains the positive entropy contributions due to

universal entropy increase, evaluated by the classical Carnot cycle of a heat engine [*Stacey*, 1992, p. 306]. That is, each thermal source provided to the core at temperature T_S, is multiplied by the efficiency factor $(1/T_{cmb} - 1/T_S)$, which defines the (ideal) Carnot efficiency of an engine working over an adiabatic temperature range. Consequently, the secular cooling and the radioactive heating enter the entropy equation with a small efficiency, since these heat sources are distributed over the whole core [*Labrosse and Macouin*, 2003], whereas the entropy produced by the heat released at the ICB is calculated using the higher efficiency factor $(1/T_{cmb} - 1/T_{icb})$. The energy released by the gravitational differentiation at the ICB, although it does not create entropy at this horizon, consists of the work done by the hot, buoyant material at the CMB, and therefore enters the entropy balance with a much larger factor, as $1/T_{cmb}$. This efficiency factor was used by *Braginsky* [1991], and more recently by *Nimmo et al.* [2004], *Labrosse* [2003] and *Labrosse et al.* [2001].

Physically, equation (2.75) states that the entropy of dissipative processes and of the heat conducted down the adiabat must be sustained by the entropy production of various heat sources in the core. If there is not enough entropy gain in the system to overcome the thermal conduction, there is not enough entropy of dissipation, hence there is no generation of magnetic field. It can also be noted that the effects of core cooling are more significant in the heat balance than in the entropy production, where compositional terms predominate. It is uncertain as to to how much entropy of ohmic dissipation must be available in order for a magnetic field to be present and most likely these minimum conditions are dependent on shell geometry [*Heimpel et al.*, 2005]. Extrapolations from numerical dynamo simulations infer that $1 - 2$ TW are required to power the dynamo [*Roberts et al.*, 2003], whereas *Christensen and Tilgner* [2004] give a range of $0.2 - 0.5$ TW, based on numerical and laboratory results. *Buffett* [2002] estimates $0.1 - 0.5$ TW. Consequently, given the fact that the temperature at which the Ohmic dissipation occurs is model-dependent, this quantity is generally regarded as currently unknown. Therefore, in all the subsequent analyses, I have made a minimal assumption that a magnetic field can be generated if there is positive entropy rate available for Ohmic dissipation.

2.7 Magnetic Field Model

The Joule heating law states that the work done by electrical forces is converted into heat in a resistor. The power delivered through Joule heating is proportional to the square power of the electric current [*Griffiths*, 1999]. Hence, Ohmic dissipation in a unit volume, scales as

$$\Phi_\Omega \sim \frac{1}{\sigma}\mathbf{J}^2\,, \tag{2.76}$$

where $\mathbf{J}$ is the electric current density and σ represents the electrical conductivity of the material. Ampere's law in a low-frequency approximation [*Braginsky and Roberts*, 1995] is used to relate the magnetic field $\mathbf{B}$ in the outer core to the electric current density,

$$\mu_0\,\mathbf{J} = \nabla \times \mathbf{B}\,, \tag{2.77}$$

with μ_0 the magnetic permeability of free space. (Displacement current is neglected by the low-frequency assumption). The total Ohmic dissipation in the outer core is given by [*Buffett*, 2002],

$$\Phi_\Omega = \frac{B^2(l)}{\mu_0^2\,\sigma\,l^2}\mathcal{V}\,, \tag{2.78}$$

where $\mathcal{V}$ represents the volume of the outer core and l is the typical length scale of dissipation for a spherical harmonic component of the field. For instance, the length scale of dissipation for an output numerical model core field of 2.5 mT is $l \cong 200$ km [*Buffett*, 2002]. The magnitude of the magnetic field can be estimated from (2.78),

$$B = \mu_0\,l\left(\frac{\sigma\,\Phi_\Omega}{\mathcal{V}}\right)^{1/2}\,. \tag{2.79}$$

In these calculations, a purely electrically insulating mantle is assumed and therefore the ohmic dissipation possibly produced by electric currents that leak from the core and into the mantle [*Kuang and Chao*, 2003], or by electric currents induced in the lowermost mantle by time-varying fields in the core [*Costin and Buffett*, 2004] are neglected. It is also to be noted that *Christensen and Tilgner* [2004] suggest a linear dependence of the magnetic field with the Ohmic dissipation (rather than a square-root power scaling), based on numerical dynamo simulations and experimental dynamo

results. The scaling law is of the form [*Christensen and Tilgner*, 2004],

$$E_{mag} \propto \frac{l_B^2 \, \Phi_\Omega}{2\eta} \,, \tag{2.80}$$

where E_{mag} , l_B and η are respectively, magnetic energy, characteristic diffusive length scale of the field and magnetic diffusivity.

The model magnetic field calculated in (2.79) can be regarded only as a first-order approximation to the measurable field at the surface, as the toroidal part of the field generated in the core is not observable at the surface, and the poloidal and toroidal components may have varied through time independently. In addition, it is possible that small-scale motions in the core may generate most of the Ohmic dissipation [*Matsui and Buffett*, 2005], though these spatially-high frequency field components are not contributing to the field observed at the surface. Thus, the core magnetic field is different in both intensity and frequency content from the field observed at the surface. None-the-less, the model magnetic field scaled from the entropy of Ohmic dissipation enables us to relate features of the long-term secular variation to the coupled dynamics of the core and mantle and analyze, to first-order, the effects of different scenarios of mantle convection on the secular variation of the magnetic field. Paleo-secular variation (PSV) has shown that the axial dipole field was dominant throughout Earth's history, over timescales greater than a few thousand years [*e.g., Valet*, 2003]. Therefore, within the limitations explained above, the evolution of the model magnetic field emulates the evolution of the axial dipole field over the Earth's lifetime.

2.8 Practical Implementation of the Models

The output from the 2D axi-symmetric numerical model is used to compute the adiabatic temperature inside the core and the radius of the inner core as a function of time. Since the value of the inner core radius is undoubtedly the strongest constraint we now have from seismological observations, I use the temperature at the CMB at the end of simulation and the present-day value of the IC radius to compute the parameter Γ. In order to choose a value for Γ such that the inner core is the correct final size, I consider (2.62) for the time when the inner core has just started to

form and for the present-day Earth. Quantities evaluated at these times are indicated by using superscripts 0 and p, respectively. For instance, the temperature at the time of IC initiation and final CMB temperature from the simulations are T^0_{cmb} and T^p_{cmb}, and the corresponding radii are $R^0_{ic} = 0$ and $R^p_{ic} = 1221$ km. Substituting the known value of R^p_{ic} into (2.62) and solving for Γ we obtain the following result

$$\Gamma = \frac{T_L(0) - \Lambda\,(R^p_{ic})^2}{T^p_{cmb}}. \tag{2.81}$$

The value of T^p_{cmb} is unknown before the start of the simulation. However, we can estimate the total change in the temperature of the core if all of the latent and gravitational energy resulting from growing a present-day inner core were used to increase the temperature of the core. Using χ_L and χ_G from above, the change in temperature $\Delta T = (\chi_L + \chi_G)/C_{pc} = 72$ K, which is generally much smaller than the total change in the temperature of the core during the whole 4.55 Gyr course of a simulation. As a result, the thermal effects of the solidification of the inner core can be considered as a perturbation to the thermal evolution of the core. This observation allows us to determine the parameter Γ for each simulation.

In practice, I first run a simulation for the full age of the Earth with zero χ_L and χ_G in order to obtain a 0^{th} order estimate of the final temperature at the CMB, $T^{p,0}_{cmb}$. I then make the first order approximation that all of the latent heat and gravitational energy released is maintained in the core to obtain an improved estimate of the final temperature at the CMB, $T^{p,1}_{cmb} = T^{p,0}_{cmb} + \Delta T$. This estimate for $T^{p,1}_{cmb}$ is then used in (2.81) to obtain an estimate of the value of Γ required to grow an inner core of the same size as the one found in the real Earth. Using this value of Γ, it is possible to calculate T^0_{cmb} and by looking at the time evolution of T_{cmb} for the first run (in the absence of χ_L and χ_G), the age of the inner core was determined. The model is then re-run starting from a time just before the formation of the inner core using as initial conditions output from the appropriate time of the first run and including the effects of χ_L and χ_G and evolving the radius of the inner core according to (2.62). If the inner core were too large or too small after this second model run, I make a new estimate of Γ calculated from (2.81) using an approximate final temperature at the CMB of $T^{p,2}_{cmb} + \Delta T_2$ where $T^{p,2}_{cmb}$ is the final temperature at the CMB from the new simulation and

ΔT_2 is the change in the core temperature associated with melting or solidifying the extra amount of core material required to make the model core of the same size as the real core in the Earth. Iterations are stopped if the inner core radius has around 20 km error ($< 2\%$ of the real Earth). It usually takes less than 3 iterations to achieve an acceptable radius for the IC.

In the formulation of *Labrosse et al.* [2001], the parameter Γ takes on the form $\Gamma \equiv \exp[(R_{cmb}^2 - r^2)/D^2]$, where D depends on physical parameters such as the thermal expansivity, heat capacity, and acceleration due to gravity in the core. There are significant uncertainties in the values of the first two of these quantities resulting in values of Γ that lie between 1.21 and 1.64; Γ should also decrease as the inner core grows since the adiabatic gradient will extend over shorter distances. I ignore this last effect (which produces an error of roughly 6%) and treat Γ as a constant in each simulation.

In order to estimate the mean temperature in the core, required to compute the entropy production from secular cooling ($\pm$ internal heating) term, a Gaussian adiabatic temperature profile in the core is assumed [*e.g., Nimmo et al.*, 2004, *Labrosse et al.*, 2001]. Consequently, using Γ_{mean} defined as:

$$\Gamma_{mean} = \frac{3}{4\ln\Gamma}\left[\Gamma\left(\frac{\pi}{\ln\Gamma}\right)^{0.5} Erf[(\ln\Gamma)^{0.5}] - 2\right], \tag{2.82}$$

the mean temperature in the core can be expressed as a function of the numerical output T_{cmb}, i.e., $< T_C > = \Gamma_{mean} \times T_{cmb}$. Further, Γ_{mean} is always less than Γ. In practice, all the entropy terms in the core are expressed as a function of the output temperature T_{cmb} and the values of Γ and Γ_{mean}. Hence, the expressions for entropy terms (S), updated at each time step from the numerical output of mantle convection are given by [*Costin and Butler*, 2006],

$$\begin{aligned}
S_{adb} &= \frac{16\pi}{5} R_{cmb}\, k_c\, (\ln\Gamma)^2, \\
S_r &= \frac{\chi_r}{T_{cmb}}\left(1 - \frac{1}{\Gamma_{mean}}\right), \\
S_{sec} &= \frac{\chi_C}{T_{cmb}}\left(1 - \frac{1}{\Gamma_{mean}}\right), \\
S_L &= \frac{\chi_L}{T_{cmb}}\left(1 - \frac{1}{\Gamma}\right), \\
S_G &= \frac{\chi_G}{T_{cmb}}.
\end{aligned} \tag{2.83}$$

It will be noted that S_{adb} has a constant value throughout each simulation, however, it differs from one simulation to another as Γ is allowed to vary due to the modern-day IC radius constraint. For consistency, the entropy of thermal conduction is also calculated assuming a Gaussian adiabatic temperature profile in the core. As a result, when comparing simulations for which different values of Γ are used, it is often useful to compare the sum of the entropy available for ohmic dissipation and thermal conduction down the core adiabat as a measure of the vigor of geodynamo action.

Lastly, for the sake of comparison, when I plot the magnetic field as a function of time, I normalize the field for each case scenario by the same reference value, namely the value of the present-day magnetic field intensity for the nominal run. The values of the physical constants used in calculations are listed in Table 2.2.

Constant	Value	Units
T_{uf}	2099	K
T_{lf}	2931	K
T_A	55,000	K
η_{l0}	2.17×10^{23}	Pa s
η_{e0}	8.52×10^{22}	Pa s
η_{u0}	4.07×10^{23}	Pa s
ϕ_{le}	0.75	non-dim
ϕ_{eu}	0.92	non-dim

Table 2.1: Constants used to define the viscosity profiles in equations (2.39) and (2.40).

Parameter	Symbol	Value	Units
Mean density (outer core)[a]	ρ_c	1.1×10^4	kg m^{-3}
Mean density (inner core)[a]	ρ_{ic}	1.255×10^4	kg m^{-3}
Density at the Earth's centre[a]	ρ_{cen}	1.3×10^4	kg m^{-3}
Density jump at the ICB[*b]	$\Delta\rho_{icb}$	400	kg m^{-3}
Density at the base of the mantle	ρ_L	5575	kg m^{-3}
Radius of the Earth[a]	R_s	6370×10^3	m
Radius of the outer core[a]	R_c	3480×10^3	m
Radius of the inner core[a]	R_{ic}	1221×10^3	m
Thermal expansion in the core[a]	α_c	10^{-5}	K^{-1}
Thermal expansion at the base of mantle [a]	α_L	10^{-5}	K^{-1}
Specific heat capacity-core [a]	c_{pc}	675	J kg^{-1} K^{-1}
Specific heat capacity-lowermost mantle [a]	C_{pL}	1256	J kg^{-1} K^{-1}
Latent heat of inner core solidification[b]	$\mathcal{L}$	7.5×10^5	J kg^{-1}
Solidification temperature at Earth's centre[c]	$T_L(0)$	5700	K
Pressure gradient for solidification temperature[b]	dT_L/dP	7×10^{-9}	K/Pa
Thermal conductivity at the base of the mantle[a]	k_L	12	W m^{-1} K^{-1}
Thermal conductivity in the core[a]	k_c	36	W m^{-1} K^{-1}
Electrical conductivity in the core[a]	σ	3×10^5	S m^{-1}
Gravitational acceleration at CMB[a]	g_c	10	m s^{-2}

Table 2.2: Constants and parameters used in this study. *Due to compositional changes across inner core boundary [a]Stacey, 1992. [b]Buffett *et al.*, 1996. [c]Anderson, 2002.

Chapter 3

Modeling the Effects on Internal Heating in the Core and Lowermost Mantle on the Earth's Thermal and Magnetic History

In this contribution I analyze the consequences of the presence of radioactive sources in the core or at the base of the mantle, as possible scenarios that have been brought forth to reconcile the geodynamo power requirements with a realistic thermal history in the core. In addition, the effects of other factors such as initial core temperature, mantle viscosity and distribution of internal heat sources in the mantle are briefly analyzed.

The concentration of volatile lithophile elements, such as potassium, in Bulk Silicate Earth (BSE) models is significantly lower than the concentration in C1 chondrites. An estimate of potassium concentration in BSE yields 120 to 300 ppm, and a K/U ratio in the range 700 to 1200 [*Lassiter*, 2004], while a more recent estimate yields 190 ± 40 ppm K in BSE (*Lubetskaya and Korenaga*, 2007). The same ratio in chondrites is roughly one order of magnitude higher [*e.g., Hart and Zindler*, 1986], showing a strong depletion in terrestrial potassium. One possible explanation is that much of the potassium was evaporated and lost into space in the early, hot stages following planetary accretion [*e.g., McDonough and Sun*, 1995], or due to large impacts. Alternatively, some of the Earth's potassium could have been sequestered in the core at the time of Earth's formation. The presence of ^{40}K in the core is inferred from recent high pressure analyses, which indicate that potassium may alloy with iron in a strongly temperature-dependent fashion, especially in the presence of S and/or Ni [*Murthy et al.*, 2003; *Lee and Jeanloz*, 2003; *Gessman and Wood*, 2002]. The conditions required for potassium dissolution vary from one model to the other, as well as

the predicted potassium concentration that could be found in the core. However, as mentioned in the first chapter, there remain still strong geochemical arguments against large concentrations of potassium in the core [*e.g.*, *McDonough*, 2004].

Recent high-precision measurements of samarium-neodymium isotopic data for chondritic meteorites suggest that most of the BSE reflects a non-chondritic Sm/Nd ratio; a chondritic BSE for these isotopes could be accounted for if a differentiation event took place within the first 30 million years of the Earth's formation, possibly resulting in a complementary reservoir located at the base of the mantle [*Boyet and Carlson*, 2005]. Arguments for an early-isolated, incompatible-element-bearing reservoir also come from global geochemistry studies on noble gases. It is proposed that a geochemically-distinct layer at the base of the mantle formed during the first $\sim 4500-4400$ Myr (in agreement with Xe systematics) due to a sequence of events that generated a deep layer composed of a late-veneer with solar-like rare gases signature and of basaltic crust [*Tolstikhin and Hofmann*, 2005]. The enriched layer would contain radioactive elements (U, Th, K) in excess of the BSE of 20% [*Tolstikhin and Hofmann*, 2005] to $\sim$ 40% [*Boyet and Carlson*, 2005], leading to 4 to 9 TW additional heat production in the lowermost mantle. The early-formed, enriched layer envisaged in these studies is quite small, of the order of the seismically imaged D$''$ region, and has a very limited mass exchange with the rest of the mantle due to its enrichment in Fe, which would make it compositionally denser than the overlying material. Increased radiative thermal conductivity of perovskite and ringwoodite with pressure [*Badro et al.*, 2004; *Keppler and Smyth*, 2005] and the resulting enhanced radiative heat transfer might also be a mechanism that would result in a long-lived layer at the base of the mantle that has not efficiently participated in producing rocks sampled at the Earth's surface. The early-isolated reservoir could be present at least locally at the base of the mantle, as increased resolution in seismic tomography studies allow for lateral complexity in the lowermost mantle, or could possibly reside in regions of partial melt [e.g., *Williams and Garnero*, 1996; *Russell et al.*, 1998], as a relic from a basal magma ocean [*Labrosse et al.*, 2007]. A chemically heterogeneous layer at the base of the mantle could also be the cause of the ultra-low velocity zone seen in D$''$[*Lay et al.*, 2004]. *Coltice and Ricard* [1999] also proposed a layer that is

enriched in heat producing elements at the base of the mantle that was the result of the separation of subducted oceanic crust that grows over time.

Previous studies of Earth's geodynamo power requirements generally used prescribed heat flux across the CMB or parameterized models for the energetics of the core and the mantle. The present paper calculates the entropy production in the outer core as a function of time based on numerical simulations output for mantle convection. Further, the Earth's magnetic evolution is modeled based on the Ohmic dissipation in the outer core. The energy balance and entropy production in the core are computed as a function of the heat flow and temperature at the CMB at each time step in the numerical simulation, allowing therefore a complete feed-back between the dynamic processes in the core and mantle. As shall be presented in the following sections, coupling the cooling history of the core and the inner core growth model with the thermal history of the mantle, which accounts for temperature-dependent viscosity, internal heating and layering, yields results difficult to predict from parameterized models, as short timescale mantle events, which are not captured by parameterized models, can considerably affect the thermal and magnetic history in the core. In addition, the use of the numerical model allows us to investigate the effects of laterally varying mantle properties.

In the following, I first describe the results from the nominal model (B0) which has no internal heating in the core and no increased concentration of radioactivity in the lowermost mantle, and show why the nominal model falls short in meeting all the required criteria for successful evolution scenarios. Subsequently, I explore the effects on thermal and magnetic history of increasing the initial core temperature, varying the degree of internal heating in the core and varying the degree of internal heating in the mantle. The output of various simulations performed are listed in Table 3.1. The thermal results for the B series models which have varying degrees of internal heating in the core and the C series which have different initial core temperatures were also discussed in *Butler et al.* [2005]. The D series models explore the effects of high concentrations of radioactive internal heat sources in the lowermost 200 km of the mantle, while model H1 is used to explore the effects of high internal heating throughout the mantle. Section 3.5 comprises a brief discussion on the scaling

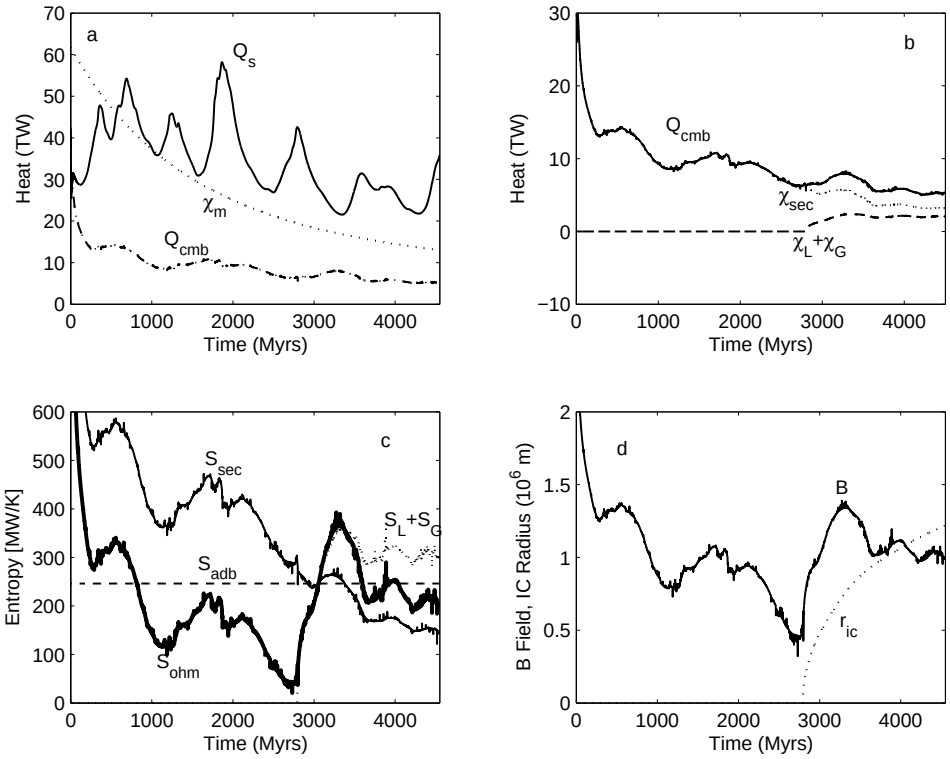

Figure 3.1: Results of nominal model (B0). a) Time variation of the surface heat flow (solid line), internal heating rate in the mantle (dotted line) and heat flow at the CMB (dashed line). b) Time variation of the CMB heat flow (solid line), secular cooling rate of the core (dotted line), and sum of the energy release due to latent heating and gravitational energy release associated with the solidification of the inner core (dashed line). c) Entropy of Ohmic dissipation (thick solid line), of secular cooling (thin solid line), associated with conduction along the core adiabat (dash-dot line) and the sum of the entropy associated with latent heat and gravitational energy release (dotted-line). d) Normalized magnetic field, and the radius of the inner core. (*Costin and Butler*, 2006. *Elsevier* re-print permission, 2009)

of the inner-core growth with time. Most of the results from this chapter have been published in *Costin and Butler* [2006].

3.1 A Model Thermal and Magnetic History

Figure 3.1 shows the results of the nominal run, B0, which assumes 13 TW (final rate) internal heating in the mantle, no internal heating in the core and starts with an initial CMB temperature of 4300 K. The initial azimuthally-averaged radial mantle temperature profile is adiabatic and set so as to be at the solidus temperature of *Boehler* [2000] for the upper mantle. The initial lateral

variations in mantle temperature are taken from a previous convection simulation with a similar effective Rayleigh number. The same initial mantle temperature distribution is used in all of the simulations. Figure 3.1a displays the heat flow at the Earth's surface (solid line), the internal heating rate in the mantle (dotted line) and the heat flow conducted across the CMB (dashed line). The variation in the surface heat flow is strongly time dependent, while the heat flow at the CMB shows only relatively minor short timescale (100 Myr) fluctuations on top of a long-term downward trend. The difference in the variability of the two heat fluxes is due to the much higher viscosity in the lower mantle, as well as the relative proximity of the 660-km endothermic phase transition, which causes much of the short timescale variability in the heat flow at the surface. The final surface heat flow in this case is similar to that for the real Earth of roughly 36 TW, for the mantle derived component [*Pollack et al.*, 1993], but only as a consequence of a mantle avalanche occurring near the end of the simulation.

Because there is no internal heating in the core, secular cooling is the only contribution to the heat flow across CMB before the onset of inner core growth. As can be seen in Figure 3.1b, the secular cooling is quite high, revealing a rapid cooling of the core. As can be noted from Table 3.2, the final CMB temperature for this case is 3505 K, which is low compared with most estimates for this quantity [*e.g., Alfè*, 2007; *Anderson*, 2002; *Boehler*, 2000]. The CMB heat flow exceeds the secular cooling once the inner core starts to form and latent heating and gravitational potential energy release occur. As mentioned earlier, although these are quite small in terms of their contribution to the energy budget of the core, they make the largest contribution to the entropy of Ohmic dissipation over the final 1 Gyr of the simulation, as seen in Figure 3.1c (dotted line) due to their relatively high efficiency factors. The entropy production due to secular cooling (thin solid line) is very large early on, when the core is cooling rapidly, but declines significantly over the course of the calculation. The entropy of Ohmic dissipation (thick solid line) jumps significantly when the inner core begins to form and the contributions of latent heating and gravitational energy release become significant. Table 3.2 lists the quantity Σ_{ent}, which was defined as the ratio of the minimum of $< S_{ohm} + S_{adb} >$ to the average for this quantity over the lifetime of the inner core,

thus giving a measure of the variability of geodynamo power. For this calculation, Σ_{ent} takes on a relatively modest value of 0.54.

It will also be noted that for this simulation, the onset of inner core solidification occurs just before the time when the geodynamo action is about to cease, as S_{sec} drops below S_{adb}. The contribution of $S_G + S_L$ becomes significant just as the secular cooling cannot sustain the adiabatic gradient and therefore makes possible the existence of the geodynamo. However, part of the reason for the dramatic decrease in S_{sec} is the warming of the core due to the effects of inner core solidification. Still, based on the slope of S_{sec} before the onset of inner core solidification, it appears that were the onset of inner core solidification delayed just by a few hundred Myr, there would have been a period without a magnetic field for this case. The magnetic field is normalized by the final value. To ease comparison, I retain this final value of the nominal case and employ it to normalize all subsequent results. Panel 'd' of Figure 3.1 displays the normalized magnetic field, B, and the radius of the inner core as a function of time. The magnitude of the magnetic field displays fluctuations on a large timescale, and jumps abruptly by a factor of three at the time of onset of inner core solidification, which is not desirable, but which cannot be ruled out by palaeomagnetic evidence [e.g., *Macouin et al.*, 2004]. *Smirnov et al.* [2003] showed evidence for an increase in the strength of the Earth's magnetic at 2.5 Gyr which they attribute to the initiation of inner core growth. It can be observed that the secular variation is largely reflecting the temporal variability in the CMB heat flux. This scenario produces a magnetic field throughout geological time, however, continuous generation of the magnetic field is merely coincidentally realized through the onset of the inner core freezing. In addition, an unrealistic final CMB temperature is rendered.

This calculation illustrates some of the challenges mentioned earlier. The most efficient heat sources in generating magnetic fields are those associated with inner core solidification. It is difficult on thermal grounds to have had an inner core throughout the lifetime of the Earth, however, and it is necessary to drive the geodynamo in a purely thermal manner at early times. This implies that if we require a positive entropy of Ohmic dissipation just prior to the formation of the inner core, particularly if we require similar Ohmic dissipation before and after the inner core begins to freeze,

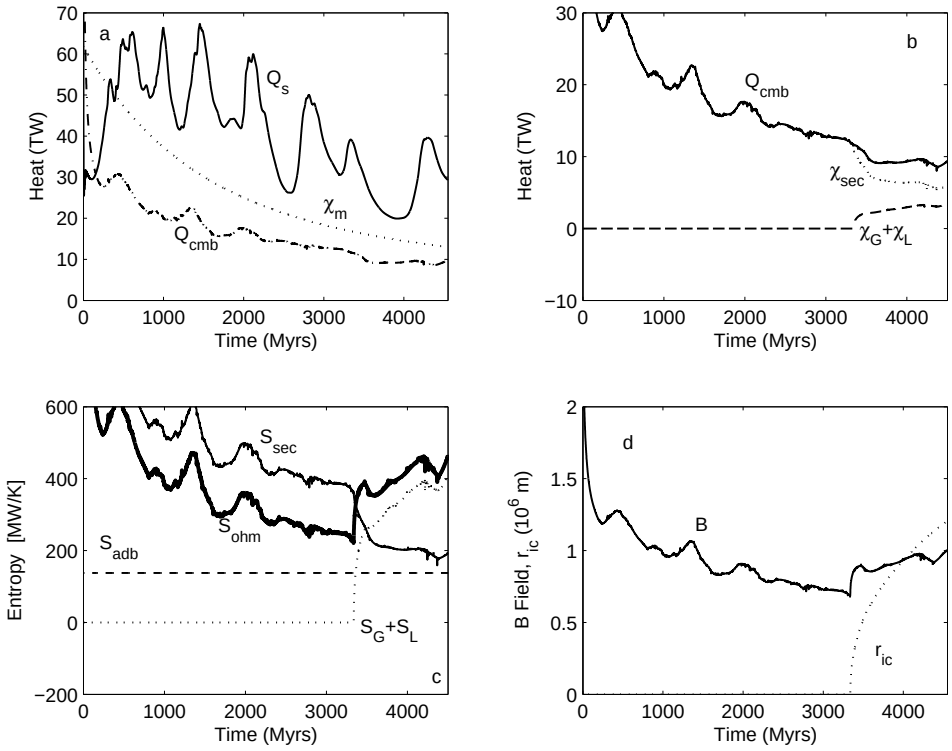

Figure 3.2: From calculation C0 (High initial CMB temperature). a) Mantle heat flows and sources. b) Core heat flows and sources. c) Entropy sources in the core. d) Normalized magnetic field and the inner core radius.

there must be a large degree of either secular cooling or internal heating in the core. If the degree of secular cooling is large, a high initial core temperature is required in order to avoid a final CMB temperature which is too small.

3.2 Effects of Increasing the Initial Core Temperature

Figure 3.2 displays the results of simulation C0, a calculation identical to B0 except that the initial CMB temperature has been increased to 5500 K and the adiabatic parameter, Γ, has been consequently decreased. Such a scenario could be envisaged if a significant amount of the heat due to core differentiation were stored in the core. Most likely, this scenario would also have resulted in a significant degree of partial melting in the lowermost mantle at early stages. The survival of a melt layer at the base of the mantle was recently discussed by *Labrosse et al.* [2007]. As can

be seen in Figure 3.2a, the heat flow at the CMB is significantly higher than for simulation B0 The final CMB heat flow for this calculation is 9.6 TW and the final CMB temperature is 3923 K, within the range for high pressure physics estimates of this quantity. It can also be seen that the final surface heat flow is close to the observed value of 36 TW, although this is partly because of a recent mantle avalanche event. It is possible that the heat flow observed today might also reflect an active state of the mantle. In this calculation, the onset of inner core solidification is accompanied by a very precipitous drop in the secular cooling rate of the core. This is largely due to the fact that the inner core is very young in this model and so solidification occurs at a very rapid rate, resulting in the large magnitudes of the latent heating and gravitational energy release effects. In fact, this case has the fastest growing rate for the inner core and the youngest inner core from all of the simulations performed.

The entropy of secular cooling remains large in this model right up to the time of inner core formation and as a net result, the drop in the secular cooling evens out the jump in entropy production due to latent heating and gravitational energy release and there is a relatively small increase in the entropy of Ohmic dissipation with the onset of inner core solidification. Consequently, the normalized magnetic field displays only a small increase at the time of the onset of the inner core growth, on a slightly decreasing magnetic evolution trend, which lacks a high degree of variability.

In contrast with the B0 case, the mantle avalanches do not trigger a high variability of the magnetic field, due to the high rate of core secular cooling which maintains vigourous convection and stabilizes the geodynamo. The inner core is quite young in this simulation (1221 Myr) and grows fast to achieve the present-day value. It should be noted that the adiabatic gradient used in this calculation is shallower than for B0 because of the higher final core temperature. As a result, the entropy associated with the core adiabat is significantly less, therefore increasing the availability for Ohmic dissipation. Still, comparing the results listed in Table 3.2, the quantity $< S_{ohm} + S_{adb} >$ is significantly larger for simulation C0 than B0, implying a greater probability for an active geodynamo.

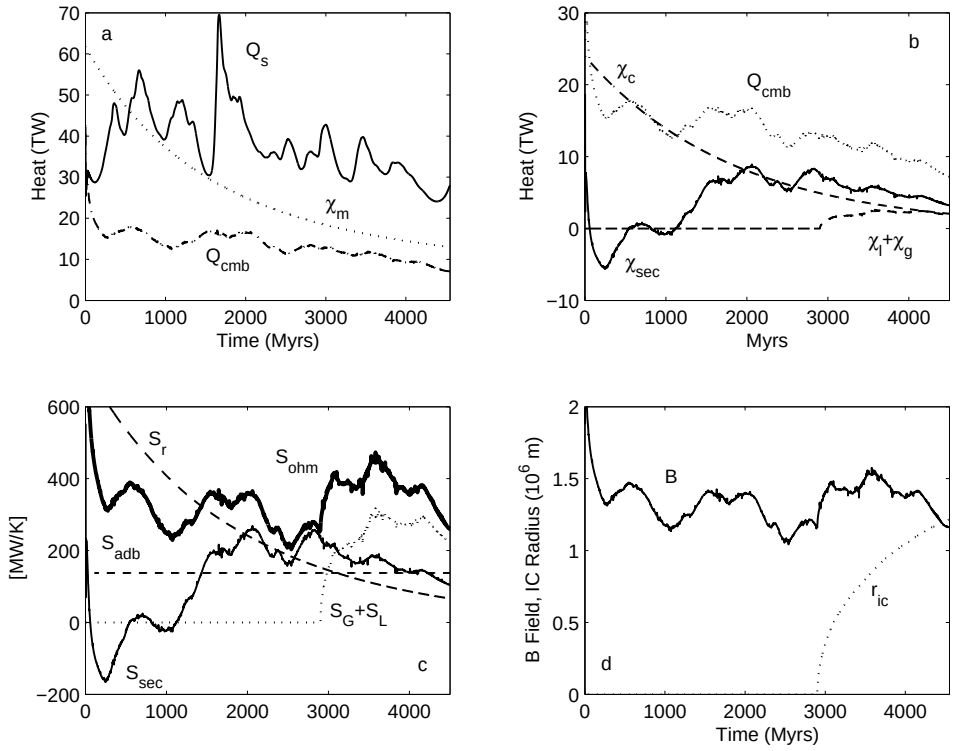

Figure 3.3: Results from calculation B2 (2 TW in the core). a) Mantle heat flows and sources. b) Core heat flows and sources. c) Entropy sources in the core. d) Normalized magnetic field and the inner core radius. (*Costin and Butler*, 2006. *Elsevier* re-print permission, 2009)

3.3 Effects of Internal Heating in the Core

Figure 3.3 displays the results of simulation B2 with 2 TW of internal heating (final rate) in the core, corresponding to 300 ppm potassium. The heat flow at the CMB is quite high, with a final value of 7.1 TW and its evolution over the latter half of the calculation is similar to the case C0 (corresponding to a high initial core temperature and no internal heating in the core). At early times the core is warming up due to the presence of the internal heating sources in the form of ^{40}K. Although there is no CMB heat contributed from the secular cooling term, the radioactive decay produces enough heat to maintain a CMB heat flow around $15-20$ TW. The relatively short half-life of ^{40}K, compared to the age of the Earth, results in fast diminishing of the internal heating and eventually the mantle is able to extract enough heat as to allow the core to start cooling. In

this model, this happens before 1 Gyr of evolution. The increased amount of heat across CMB softens the lower mantle and possibly contributes to the peak event at the surface around 1.6 Gyr. Both the CMB and surface heat flow display some degree of variability, which can be observed from Figure 3.3a The surface heat flow at the end of the simulation is less than 30 TW.

While the core is warming up, there is negative entropy contribution from secular cooling. The entropy associated with internal heating more than makes up for this, however, and as shown in Figure 3.3c, the entropy available for Ohmic dissipation is fairly constant throughout the entire calculation. It will be noted that secular cooling and internal heating power the dynamo with equal efficiency factors. In this case, there is a relatively small increase in the magnetic field at the time of onset of inner core solidification. The average entropy available for Ohmic dissipation over the lifetime of the Earth increases with the degree of internal heating in the core (see Table 3.2), however, all of this increase can be attributed to the change in the entropy required for the adiabatic gradient. If these terms are summed, the total entropy available for Ohmic dissipation and conduction down the adiabat is roughly unchanged with the degree of internal heating in the core. This can be explained by two effects. One effect is that models with high degrees of internal heating have higher core temperatures which decrease the efficiency factors for all of the heat sources and fluxes. The other effect is that as internal heating in the core is increased for models that are otherwise the same, an increasing amount of the heat energy goes into warming the core, decreasing the secular cooling term.

A simulation with a higher initial core temperature and 2 TW of internal heating in the core in the final state (not shown) resulted in a greater degree of core cooling. This indicates that, with an initially hotter core, radioactive internal heating causes a more significant increase in the entropy available for dissipation as can be seen by comparing the results of simulations C0 and C2 in Table 3.2. Model C2 was run with an initial temperature of 5500 K and with 2 TW of internal heating in the core in the final state. The effects of inner core formation for model C2 are not included. For these calculations, even with no energy release from the inner core solidification, and with a significantly higher core temperature, case C2 has significantly higher entropy for Ohmic

dissipation and thermal diffusion than does model C0.

The magnetic field in B2 is present throughout the entire simulation and although it displays some long timescale variability (of the order of several hundred Myr), the amplitude of the fluctuations is less than in the nominal case B0, which makes this case a potentially viable scenario for the magnetic evolution. The final magnitude of the magnetic field is also slightly greater than for case B0 as can be seen in Figure 3.3 (the final value of B is greater than 1). In fact, throughout the entire evolution, the intensity of the magnetic field stays higher than the modern-day magnetic field of the nominal case B0, due the contribution of the internal heating in the core.

In one instance, a long period of high magnetic field intensity (between roughly 1.2 and 2.2 Gyr) is caused by fluctuations in convection in the mantle, whereas as the mantle activity lessens in vigor towards the last 1 Gyr of the simulation, another period of high magnetic field occurs due to the addition of compositional terms in the entropy balance with the onset of inner core freezing. The high intensity periods are separated by low intensity periods, reminiscent, for instance, of the Mesozoic dipole low [e.g., *Tanaka et al.*, 1995]. The interesting feature displayed by the magnetic evolution for this case is that the field intensity fluctuates about an apparent steady trend, which is more likely supported by palaeomagnetic data, in that the paleointensities at earlier times in the Earth's evolution have shown lower or similar values to the Cenozoic data [*e.g.*, *Hale*, 1987; *Prévot et al.*, 1990; *Macouin et al.*, 2004]. An actual comparison with PSV data is hard to include in this analysis, as generally a paleo-secular record spans a short geological time compared to the time scale of the plots which span the entire 4.55 Byr of evolution.

3.4 Effects of High Internal Heating in D″

Figure 3.4 displays the results of calculation D1 with 13 TW (final rate) of internal heating concentrated in the lowermost 200 km of the mantle. This represents an end-member model, where all of the radioactive heating is concentrated in the lowermost mantle which we know is not exactly the case, but it serves to illustrate a number of features of models of this kind. In this case, it was found necessary to decrease the liquidus parameter, Λ, in order to achieve an Earth-like inner core

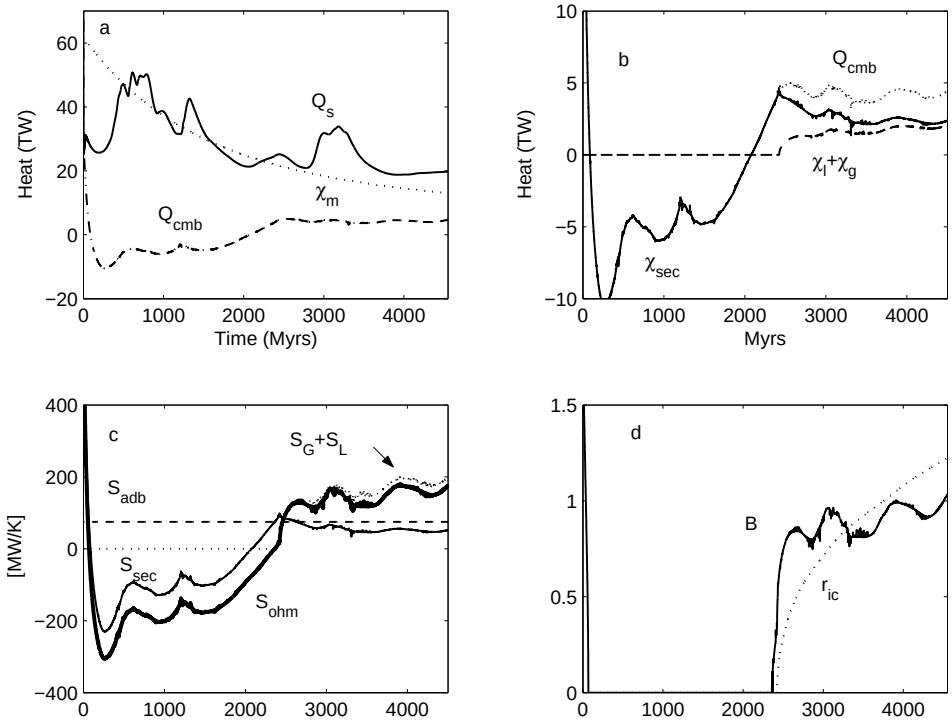

Figure 3.4: Results from calculation D1 (13 TW in D″). a) Mantle heat flows and sources. b) Core heat flows and sources. c) Entropy sources in the core. d) Normalized magnetic field and the inner core radius. (*Costin and Butler*, 2006. *Elsevier* re-print permission, 2009)

size. The value of the slope of the liquidus, dT_L/dP implied herein is 4.4×10^{-9} K/Pa, slightly smaller than high pressure physics estimates for this quantity.

For this scenario, heat is flowing from the mantle into the core for roughly the first half of this simulation due to the extremely high concentration of radioactive elements at the base of the mantle. A direct consequence is a more modest heat flow at the surface, compared to the nominal run B0. The heating of the core can be observed from Figure 3.5 where the CMB temperature for model D1 is increasing during this time. As a result, there cannot be a magnetic field until the radioactive heat sources have diminished to the extent that heat flow at the CMB can reverse direction. In this calculation, this happens at essentially the same time that the inner core begins to form. Therefore, for this case the magnetic history is strongly dependent on the onset and growth of the inner core, which has existed for roughly 2 Gyr. Another consequence of the increasing the

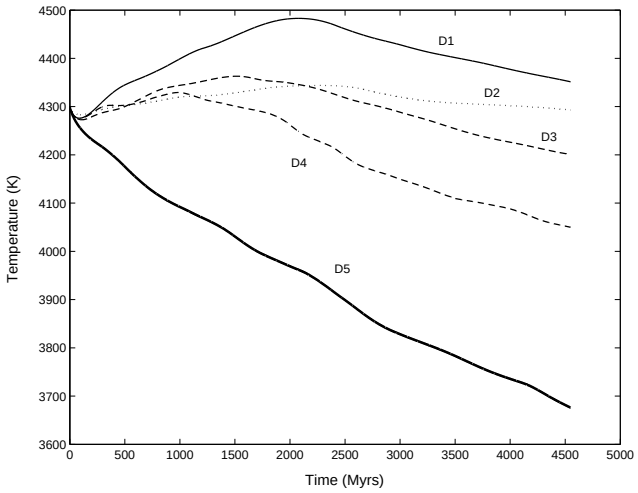

Figure 3.5: The evolution of the temperature at the CMB for the various D series models. (*Costin and Butler*, 2006. *Elsevier* re-print permission, 2009)

heat across CMB is that the surface heat flow also increases for a short period of time, roughly 0.6 Gyr after the inner core starts to freeze. The surface heat flow remains low until the end of the simulation, showing the lower efficiency of heat transport in the mantle, if the lower mantle were to bear all the internal heating inventory.

This scenario might not be plausible for the Earth's case, however, it might explain observations from other terrestrial bodies (*e.g.*, Venus has currently no magnetic field, possibly because its core is not cooling at present, *Nimmo*, 2002). It must be pointed out that in this calculation, the possibility of an initial inner core that melted and then refroze was not considered, and only the effects of a solidifying core during the cooling phase of the simulation were considered. A simulation that includes an initial core that partially melts and refreezes will be discussed below. The data in Table 3.2 show that the final CMB temperature of 4351 K is actually higher than the initial value and the final CMB heat flow is 4.68 TW.

Figure 3.6 displays the geotherm for this calculation after 1000 Myr and 4550 Myr of evolution. At the earlier time, the geotherm has a maximum above the CMB implying that heat is flowing both into the core and into the mantle from this hot lower layer. At 4550 Myr, heat is no longer flowing into the core, but the geotherm still shows a significant degree of curvature in the basal

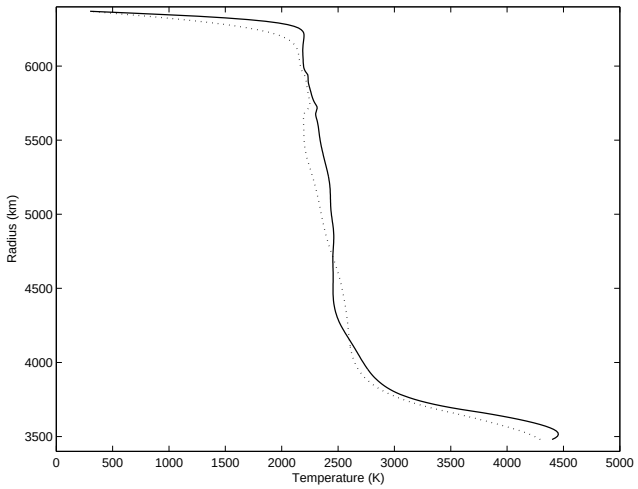

Figure 3.6: The geotherm from calculation D1 at times 1000 (solid line) and 4550 Myr (dotted line). (*Costin and Butler*, 2006. *Elsevier* re-print permission, 2009)

thermal boundary layer which is indicative of the high internal heating rate in that region. This also implies that the heat flow from the lowermost layer into the rest of the mantle is higher than the heat flow at the CMB. In order to arrive at an Earth-like final-sized inner core for this model, both the liquidus parameter and the core adiabat needed to be decreased because of the very small decrease in the temperature of the CMB in the latter half of the calculation.

Figure 3.7 displays the results of calculation D2 with high internal heating in the lowermost 200 km of the mantle over 1/2 of the hemisphere of the core. This simulation is intended to model the effects of laterally heterogeneous internal heating. It must be pointed out that the viscosity in the mantle is allowed to vary only radially and some of the effects of laterally heterogeneous internal heating on mantle heat transport may not be captured in this model. In this calculation, the temperature at the CMB showed very little variation throughout the simulation as can be seen in Figure 3.5. This is the result of heat entering the core on the hot part of the CMB and leaving on the cold part. In addition, the surface heat flow is far less variable than in all other cases described before, as can be seen from Figure 3.7a. The modern-day heat flow at the surface is less than 30 TW, and displays small departures from a slowly decreasing trend for the past 2.5 Gyr.

It was not found possible to achieve a correct-sized inner core by means of any reasonable combination of the parameters T_{L0}, Λ and Γ when a model was started with no initial inner core.

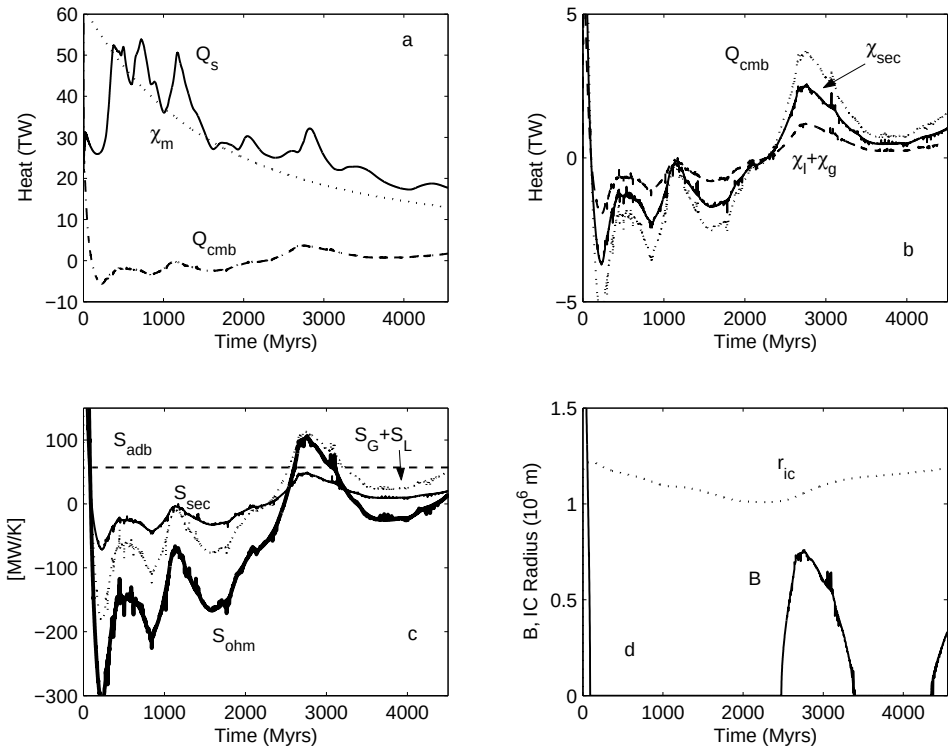

Figure 3.7: Results from calculation D2 (13 TW in D″, hemispheric distribution). a) Mantle heat flows and sources. b) Core heat flows and sources. c) Entropy sources in the core. d) Normalized magnetic field and the inner core radius. (*Costin and Butler*, 2006. *Elsevier* re-print permission, 2009)

Hence, the model was started with a primordial inner core of radius of 1171 km. The hypothesis of an IC that was present from the early stage of accretion, melted as the core heated up and began to re-solidify at a later stage was discussed in other studies [*e.g., Buffett*, 2002]. This assumption is however less likely, on account that the potential energy released by the Earth accretion would have resulted in a hot, entirely liquid core. Such a scenario may however be envisaged for smaller terrestrial bodies.

The thermal history in Figure 3.7 reveals that, except for a very brief initial period of core cooling, heat is flowing from the mantle into the core until roughly 2500 Myr into the simulation. As a result, the inner core is gradually melting during this period and gradually grows over in the latter part of the simulation. During the growth of the inner core phase, there is only a period of roughly 1 Gyr when there is sufficient entropy to maintain both Ohmic dissipation and conduction

down the adiabatic gradient, therefore there is only an episodic, weak, magnetic field throughout the simulation.

It will also be pointed out that *Glatzmaier et al.* [1999] found that geodynamo simulations produce the most Earth-like magnetic fields when the CMB heat flow is close to spatially uniform and *Olson and Christensen* [2002] demonstrated that geodynamo simulations where the magnitude of the spatial variation is greater than the mean value of the heat flow at the CMB, usually fail to produce a magnetic field. As a result, it is possible, given the very large spatial variations in the CMB heat flow in the D2 simulation, that a magnetic field would not have been produced even at times when there is entropy available for Ohmic dissipation and if present, it would have had a very strongly non-dipolar character.

The short-lived magnetic field is reminiscent of the short-lived early Martian magnetic field [*Acuña et al.*, 1999]. In this scenario, the episodic field is driven largely by the compositional terms, in contrast with models for the Martian field which indicate a thermally short-lived magnetic field [*e.g., Breuer and Spohn*, 2006]. Recently, numerical simulations have shown that imposing hemispheric distribution for the CMB heat flow in dynamo models for the Martian core may explain the crustal magnetization variability between the two hemispheres, and may have contributed to the demise of the magnetic field. The Y_1^1 distribution for the temperature anomaly at the Martian CMB could be the result of radial viscosity variations in Mars' mantle, superplumes resulting from destabilization of a thermal boundary layer, or the effect of a large, low-angle impact that swept the Northern hemisphere [*Stanley et al.* 2008]. In our case D2, the degree-1 symmetry of the CMB heat flow is due to the distribution of radioactive sources in the mantle.

The final inner core radius for model D2 is only slightly greater than its initial value, and the CMB temperature is very close to constant throughout this entire simulation. As explained before, part of this is caused by the laterally heterogeneous high internal heating at the base of the mantle. The other factor is that the effects of latent heating/cooling are present throughout this entire simulation which act to increase the effective heat capacity of the core, resulting in reduced variations of the core temperature.

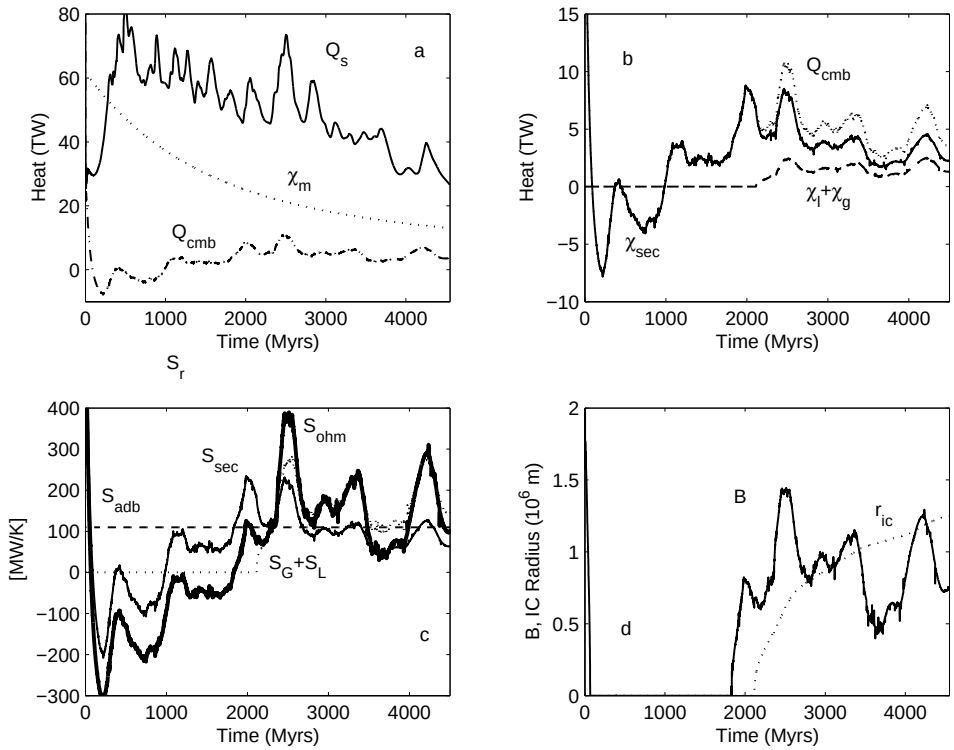

Figure 3.8: Results from calculation D4 (13 TW additional heating in D″). a) Mantle heat flows and sources. b) Core heat flows and sources. c) Entropy sources in the core. d) Normalized magnetic field and the inner core radius. (*Costin and Butler*, 2006. *Elsevier* re-print permission, 2009)

Simulation D3 was run with an identical configuration to model D1 with the exception that the initial viscosity of the mantle was decreased everywhere by a factor of two. As can be noted from Figure 3.5, the temperature of the core increases for a shorter period of time and to a significantly lesser extent than it did in simulation D1. Inspection of the data in Table 3.2 reveals that the inner core in this simulation is roughly 400 Myr older than in simulation D1 and there is entropy available for Ohmic dissipation for roughly 200 Myr longer, due to the increased efficiency by which the mantle can cool off the core.

Figure 3.8 displays the results of simulation D4. This simulation is similar to D1 in that there is now 13 TW of internal heating throughout the mantle as well as a hot layer with 13 TW of internal heating at the base of the mantle as in D1 [*e.g., Lassiter*, 2006; *Boyet and Carlson*, 2005] . In contrast with runs D1 or D3, the CMB temperature increases for a significantly shorter period of

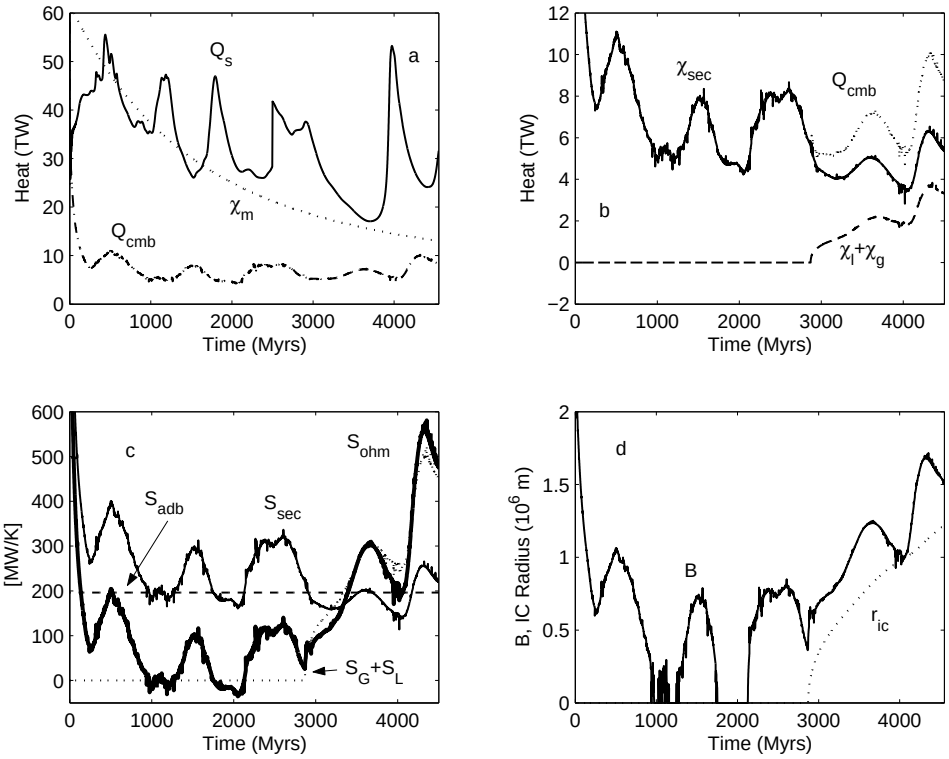

Figure 3.9: Results from calculation D5 (4 TW additional heating in D″). a) Mantle heat flows and sources. b) Core heat flows and sources. c) Entropy sources in the core. d) Normalized magnetic field and the inner core radius. (*Costin and Butler*, 2006. *Elsevier* re-print permission, 2009)

time and thereafter decreases significantly more over the latter part of the simulation. This occurs because the extra heat sources in the mantle act both to increase the convective vigor in the mantle directly and they raise the temperature in the mantle, lowering the viscosity, which further leads to more vigorous mantle convection and efficient transport of heat to the Earth's surface. The heat flow at the surface is quite high for the most of the geological time with a high degree of variability, however displaying a decreasing trend, and reaches about 30 TW at the end of the simulation.

The final CMB temperature in this model is roughly 4000 K, which is close to the assumed value for this quantity. The plot in Figure 3.8b reveals that the heat is flowing from the mantle into the core for roughly the first 1 Gyr of this simulation. There is no entropy available for Ohmic dissipation for almost another 1 Gyr, however, as the CMB heat flow remains quite modest

($\sim$ 5 TW). In this case, the model geodynamo starts and remains active from a time just before the onset of inner core growth until the end of the simulation. The emergence of the magnetic field is occurring at the moment when the secular cooling becomes positive and hence the entropy produced by this term overcomes the entropy of the adiabatic term. A sudden swing in magnetic field intensity is observed once the compositional terms produce entropy due to the IC solidification. There is a significant decrease in intensity around 3.6 Gyr, correlated with fluctuations in mantle convection. Inspection of Figure 3.8d reveals the sensitive response of the magnetic field to the mantle dynamics and the influence of the cooling history at the CMB on the rate of growth of the inner core. Furthermore, the magnetic field is relatively weak in this case since it is almost entirely correlated to the compositional terms which enter the entropy production and there was a only brief period of thermally driven geodynamo prior to IC solidification.

The liquidus temperature in the core is reached after approximately 2 Gyr of evolution, yielding an older inner core, and it can be noted that the rate of growth is not constant, with an apparent faster growth of the inner core at the beginning. A varying regime for the inner core growth, also observed in other simulations, might be responsible for disturbing the hexagonal close-packing of the iron atoms, and possibly contributing to the inner core anisotropy [*e.g., Tromp*, 2001].

In Table 3.2 I also list the results of simulation H1, having the same total degree of radioactive internal heating as simulation D4, but where the internal heating has been uniformly distributed throughout the mantle. It can be seen that the CMB temperature decreases significantly more and the total entropy available for Ohmic dissipation are significantly higher for this case. When the internal heat sources are uniformly distributed throughout the mantle, convection in the mantle is much more efficient, leading to much more rapid core cooling and at no time is the temperature of the lower mantle hotter than the temperature of the core. Simulation H1 does show significant temporal variations in the entropy available for dissipation as can be seen by the value of Σ_{ent} of 0.38.

Figure 3.9 displays the results of simulation D5 with 4 TW of internal heating in the lowermost 200 km of the mantle in the final state and 13 TW distributed throughout the rest of the mantle.

This calculation corresponds to the internal heating generated in the heterogeneous isotopic layer described in *Tolstikhin and Hofmann* [2005]. The heat flow at the surface shows a high variability, with very few distinct, punctuated events, reminiscent of episodic mantle avalanches. However, there is no decreasing trend in the surface heat flow and the final value of the simulation is just over 30 TW.

The heat flows from the core into the mantle throughout the entire time of the simulation and as can be seen in Figure 3.5, the CMB temperature drops by roughly 624 K over the time of the simulation. In this case, although the CMB heat flow remains positive, it does drop to roughly 4 TW at times due to dynamical variations in convection in the mantle. During these CMB heat flow lows, before the onset of inner core growth, there is no entropy available for Ohmic dissipation at times, and the model magnetic field vanishes. The magnetic field displays a high final value and also a higher variability than in the case B2 and even B0, since its generation is related solely to the secular cooling term prior to the inner core freezing, and does not benefit from the more stabilizing regime given by the internal heating in the core. The higher variability is also related to a higher degree of variability in the heat flux at the CMB, undoubtedly due to the increased heat production of the lowermost mantle.

It is worth noting that the degree of variability of the heat fluxes caused by mantle avalanches may be reduced if the simulations are performed in three dimensions [*e.g., Tackley et al.,* 1993]. Nonetheless, some features in the modeled magnetic field are found in the palaeomagnetic database, as for instance lower intensities at the early times [*Macouin et al.*, 2004]. An interesting observation that arises from this simulation is the fact that the apparent re-instatement of the magnetic field, after a period of inactivity, occurs before the onset of inner core crystallization, hence there is no absolute correlation between these two events.

Figure 3.10 displays the results of calculation D6 which has the same configuration of mantle internal heating as simulation D1 (i.e., a basal layer bearing all the 13 TW of internal heating), but the initial CMB temperature has been increased to 5500 K. This scenario resembles probably the closest to the Earth evolution model of *Labrosse et al.* [2007], as it assumes a high initial CMB

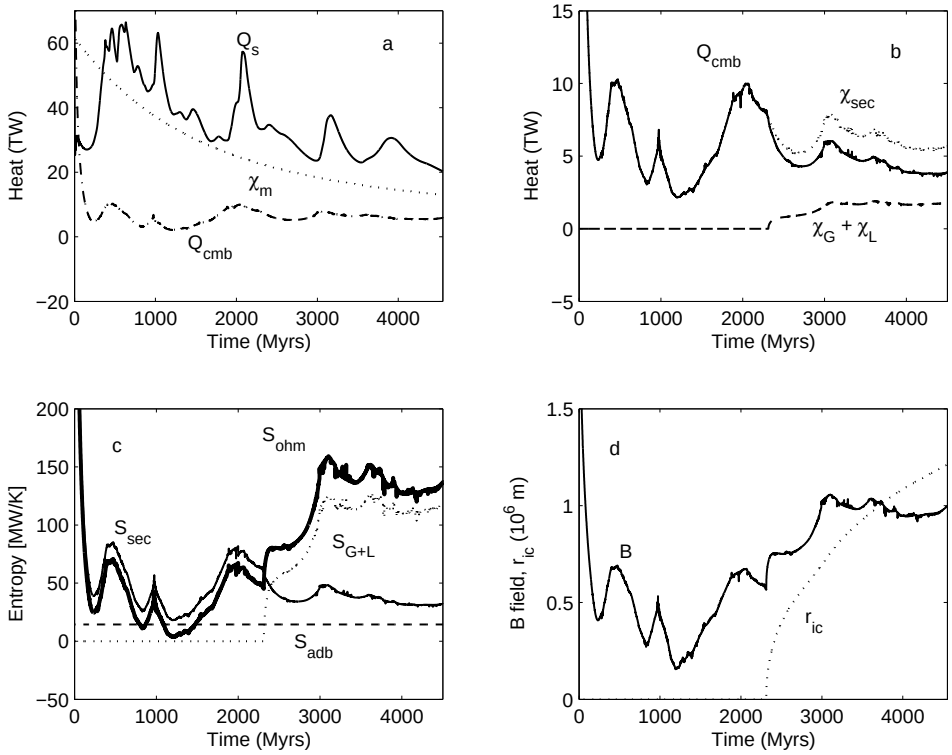

Figure 3.10: Results from calculation D6 (13 TW internal heating concentrated in in D″and high initial CMB temperature). a) Mantle heat flows and sources. b) Core heat flows and sources. c) Entropy sources in the core. d) Normalized magnetic field and the inner core radius.

temperature, consistent with a lower mantle that is entirely liquid, and additionally, it bears internal heating, in agreement with the aforementioned study . However, case D6 does not account for a molten layer, as it does not contain the effects of latent heating caused by the slow solidification of the basal magma layer.

In contrast with model D1, it can be seen that the heat at the CMB is flowing from the core into the mantle at all times and the CMB temperature decreases in this simulation by 409 K. The amount of entropy available for Ohmic dissipation is still very low, however, and the model geodynamo comes very close to vanishing after about 1 Gyr of evolution. However, since all of the internal heating is concentrated at the base of the mantle, the viscosity in the lower mantle decreases, therefore allowing the mantle to cool the core and the intensity of the model magnetic

field starts to increase before the onset of inner core solidification. At the time of inner core inception, there is a second increase in the magnetic field intensity, however. The weak magnetic field present in the first billion years is reminiscent of the lower intensities detected by paleointensity studies in a single crystal [*e.g., Tarduno et al.*, 2006]. These facts can also be seen from the results in Table 3.2, from where it can be noted that both $< S_{ohm} >$ and $< S_{ohm} + S_{abd} >$ are significantly lower than in the B and C series runs and Σ_{ent} has the very low value of 0.13. The entropy required by conduction down the core adiabat is also very low in this calculation as it was necessary to use a very shallow core adiabat in order to achieve the correct-sized final inner core. It will also be noted from the results summarized in Table 2 that the final core temperature is 5091 K, which is significantly higher than estimates of modern core-mantle boundary temperatures.

3.5 Scaling of Inner-Core Growth with Time

The last column in Table 3.2 contains the values for the parameter, α, which is calculated as the best fitting value in a least-squares sense for a model of inner core growth of the form $r = r_{ic}^{p}(\frac{t-t^{in}}{t^{p}-t^{in}})^{\alpha}$ where r_{ic}^{p} and t^{p} are the final inner core radius and time and t^{in} is the time of inner core growth initiation. A value of $\alpha = 0.5$ has been assumed in some previous work [*e.g., Aurnou et al.*, 2003] for the scaling between the inner core radius and time. Inspection of equations (2.62) and (2.63) indicates that the inner core radius in the present model scales like the square root of the difference between the liquidus temperature at the center of the Earth and the adiabatically extrapolated temperature at the CMB. As a result, if the core temperature decreases at a constant rate then α will be 0.5, while if the core secular cooling rate decreases over the lifetime of the inner core, α will be less than 0.5 which is the case in most of the simulations. This might be expected as the temperature difference between the core and mantle decreases with core cooling. There is no systematic variation in the value of α with the control parameters of the simulation, indicating that most of the variation in α is due to fluctuations in the dynamical simulation in the mantle for any particular simulation.

3.6 Discussion

This chapter shows the results from a number of simulations of the Earth's thermal and magnetic evolution with various configurations of internal heating and core initial temperatures. The goal of the study has been to find models of the Earth's thermal evolution for which the final CMB temperature is in the range indicated by high pressure physics studies and the entropy available for Ohmic dissipation is positive throughout the latter 3500 Myr of the simulation. It is also desirable if the entropy available for Ohmic dissipation has not fluctuated too much over the course of a simulation. The nominal simulation, B0, which starts with $T_{cmb} = 4300$ K, with no internal heating in the core and homogeneous internal heating throughout the mantle, produces a magnetic field throughout its history but the final CMB temperature is quite low and the magnetic evolution features a high degree of variability in the magnetic field intensity.

Model B2 with 300 ppm potassium in the core gives the magnetic field with the smallest temporal fluctuations. It also has a final CMB temperature that is within the bounds given by high pressure physics and the initial CMB temperature is at the solidus point for lower mantle materials. This is in general agreement with the results of *Nimmo et al.* [2004] and *Labrosse* [2003]. In these simulations, the effects of increasing internal heating did not substantially increase the entropy available for dissipative processes since a great deal of the heat energy remained in the core and prevented the secular cooling of the core. If convection in the mantle were more efficient, or if the temperature difference between the core and mantle were greater, then internal heating has a greater direct effect in increasing the entropy available for Ohmic dissipation. There is a long standing debate in the geochemical and high pressure physics communities as to whether there can be significant quantities of potassium in the core [*e.g., Chabot and Drake*, 1999; *Murthy et al.*, 2003; *McDonough*, 2004]. If it emerges that it is possible that significant quantities of potassium are sequestered in the core, then internal heating in the core is an attractive scenario.

Various scenarios for layers with high internal heating at the base of the mantle exist. Here only the effects of a layer with a high degree of internal heating in direct contact with the core,

as described in recent global geochemical models have been examined [*Tolstikhin and Hofmann*, 2005; *Boyet and Carlson*, 2005]. Geodynamo simulations have also shown that Earth-like magnetic fields are best produced by models with roughly spatially uniform CMB heat flows which argues that any layer at the base of the mantle with a high degree of radioactive internal heating must be close to spatially homogeneous [*Glatzmaier et al.*, 1999; *Olson and Christensen*, 2002]. Most of the models with high degrees of internal heating at the base of the mantle have heat flowing from the mantle into the core for roughly the first two billion years of the simulation, a situation for which the operation of a geodynamo is clearly impossible. Even simulation D5, with a relatively modest 4 TW of internal heating in the lowermost layer, which did allow for heat flow from the core to the mantle throughout its history showed a magnetic field that vanished at times. A later simulation (not shown in this chapter), containing only 2 TW of present-day additional internal heating in the D″region, has yielded a continuous magnetic field, therefore if the additional internal heating in D″is lower than geochemical models suggest, plausible scenarios may be envisaged. It has been also shown in this analysis that if convection in the mantle is made more efficient by decreasing the viscosity of the mantle or by increasing the degree of internal heating in the mantle or if the initial core temperature is increased, it is possible to increase the degree of core cooling.

Given the very high degree of heating in the very early Earth implied by radioactive decay in the hot basal layer, convection in the mantle would have to have been very efficient at early times in order to cause heat to flow from the core to the mantle. In such a case, a great deal of the Earth's early internal heat energy would be lost to the surface at early times which would make reconciling the Earth's relatively high current surface heat flow [*Pollack et al.*, 1993] with geochemically constrained internal heating rates in the mantle [*e.g., Hart and Zindler*, 1986] more difficult. As such, with very careful tuning of the above mentioned parameters, a model may exist for which gradual cooling of the core occurs over the lifetime of the Earth leading to an old inner core and a magnetic field over the lifetime of the Earth due to a region with high concentrations of radioactivity at the base of the mantle. Such a layer, representing an early-isolated, incompatible-element enriched reservoir is appealing from a geochemical standpoint. However, it requires a

careful tuning in the parameter space, while from a geomagnetic perspective the additional internal heating must be less than the predicted amounts from geochemical models.

Model Name	$\chi_c(t^p)$ (TW)	$\chi_{lm}(t^p)$ (TW)	$\chi_m(t^p)$ (TW)	$T_{cmb}(t(0))$ (K)	Λ (Km^{-2})	Γ	Γ_{mean}	η_0	Cov
B0	0	0	13	4300	1.6526×10^{-10}	1.556	1.20	1	1
B1	1	0	13	4300	1.6526×10^{-10}	1.46	1.17	1	1
B2	2	0	13	4300	1.6526×10^{-10}	1.3915	1.1456	1	1
B4	4	0	13	4300	1.6526×10^{-10}	1.26	1.1	1	1
C0	0	0	13	5500	1.6526×10^{-10}	1.3915	1.1456	1	1
C2	2	0	13	5500	1.6526×10^{-10}	1.3915	1.1456	1	1
D1	0	13	0	4300	9.8798×10^{-11}	1.2759	1.105	1	1
D2	0	13	0	4300	1.6526×10^{-10}	1.2373	1.090	1	0.5
D3	0	13	0	4300	1.2770×10^{-10}	1.3108	1.117	0.5	1
D4	0	13	13	4300	1.6526×10^{-10}	1.3435	1.1288	1	1
D5	0	4	13	4300	1.6526×10^{-10}	1.4838	1.177	1	1
D6	0	13	0	5500	1.6526×10^{-10}	1.1128	1.0441	1	1
H1	0	0	26	4300	1.6526×10^{-10}	1.5617	1.203	1	1

Table 3.1: Run Summary. The symbols $\chi_c(t^p)$, $\chi_{lm}(t^p)$ and $\chi_m(t^p)$ represent the prescribed internal heating rates in the core, lowermost 200 km of the mantle, and mantle at modern times. $T_{cmb}(t(0))$, Λ, Γ, are the initial temperature at the CMB, the core liquidus parameter, adiabat parameter, and mean temperature parameter. η_0 and Cov are the initial viscosity multiplier and the fractional azimuthal coverage of the region of high internal heating in the lowermost mantle.

Model Name	$T_{cmb}(t^p)$ (K)	$< S_{ohm} >$ (MW/K)	$< S_{ohm} + S_{abd} >$ (MW/K)	Σ_{ent}	t_B (Myr)	I.C. Age (Myr)	$r_{ic}(t^p)$ (km)	α
B0	3505	223	479	0.54	4550	1756	1221	0.406
B1	3736	286	466	0.51	4550	1680	1219	0.483
B2	3921	338.4	476	0.67	4550	1647	1216	0.413
B4	4326	355.5	451	0.66	4550	1482	1228	0.437
C0	3923	397.4	535	0.66	4550	1221	1207	0.422
C2	4183	449	586.5	-	0	0	0	-
D1	4351	-11.2	75	0	2259	2127	1224	0.414
D2	4293	-180	-123	0	1206	4550	1188	-
D3	4201	14.2	106	0	2485	2541	1231	0.482
D4	4050	50.8	160.1	0	2779	2435	1253	0.385
D5	3676	153	341	0	3944	1679	1218	0.519
D6	5091	85.6	100	0.13	4550	2234	1213	0.449
H1	3499	241	491	0.38	4550	1977	1245	0.363

Table 3.2: We list the final CMB temperature, $T_{cmb}(t^p)$, the temporal average entropy of Ohmic dissipation $< S_{ohm} >$ and entropy of Ohmic dissipation and conduction down the core adiabat $< S_{ohm} + S_{adb} >$, the ratio of the sum of the minimum entropy of Ohmic dissipation and entropy due to the adiabatic gradient to the temporal average of this quantity over the lifetime of the inner core, Σ_{ent}, the total time for which the entropy of Ohmic dissipation is positive, t_B, the age of the inner core, the final radius of the inner core, $r_{ic}(t^p)$ and the best-fitting scaling exponent between inner-core growth and time, α.

Chapter 4

Stagnant Basal Layer in D″: Implications for the Thermal History of the Core and Geodynamo Energetics

Our understanding of the lowermost region of the mantle, located in direct contact with the core, is changing. The old paradigm of a sharp transition between the fluid metallic core and the silicate mantle is challenged by increasing evidence for chemical reactions between the fluid iron and the silicates, causing a compositionally-distinct, iron-enriched layer [*Mao et al.*, 2006; *Mao et al.*, 2005; *Kavner and Walker*, 2006; *Anderson*, 2005], which could be responsible for the anomalous velocities detected above the CMB (Figure 4.1).

As described in Chapter 1, the lowermost part of the mantle may be enriched in iron-bearing minerals. The presence of several Fe-bearing compounds such as $FeSiO_3$ and FeO in D″, in larger quantities than the rest of the mantle may increase the local density of the mantle material and may have implications from the standpoint of heat transport. Advances in the study of spin pairing in Fe atoms in Fe-bearing minerals, such as (Mg,Fe)$Si0_3$ perovskite and (Mg,Fe)O ferropericlase, appear to be relevant at pressures and temperatures corresponding to D″. Several studies [*e.g., Badro et al.*, 2003, 2004] have shown that the documented low spin state in Fe atoms increases the transparency of minerals in the red and infrared region, therefore an increase in the radiative and conductive properties of minerals is likely to occur at 120 GPa . However, other studies indicate that the low-spin (Mg, Fe)O will exhibit lower radiative thermal conductivity than the high-spin (Mg, Fe)O [*e.g., Goncharov et al.*, 2006; *Lin and Tsuchiya*, 2008]. Changes induced by a high-spin to low-spin transition in Fe-bearing minerals may also affect other physical properties, such

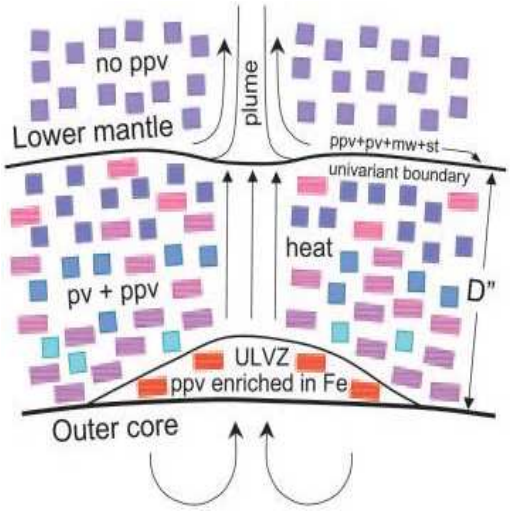

Figure 4.1: Schematic cross-section of the D″region, with iron enrichment in mantle silicates (from *Mao et al.*, 2004).

as elastic moduli, at depths where spin transitions occur and may be responsible for seismological anomalies in D″ [*e.g., Speziale et al.*, 2005]. Increases in the density and the incompressibility of the lower-mantle minerals, including ferropericlase, silicate perovskite, and possibly in post-perovskite, at lower-mantle pressures are reported by *Lin and Tsuchiya* [2008], who also indicate a reduction in sound velocities within the spin transition. In contrast, preliminary results of *Masters* [2008] conclude that the effect on elasticity of the spin crossover at high temperatures must be much less than that observed at low temperatures, and therefore the speed of sound waves is not significantly affected.

The notion of a dense, chemically-distinct layer in D″ has been suggested in the past. Previous theories for its origin include a relic layer from core formation or continuous deep slab subduction [*e.g., Hansen and Yuen*, 1988], a very dense D″ as the result of iron enrichment [*e.g., Anderson*, 2005], and an isolated, 7% denser layer roughly corresponding to D″, composed of chondrite-like material and basaltic crust [*Tolstikhin and Hofmann*, 2005; *Tolstikhin et al.*, 2006], as described in the Chapter 1.

Geodynamical simulations of *Christensen and Hofmann* [1994], *Tackley* [1998], *Nakagawa and Tackley* [2005] and *McNammara and Zhong* [2004] have suggested that dense, subducted MORB

crust is accumulating in chemically distinct piles in the D″region at the bottom of the mantle. These studies suggest that accumulation of dense MORB material at the bottom of the mantle could be responsible for the strong seismic velocity heterogeneities detected in the lowermost 200 km of the mantle and could explain the large low shear velocity provinces (LLSVP) regions (such as underneath Africa), which appear to be dense and chemically distinct from the surrounding mantle [*Lay and Garnero*, 2004].

Moreover, the review by *Jellinek and Manga* [2004], based on laboratory experiments and theoretical scalings, brings evidence that the source region for deep mantle plumes is partly composed of dense, low-viscosity material. Additionally, they show that the deformation of the dense material originating at the base of the mantle and subsequent entrainment into plumes, can stabilize the positions of plumes for hundreds of millions of years, and ultimately can explain the fixity of hot spots.

Montague and Kellog [2000] numerically investigated the implications on lower mantle dynamics of a dense, low viscosity, layer located in the lower mantle. They found that increased thermal diffusivity in D″, which simulates metal enrichment in this region, enhanced the heat conduction and suppressed internal convection within D″. They concluded that for a buoyancy number (i.e., the ratio of chemical to thermal buoyancy) in excess of 0.6, a chemical layer may remain stable for long periods of time. *Naliboff and Kelogg* [2007] explored the mantle entrainment of a basal mantle layer characterized by variations in thermal conductivity and viscosity, as suggested by the experiments of *Badro et al.* [2003, 2004]. The authors found that varying these physical properties of the lowermost mantle alone are not sufficient to preserve a long-lived, isolated, geochemical mantle reservoir and that density contrasts may be required to avoid mantle mixing.

The experimental studies of *Davaille et al.* [2003] have shown that for a Buoyancy number B in excess of 0.4, a dense layer may persist at the base of the mantle for all of geological time, without mantle entrainment. In addition, convection would not occur in such a layer, if the $Ra < Ra_{crit}$ ($\sim$ 1000). This translates to a density contrast in excess of 5%, for a lower mantle layer (*i.e.*, D″), assuming a value for the thermal expansion coefficient of 3×10^{-5} K^{-1} [*Davaille et al.*, 2003],

and a temperature drop in the stratified layer around 1000 K. These scalings apply to a scenario where the viscosity in the lower layer is one order of magnitude lower. The experimental studies of *Jaupart et al.* [2006], have taken into account a viscosity ratio 1, *i.e.*, there is no significant viscosity variation between the layer and the overlying material. They also find that the critical B number for which the layer remains stratified is around 0.4, whereas $Ra_{crit} \sim 1000$. For the cases with the above specified parameters, there is no significant flow in the layer, which remains stably stratified. Additionally, these analyses pertain to a ratio D/d for the thicknesses of the two regions equal to 19, which is in the range of a stagnant layer in D″, assuming D = 2900 km and d = 200 km.

The accumulation mechanisms or the extent of a reaction layer between core and mantle resulting in iron enrichment in D″, remain poorly constrained. Hence, quantifying its importance for planetary dynamics is a challenging task [*Buffett*, 2007]. Moreover, geochemical models have shown that if the molten outer core is in chemical equilibrium with the mantle, FeO ferropericlase could be significantly depleted at the core-mantle boundary [*Ozawa et al.*, 2008]. However, the depleted layer would be extremely thin, in the order of centimeters to meters, due to the very low Fe-Mg interdiffusion coefficients in minerals found at the pressures of the lowermost mantle [*Holzapfel et al.*, 2005].

A compositionally-distinct, insulating layer may be present not in the mantle side, but in the outermost core. Its existence has been suggested from analytical models, required to dynamically stabilize the chemical heterogeneity in the outer core [*Braginsky*, 1991; *Lister and Buffett*, 1998]. To date, several studies based on the multiple reflections of the transmitted P-wave phases originating in the S-waves that graze the core (*i.e.*, SmKS phases) have suggested the presence of a thin layer at the top of the core, which exhibits low P-wave velocities [*e.g., Eaton and Kendall*, 2006; *Tanaka*, 2007]. *Eaton and Kendall* [2006] supported this possibility based on their analysis of an anomaly in the S4KS/S3KS amplitude ratios, which do not fit the PREM models for the outermost 150 km of the core. The low P-wave velocity layer is interpreted as a stably stratified layer at the top of the core. The thickness of the layer in the models of *Tanaka* [2007] ranges from 90 to 140 km.

Helffrich and Kaneshima [2004] demonstrated that, for a plausible range of Fe-O-S compositions, a low-density layer at the top of the core could also exist as one of two immiscible fluid phases, but these authors were not able to detect any evidence for such a layer from the analysis of P4KP and PcP waveforms.

Together with a density increase due to compositional changes in mantle minerals found in the core proximity, the increased translucence to the infrared radiation might suggest non-convective layers, although this issue is still debated. It is likely then that in the denser, iron enriched layer, the stabilizing chemical density anomaly prevails over the destabilizing thermal density anomaly to yield a basal stagnant layer [*Davaille et al.*, 2003; *Williams*, 1998]. If convecting, the Nu number may be small enough that it is still a good insulator.

In this contribution, I investigate the effects of a chemically-distinct layer, which is thermally resistive to the core heat flow. I assume that the lowermost mantle heterogeneities (corresponding to D″), inferred from strong seismic velocity anomalies [*e.g., Garnero and Helmberger*, 1995; *van der Hilst et al.*, 2007], may at least partially be due to a compositionally distinct layer. The compositional effect may be attributed to an (1) iron enrichment of the post-perovskite and ferropericlase minerals, due to core-mantle interactions or to a relic layer from core formation [*e.g., Mao et al.*, 2006; *Auzende et al.*, 2008]; (2) the spin crossover of iron atoms which can significantly change the physical properties of the minerals [*e.g., Lin et al.*, 2005; *Lin and Tsuchiya*, 2008]; (3) deep subduction of MORB material [*e.g., Lay and Garnero*, 2004]; or (4) due to an early isolated geochemical reservoir, enriched in incompatible elements [*e.g., Tolstikhin et al*, 2006].

The insulating effect of the layer on the core can be estimated by calculating Bi (2.31). Assuming a thickness of the lid of 200 km (roughly corresponding to D″), a thickness of 2260 km for the fluid outer core, and the thermal conductivities indicated in Table 2.2 for the lower mantle and the liquid core, the calculated $Bi = 3.77$. Conversely, if the insulating layer were to reside in the outermost core, the same insulating effect would be realized by a 420 km-thick layer. The thickness of the core layer was obtained estimating a thermal conductivity $k_{strat} = 25$ W m^{-1} K^{-1}. This value was assumed to be higher than the lower mantle conductivity, but less than the core conductivity, as

such a layer may be formed by stratification due to accumulation of lighter components expelled at the ICB [*e.g., Lister and Buffett*, 1998].

As mentioned earlier, the existence of a stably stratified layer was suggested from seismological observations, however the extent of such a layer was estimated to be at at most 140-150 km in the outermost core [*e.g., Eaton and Kendall*, 2006; *Tanaka*, 2007]. The existence of a 420 km-thick layer is highly unlikely. Such a layer, bearing a density contrast with the underlying fluid would be easily detected from seismic imaging, as it is above the resolution threshold for seismic data, and the misfit obtained from slowness models would be hard to overlook.

On the other side, strong evidence of such a layer would be inferred from the secular variation (SV) of the magnetic field. For instance, the classic paper by *Whaler* [1980], suggests that upwelings (or downwellings) of the liquid from deep inside the core can be measured at points of maximum (or minimum) of $\mathbf{B}_r$, the radial component of magnetic field (measured at the surface and downward continued to the CMB). If the outermost last 420 km of the core would not be convecting, the SV would not show any extrema in the radial component of the magnetic field projected onto the core surface. However, SV shows variations in upwellings and downwellings, although surprisingly small [*Gubbins*, 1982], which cannot rule out a stratified layer of 100 km [*Whaler*, 1980]. Since there is evidence of the variation in $\mathbf{B}_r$ at the core surface, it follows that it is not screened by a 420 km-thick layer. I also speculate that a 420 km-thick layer would completely filter out the secular 'acceleration' (second derivative of magnetic field), hence geomagnetic 'jerks' would not be observable at the surface.

Additionally, numerical dynamos suggest that some distinctive features in the core field might develop in the stratified layer through interactions with the motions of the underlying convective fluid [*Zhang and Roberts*, 2000], which would probably map in the westward drift.

The dense layer in the lowermost mantle may be stabilized against the overlying convecting mantle as a result of the increased density due to compositional changes. The increased density in the layer may be suggested by the iron enrichment of the lowermost mantle, which can give a density increase up to 20% [*Mao et al.*, 2004], or due to an isolated geochemical reservoir which

require a 7% density increase [*Tolstikhin and Hofmann*, 2005]. The Buoyancy number for a 200 km-thick layer, for a density contrast of 5%, calculated from (2.79) is around 2, therefore, a density contrast in the lower mantle of 5% is sufficient to maintain the layer virtually un-entrained in the overlying mantle flow. In addition, even though that for a lower B number (which can arise if the value of the thermal expansion coefficient α_L is higher than 10^{-5} K^{-1}), the interface between the mantle and the layer may develop in domes and denser piles, locally, but the strong chemical stratification may persist [*e.g., Davaille et al.*, 2003]. If the denser piles still preserve a low spatial frequency heterogeneity, the CMB heat flow may be only locally affected, and the effects on core thermal history may be still well approximated by a continuous layer. As it will be shown in Section 4.1, convection in a stagnant 200 km-thick layer in D″may not be occuring, therefore the denser layer is also acting as a thermal insulator. This has significant implications for the thermal history of the D″region and the evolution of the Earth's core. These effects are the main focus of the present chapter.

Chapter 4 is outlined as follows: in Section 4.1, I describe the implementation of a stagnant layer in a numerical model for mantle convection. In Section 4.2, I show the core thermal histories for various internal heating scenarios in the basal mantle layer and include an analysis of the inferred thermal parameters of the core and how they compare with other work. Implications for the core thermal and magnetic evolution due to the presence of a stagnant layer are discussed in Section 4.2. Further, I analyze scenarios for which a stagnant layer becomes entrained in mantle convection, roughly after 2 Gyr of evolution. The thermal and magnetic effects for cases with a transition from conductive to convective regimes are described in Section 4.4.

4.1 Stagnant Layer Model

The model couples a finite difference 2D axi-symmetric spherical model for mantle convection [*Butler and Peltier*, 2000, and references therein], with parameterized energy conservation and entropy production equations for the core [*Butler et al.*, 2005; *Costin and Butler*, 2006]. The fully dynamical mantle model allows for a thermal history closer to the real Earth's than the

parameterized models. It accounts for effects due to mineral phase changes, temperature-dependent viscosity and heterogeneous distribution of radioactive sources. However, the model does not include the effects of plates and continents.

A 200-km theoretical layer is designed between the core and the mantle, to model a reaction layer which may be stabilized against mantle overturn. The extent of the designed layer is similar with the distinct, deep, 'DDP' geochemical reservoir of *Toltstikhin and Hofmann* [2005], obtained from a global mass balance for Nd isotopes. They assume that the long-lived reservoir, 7% denser than the rest of the mantle, which has not been entrained in mantle flow, resides in the mantle's D″region. Other numerical studies have considered similar models for a chemically-distinct layer at the CMB. *Montague and Kellogg* [2000] assume a 100 to 300 km thick boundary layer, as a starting point for their analysis performed to illustrate the consequences of a dense, low-viscosity layer which simulates metal-enrichment at the base of the mantle; the majority of their models, however, assume a thickness of the boundary layer of 200 km. The choice of the layer extent is also consistent with the analysis of *Lassiter* [2006], who proposes a thermally-conductive layer above the core, based on CMB heat flow estimates required to maintain the magnetic field inside the core. The studies of *Lassiter* [2006] and *Toltstikhin and Hofmann* [2005] also require enhancement in radioactive elements in the deep layer.

I assume that the density of the layer is increased by at least 5% with respect to the overlying material, due to iron enrichment. The initial temperature drop in the layer is $\delta T = 1300$ K, reflecting the temperature difference between the mantle and the core, when the upper mantle temperatures are extrapolated down the mantle adiabat in a single convecting layer and the temperatures on the core side are extrapolated from the melting temperature of iron at the inner core boundary [*Williams*, 1998]. The nature of the heat transport in the layer is controlled by the value of the Ra number (see also (2.28)),

$$Ra = \frac{C_{pL}\alpha_L g\, {\rho_L}^2\, \delta T\, h^3}{k_L \eta}\,. \tag{4.1}$$

Using $h = 200$ km for the thickness, $\eta = 10^{22}$ Pa s for viscosity, $g = 10$ m s^{-2} for gravitational acceleration, $\rho_L = 5775$ Kg m^{-3} for the density in the layer, $C_p = 1256$ J kg^{-1} K^{-1}, $\alpha = 10^{-5}$

K^{-1}, $k = 12$ W m^{-1} K^{-1}, $\eta = 10^{22}$ Pa s for heat capacity, coefficient of thermal expansion, thermal conductivity, and dynamic viscosity respectively (Stacey, 1992), yields $Ra = 363.2$, which is lower than the critical Ra for convection onset.

As shown earlier, the possibility of increased thermal conductivity in the lowermost mantle may arise due to the increased translucence to infrared radiation of iron-bearing minerals [*e.g., Badro*, 2003, 2004]. However, since there is no unanimous consensus on the effect of the high-spin low-spin transition on thermal conductivity [*e.g., Goncharov*, 2004], the value for the thermal conductivity, k_L, used to compute the Ra number, is taken to be consistent with the lower mantle conductivity models [*Stacey*, 1992]. Studies that have used increased thermal conductivity at the base of the mantle include those of *Lassiter* [2006], who uses a conduction-dominated 200-km thick layer at the CMB to constrain the CMB heat flow from geochemical and geodynamo perspectives, *Naliboff and Kellogg* [2007], and *Matyska and Yuen* [2005] who also use increased thermal conductivity (due to the radiative term) in the lowermost mantle, motivated by the Fe^{2+} spin transition effects in oxides and silicates [*Badro et al.*, 2004].

If the entire layer is 20% denser than the overlying mantle (*i.e.*, $\rho = 6600$ Kg m^{-3}), as suggested by post-perovskite iron enrichment in the study of *Mao et al.* [2004], the estimated Ra becomes marginally critical. However such a density increase in a 200-km thick layer is less likely, as this would affect the Earth's moment of inertia. If the value of viscosity in the layer is reduced by a few orders of magnitude, as may occur if melt pockets are present [*e.g., Lay et al.*, 2004], or due to the temperature effect on viscosity, the Ra number (for a 5% denser layer) is greater than the critical value and thus convection would likely occur in the layer. However, the Nusselt number, Nu, (describing the ratio between convected and conducted heat flow rate), which can be calculated from [*Turcotte and Schubert*, 2002],

$$Nu = 1.04 \left(\frac{Ra}{Ra_{cr}} \right)^{1/3}, \tag{4.2}$$

is only 1.84, showing that conductive and convective fluxes are of the same order of magnitude in the layer. The fact that the Nu number is not much higher than unity is due to the fact that the layer is thin and thus convection in the layer is not very vigorous. In addition, the thermal

conductivity may be higher than the value assumed in these estimates, which would further reduce the Ra number and thus the Nu value would be closer to unity. Decreasing the viscosity in the layer by four orders of magnitude, would yield $Nu = 18.38$, indicating that vigorous convection may take place if the dense layer is also molten, as suggested by *Labrosse et al.* [2007].

In this study, I limit my attention to the case where the layer is sub-critical and remains virtually un-entrained in the mantle flow over the Earth's evolution. I study several scenarios where the stagnant layer bears internal heating ($\mathcal{H}$) in excess of the mantle background, possibly due to the presence of an early-differentiated, incompatible- and radioactive-element enriched reservoir residing at the base of the mantle [*e.g., Tolstikhin and Hofmann*, 2005; *Boyet and Carlson*, 2005; *Tolstikhin et al.*, 2006; *Lassiter*, 2006; *Lubetskaya and Korenaga*, 2007]. Hence, a time-decaying radioactive source composed of U, Th and K isotopes, with ratios 1/4/10,000 [*Hart and Zindler*, 1986] and consistent with the isotopic ratio assumed for the rest of the mantle is assumed for the scenarios that assume additional internal heating sources in the layer.

The simulations performed investigate various scenarios of internal heating in the layer, from a depleted basal layer up to 4 TW of modern-day internal heating. As shown in the previous chapter, additional heating in excess of 4 TW (final rate) prevents a continuous generation of magnetic field in the core, even for a mobile basal layer, therefore I did not include in my analyses cases with concentrations of radioactive sources which would lead to internal heating in excess of 4 TW (final rate). I also study the case with a final rate of $\mathcal{H} \sim 0.5$ TW in the basal 200-km thick layer, which represents the same degree of radioactive heating in the layer and the mantle above, leading to 13 TW final rate of radioactive heating from the entire mantle.

The layer is integrated in the 2D axi-symmetric model for mantle convection; for this, I solve numerically the time-dependent heat conduction equation with internal heating ($\mathcal{H}$) in a 2D axi-symmetric spherical shell,

$$\mathcal{M} C_p \frac{dT}{dt} = k\nabla^2 T + \mathcal{H}\,, \tag{4.3}$$

where $\mathcal{M}$, C_p, T, $\mathcal{H}$, and k are the mass, specific heat, temperature, internal heat production and thermal conductivity, respectively. The initial condition for temperature distribution in the

stagnant layer is taken as the steady-state solution of (4.3),

$$T(r) = -\frac{\mathcal{H}}{6k} r^2 + C_1 \frac{1}{r} + C_2 \,, \tag{4.4}$$

where r is the radius of the spherical sector representing the layer. The integration constants C_1 and C_2 are computed separately for each case of internal heating, from the initial temperatures 4.55 Gyr ago, assuming 4300 K at the CMB, which represents the mantle solidus, and 3000 K at the upper boundary of the layer.

The layer is incorporated into the numerical model for mantle convection by requiring continuity of the heat flow and temperature at the core and overlying mantle interfaces. The mechanical boundary conditions at the layer/mantle and mantle/surface interfaces are free-slip. This implies that there is no mechanical deformation in the layer, and there is no viscous coupling with the overlying mantle. This assumption is not strictly correct, and entrainment of some quantity of dense material in mantle is undoubtedly unavoidable, unless a thin, molted layer may separate the two regions. However, it is possible that the layer would not disappear entirely over the Earth's age and to first order, it would have the same effect on core evolution, even though thinning of the layer may occur regionally. Lateral variations in the temperature field in the layer are due to the continuity of temperature and heat flow across the upper boundary, where lateral variations occur owing to the 2D axi-symmetric mantle flow. The temperature at the base of the layer is the CMB temperature, which is laterally uniform, but is variable in time, depending on the mantle and core evolutions.

The behavior and magnetic implications of a $\sim$ 2 % denser basal layer of subducted oceanic crust, or of primordial origin, mechanically coupled with the overlying mantle, was addressed by *Nakagawa and Tackley* [2004], [2005]. In these studies, mechanical movements occur in the denser layer which lead to de-stabilizing the chemically-dense material, forming thermo-chemical piles, often swept under upwelling regions. In contrast, I assume a 5% density contrast due to enrichment with iron, possibly from combined effects or enrichment in core material [*e.g., Buffett et al.*, 2000] and a relic layer due to a primordial layering at the time of core formation. For this value, the Buoyancy number is roughly 2 and the layer is stagnant, therefore I make the assumption that

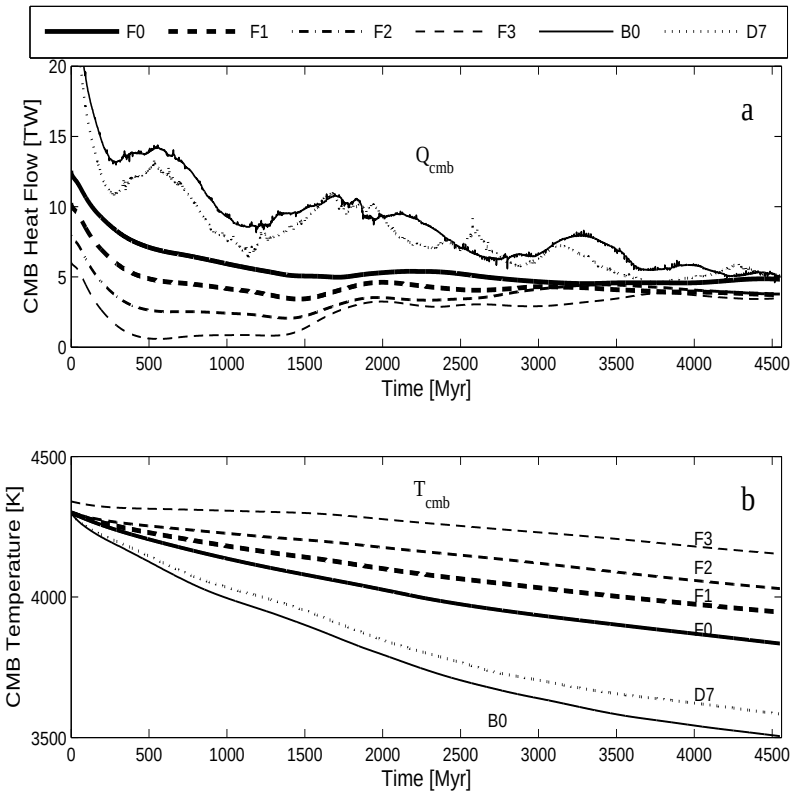

Figure 4.2: Time evolution of the heat flow (a) and the temperature at the CMB (b) for model runs indicated (see Table 4.1).

there is no exchange of material with the overlying mantle.

The model represents a starting point for a suite of future models that can be developed and refined which may include lateral variability of iron content of the silicates as a result of incomplete chemical mixing between the core material and the mantle silicates. Nonetheless, the effects of the dense, conductive layer on the core dynamics will be preserved and similar trends are likely to be observed in future models.

4.2 Core Evolution With a Stagnant Layer in D″

Simulation settings and results are summarized in Tables 4.1 and 4.2. The time evolution of the CMB heat flow, temperature, inner core radius and magnetic field are plotted in Figures 4.2 and 4.3. I show the results for a purely thermally conductive layer in D″, for which B has an approximate

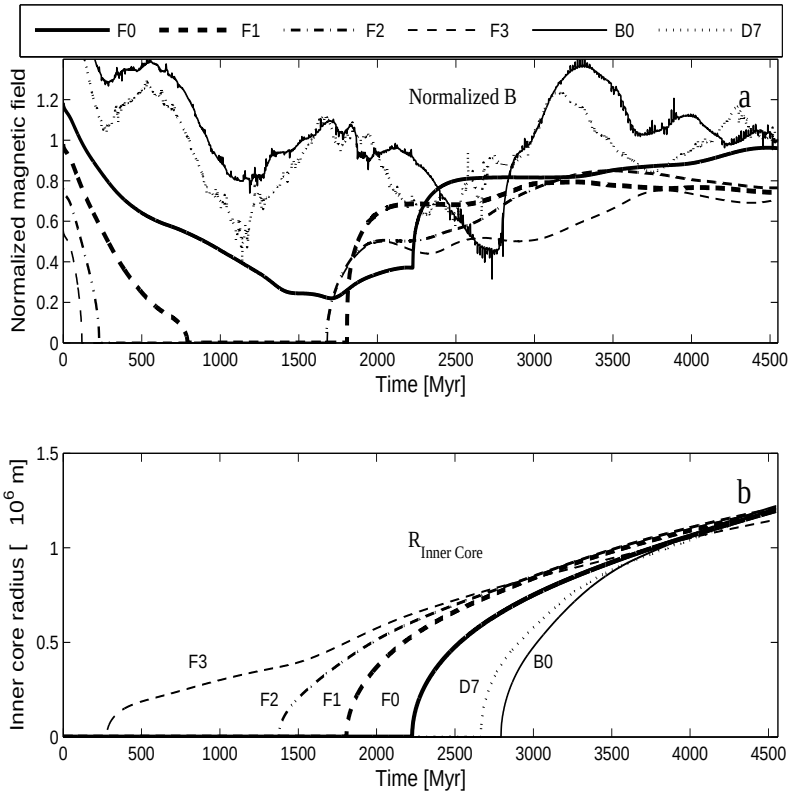

Figure 4.3: Time evolution of the modeled magnetic field (a) and growth of the inner core (b) for model runs indicated (see Table 4.1).

value of 2 and Bi is 3.77 (F cases). I compare these results with earlier results of 'whole-mantle' convection models, for which practically $B \rightarrow 0$ and $Bi \rightarrow \infty$ (D cases, investigated in *Costin and Butler*, 2006). The nominal case, B0, consists of whole-mantle convection, where there is no stagnant layer and corresponds to 13 TW final rate internal heating, distributed throughout the entire mantle.

In the absence of convection in D$''$(F series models), the amount of heat removed from the core decreases significantly compared with the D series models, and becomes even lower for the cases with additional heating in the layer, whereas internal heating in a mobile D$''$ has the effect of lowering the viscosity in the lowermost mantle and therefore the mantle can remove heat more efficiently (Table 4.1 and Figure 4.2a). The CMB temperatures at the end of the simulations increase consistently from 3500 K in the nominal run (B0) up to, and exceeding, 4000 K (Figure 4.2b). This latter value agrees with estimates of CMB temperatures resulting from *ab initio* calculations of

iron alloy melting points [*Alfè et al.*, 2007]. A high CMB temperature is also desirable from the standpoint of lighter element content in the fluid outer core. A much lower temperature would yield contamination of the core with light elements such as O and Si in excess of the known weight percentage [*Ozawa and Hirose*, 2006]. As the internal heating is increased in the layer, the cooling rate in the core decreases to the point where it reaches marginal values for thermal stratification [*Gubbins et al.*, 2004].

An important consequence of the slow rate of cooling in the core is the decrease in the calculated adiabatic gradient required to solidify an inner core to the present-day size, which in-turn affects the amount of time necessary for this process. The estimated age for the inner core increases dramatically over the range of parameters studied (Figure 4.3b). Additional heating in the layer with modern rates of 3-4 TW (F3 and F4) yield models for which the inner core has essentially the same age as the Earth. In contrast, cases D with a mobile basal layer, where the viscosity decreases due to additional internal heating, result in a more modest increase in the inner core age with the degree of internal heating.

The constrained values for Γ, which in my model formulation represents the fractional increase in adiabatic temperature from the CMB to the inner core, are listed in Table 4.1 for each case separately. Equating previous formulations [*e.g., Labrosse et al.*, 2001; *Nimmo et al.*, 2004] and my formulation for the core adiabat, the thermal expansivity of the core takes on the form,

$$\alpha_c = \frac{c_{pc} \ln \Gamma}{(2\pi/3)\,\rho_{cen}\,G\,(R_{cmb}^2 - R_{ic}^2)}\,. \tag{4.5}$$

Consequently, for the core heat capacity used in our model ($c_{pc} = 675$ J kg^{-1} K^{-1}), the thermal expansivity implied from our models ranges from $\alpha_c \approx 1.1$ to 0.90 $\times 10^{-5}$ K^{-1} (Table 4.1). These values are fairly consistent with other studies (1.25 -1.7 $\times 10^{-5}$ K^{-1} over the entire core, in *Labrosse*, 2003, 1.35 $\times 10^{-5}$ K^{-1}, in *Nimmo*, 2007, and 0.89 - 1.77 $\times 10^{-5}$ K^{-1} in *Roberts et al.*, 2003). A higher value for the thermal expansion of the core (2.5×10^{-5} K^{-1}) is used in the study of *Davies* [2007]. It can be noted that for high internal heating in the basal layer, the core cooling is very slow and this results in lower values for the adiabatic parameter Γ, and implicitly for α_c. Another reason for obtaining slightly lower values for the thermal expansion, is the use of a heat capacity in

the core somewhat lower than values employed in other studies. For instance, the ratio $\Theta = \alpha_c/c_{pc}$, scaling the adiabatic speed of sound in the core, computed from our thermal evolution for various scenarios, ranges from 1.48 to 1.63 $\times 10^{-8}$ s^2 m^{-2}, while the same ratio is 1.47 to 2.0 $\times 10^{-8}$ s^2 m^{-2} in *Labrosse* [2003] and 1.67 $\times 10^{-8}$ s^2 m^{-2} in *Nimmo* [2007]. These compare very closely with my results. As a final consistency check, I express $\Theta = \gamma\,\rho_c/K_T$, where γ is the Grüneisen parameter, $\rho = 11,000$ kg m^{-3} is the mean density in the outer core and $K_T = 970$ GPa is the isothermal mean bulk modulus [*Stacey*, 1992], and obtain a range for the Grüneisen parameter from 1.438 to 1.35, consistent with values for Grüneisen parameter in the outer core employed in other studies [*e.g. Davies*, 2007; *Gubbins et al.*, 2004; *Roberts et al.*, 2003; *Labrosse*, 2003; *Williams*, 1998]. In contrast, a value of 1.51 $\pm$0.01 is indicated by *Vočadlo et al.* [2003] for pure iron, whereas *Williams* [1998] prefers a value close to 1.4 for the Grüneisen parameter. Given the uncertainties of the light element content in the outer core which can affect the *ab initio* simulations [*Alfè et al.*, 2007; *Vočadlo*, 2007], and the difficulty of reproducing core conditions in laboratory experiments, there are still a number of uncertainties in constraining the physical parameters of the core, and therefore a wider range of thermal history scenarios cannot be excluded.

The resultant magnetic field for each case is plotted in Figure 4.3a. We can immediately observe that the evolution of the magnetic field follows two regimes, starting with a transient period at very early times when there is enough entropy created by the cooling of the core to generate an initial magnetic field. However, as the entropy of cooling decreases, so does the intensity of the magnetic field. The duration of the transient field is case dependent, and is correlated with the CMB heat flow (Q_{cmb}), illustrating the mantle control on magnetic field generation. Further, the magnetic field becomes weaker or vanishes for the cases of higher internal heating in D$''$, where the reduction in Q_{cmb} is severe. For those cases, although the inner core starts to freeze early, even with the contributions from the terms associated with the solidification process, there is still not enough entropy gain to overcome the adiabatic sink. This is due to maintaining high ambient temperatures in the core and very shallow temperature gradients at the CMB which diminish the efficiency of the cooling engine.

Once the entropy production in the model core becomes positive, the model magnetic field increases in intensity, and as can be seen, this modern magnetic field becomes more robust, keeping an almost steady trend, with highest values at the present, in agreement with paleomagnetic studies [*Selkin and Tauxe*, 2000]. An interesting result is the fact that for the cases where there is an interruption in the magnetic field generation, the modern magnetic field re-activates around the same time for all cases (after 1.6-1.8 Gyr of evolution) though the period without magnetic field varies among cases. This 'quiet' period increases with the amount of internal heating in the conductive layer, as a consequence of the lower cooling rate, and the reduced amount of heat leaving the core (Table 4.2 and Figure 4.3b). When convection penetrates D$''$ (B0 and D series models), the high variability in the magnetic field is caused by temporal fluctuations in mantle convection. Not surprisingly, these effects are smaller for conduction-dominated D$''$ (F series models), owing to the diffusive nature of thermal conduction, though large mantle avalanches may still trigger intensity swings.

For the stagnant regime in D$''$ considered in this paper, an un-interrupted magnetic field throughout geological time requires roughly 5 TW CMB heat flow for modern times, which occurs only for the radioactively depleted lowermost mantle (F0) or for a layer that has the same concentration in radioactive elements as the rest of the mantle (FF), or is very slightly enriched in radioactive elements (no more than 0.5 TW additional internal heating for the final rate in the layer). For cases with additional internal heating in excess of 0.5 TW, the CMB heat flow becomes sufficiently low to suppress the dynamo action at early times. The high temperatures in the core, due to the insulating layer affect the efficiency factors of the entropy-producing terms. This analysis shows that the low efficiency of the secular cooling to generate entropy requires a minimum CMB heat flow of roughly 4.5 TW at all times for maintaining positive values of Ohmic dissipation, and rates below this threshold fail to sustain an active dynamo from secular cooling alone. These estimates may slightly vary, since energy and entropy are quite sensitive to insufficiently constrained thermodynamic properties (*e.g.*, thermal conductivity, heat capacity). For instance, a decrease of 10% in the thermal conductivity in the core yields a continuous magnetic field for the case with

0.5 TW additional internal heating (F1), because of the decrease of the heat conducted along the adiabat. At the same time, if thermal conductivity were changed consistently, the intensity of the magnetic field would be slightly lower, due to reduced electrical conductivity predicted by the Franz-Wiedemann's relationship between the thermal and electronic conduction in metals [*Stacey*, 1992], $k = L\,T\,\sigma_e$, where L is the Lorentz constant and T is temperature.

4.3 Summary of Models With a Stagnant Layer in D″

A conductive layer in D″prevents rapid cooling of the core due to reduced heat transfer, requiring an early solidification of the inner core. If no additional heating is present in the layer, the internal magnetic field is quasi-continuously generated throughout Earth's evolution with an initial, purely thermal magnetic field weakening due to the slow cooling of the core, followed by a vigorous modern magnetic field, once the inner core starts to solidify. The total amount of Joule heating dissipated by the geodynamo is lower by almost an order of magnitude when heat is carried purely by conduction in D″, showing the ability of the stagnant layer to resolve the heat source paradox by maintaining a reduced CMB heat flow; by the same token, the mechanism produces an old inner core. This 'blanketing' effect was also noted by *Nakagawa and Tackley* [2004] when studying a thermo-chemical mobile layer, with a smaller density contrast.

The presence of additional internal heating in the stagnant layer shuts down the early magnetic field. Subsequently, when the entropy production in the system overcomes the adiabatic loss, due to the changing of cooling conditions in the core, the magnetic field is re-generated. This does not necessarily coincide with the moment of inner core inception, consistent with earlier remarks from the previous chapter. If the temperatures in the core are too high, the compositional term is still too low to sustain the geodynamo, particularly observed in cases F3 and F4. These cases refer to a stagnant D″ layer bearing rates of internal heating required by the geochemical models with 'isolated' reservoirs [*e.g., Tolstikhin and Hofmann*, 2005]. However, they are less plausible, as the quiescent period for magnetic field of about 1.5 Gyr, is not supported by paleomagnetic evidence. In addition, the thermal parameters computed on the basis of the inner core constraint

(*e.g.*, Grüneisen parameter) are slightly lower than the ones indicated by *ab initio* calculations. These scenarios may follow a totally different core thermal evolution, however, in that a significantly lower rate of cooling may generate a stratified thermal layer at the top of the core [*e.g., Braginsky*, 1991; *Lister and Buffett*, 1998]. This possibility is not accounted for in the present formulation for core evolution.

With a stagnant layer bearing no additional heating (model FF), an old inner core and a continuously generated dynamo are made possible without appealing to core potassium, a still disputed issue [*McDonough*, 2004]. The age of the inner core predicted from the models with a stagnant layer exceeds 2.6 Gyr, comparable to predictions from isotopic models and higher than those from analytical or numerical models. Similar ages are obtained by *Nagakawa and Tackley* [2005] when using 100 ppm ^{40}K in the core and a dense mantle basal layer, and by *Davies* [2007] by re-formulating the parameterized schemes for the CMB heat flow in an attempt to model complexities known to occur in D$''$, such as a thermal boundary layer with compositional variations and a post-perovskite phase. Lastly, this novel approach for heat transport at the base of the mantle generates models for Earth's thermal history that yield final core temperatures in the range of mineral physics estimates, without starting with a very high initial core temperature.

The analysis for the thermal and magnetic history in the core favors a stagnant, thermally conductive lowermost region in the mantle, with a chemically-distinct signature, where a hidden reservoir bearing no more than twice the background mantle concentration in radioactive elements may reside (case F1). For this scenario, the age of the inner core is around 2.74 Gyr and the magnetic field is generated for 80% of the Earth's history, with onset of 'modern' field in the Proterozoic. A weak, early magnetic field would have been responsible for magnetizing mid-Archean rocks, consistent with paleointensity analyses that have shown dipole moments lower by up to a factor of four in the distant past [*e.g., Tarduno et al.*, 2006; *Yoshihara and Hamano*, 2004]. The modern CMB temperature in model F1 is 3946 K. The stagnant layer in D$''$ is an appealing mechanism to maintain a high core temperature and produce an old inner core; it can only be weakly enriched in radioactive elements, however.

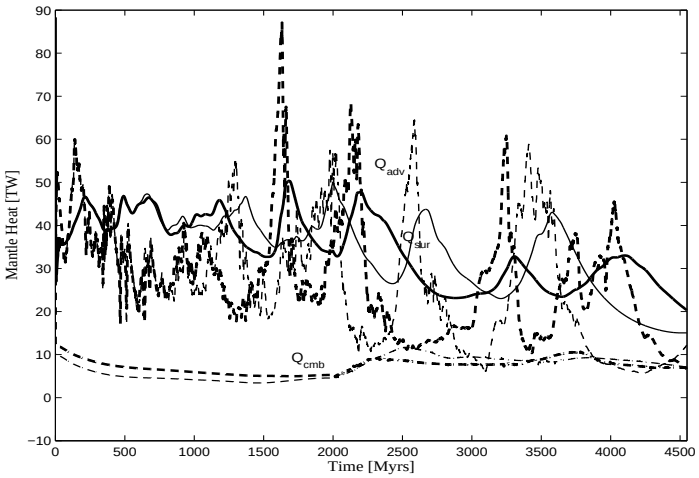

Figure 4.4: Evolution of heat fluxes for a stagnant layer in D″that breaks up after 2.0 Gyr of evolution (T1 and T2). Surface heat flow - solid lines. Advected heat at 660-km phase transition - dashed lines. CMB heat flow - dash-dotted lines. Thicker profiles represent a depleted D″layer (T1), thinner lines represent a D″layer enriched in internal heating, with 1 TW final rate (T2).

4.4 Thermal and Magnetic Consequences of Entraining the Stagnant Basal Layer in Mantle Circulation

Several studies have shown that a density contrast of $\sim 2-6\%$ is sufficient to maintain a stable layer at the base of the mantle for geologically significant lengths of time [*e.g., Montague and Kellogg*, 2000; *Sleep*, 1988; *Hansen and Yuen*, 1989], though the estimates vary slightly due to the geometry of the models employed and the viscosity contrast. *Montague and Kellogg* [2000] suggest that it may have been easier to preserve a dense layer in D″in the past, when the mantle was much hotter and had a lower viscosity. Experimental work has shown that for a low density contrast ($\sim 2\,\%$), the layer could break after $2.0-2.5$ Gyr of evolution and be entrained in the whole mantle convection due to instabilities that develop at the layer interface [*Davaille and Arndt*, 2007]. The entrainment occurs when the thermal heterogeneities at the interface induce circulations in the two layers; later, the viscous drag is strong enough to entrain thin tendrils of dense material. After a while, the entire chemical layer becomes eroded until $B = 0$ and a complete mixing is achieved [*Davaille*, 1999, *Davaille et al.*, 2003].

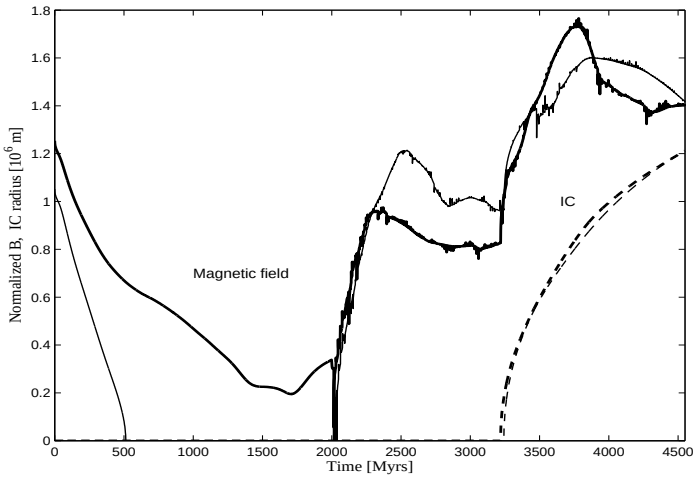

Figure 4.5: Time evolution of the modeled magnetic field and growth of the inner core for a stagnant layer in D″that breaks up after 2.0 Gyr of evolution. Magnetic field - solid lines. IC radius - dash lines. Thicker profiles represent a depleted D″layer (T1), thinner lines represent a D″layer enriched in internal heating, with 1 TW final rate (T2).

To study the effects of convection penetrating to the bottom of the mantle after a period of evolution with a stagnant layer, I have performed a set of simulations corresponding to cases with a depleted lowermost mantle (stagnant case F0) and a slightly-enriched lowermost mantle (stagnant case F1). For these cases, I have performed the first run with a conductive regime at the base of the mantle and have stopped the simulations after 2.0 and 2.5 Gyr of time evolution. Subsequently, the simulations were switched from stagnant to mobile D″ by using the final temperature distribution of the stagnant case as an initial condition for the new simulations. From this point on, the method was identical with all the other simulations with a mobile D″. The first simulation was run until the present time without IC formation and subsequently a second run was performed to grow the correct size of the inner core (T series, see Tables 4.1 and 4.2). The results from T series models are plotted in Figures 4.4, 4.5, and 4.6, 4.7 for the layer break-up after 2.0 and 2.5 Gyr, respectively.

To estimate B for these two cases, we can use a scaling law for the erosion rate for a dense layer [*e.g., Jellinek and Manga*, 2002], of the form,

$$q = \frac{C^2}{20^2\,\pi^2}\,\frac{\kappa}{H}\,\frac{Ra^{1/3}}{\lambda_d B \lambda_h^{2/3}}\,. \tag{4.6}$$

In (4.6), H is the combined height of both layers, κ is the thermal diffusivity, $C = 0.6$ is a

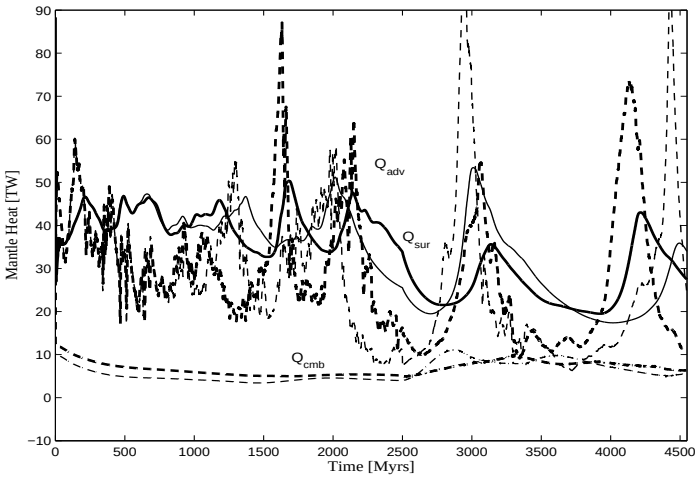

Figure 4.6: Evolution of heat fluxes for a stagnant layer in D″that breaks up after 2.5 Gyr of evolution (T3 and T4). Surface heat flow - solid lines. Advected heat at 660-km phase transition - dashed lines. CMB heat flow - dash-dotted lines. Thicker profiles represent a depleted D″layer (T3), thinner lines represent a D″layer enriched in internal heating, with 1 TW final rate (T4).

scaling constant, $\lambda_d = \mu_c/\mu_d$, $\lambda_d = \mu_c/\mu_h$, and μ_c, μ_d, μ_h are the viscosity in the ambient fluid, at the interface and in the denser layer, respectively. For a 200 km-thick layer that is completely entrained after 2.0 Gyr, the erosion rate is $q = 100$ m Myr^{-1}, whereas if the entrainment occurs after 2.5 Gyr, $q = 80$ m Myr^{-1}. Typical values for the Earth are $Ra = 10^7 - 10^8$, $\kappa = 10^{-6}$ m s^{-2} and $H = 3 \times 10^6$ m [*Jellinek and Manga*, 2002]. Using these values, $B = 0.4089$ for a layer that is completely mixed after 2.0 Gyr, whereas $B = 0.5111$, for a transition which occurs after 2.5 Gyr of evolution. Further, the density contrasts are 1.09 % and 1.28 %, respectively.

When the thermally conductive layer is allowed to enter the whole mantle convection, the mantle can remove heat from the core more efficiently. The CMB heat flow increases as the more effective convective heat transport penetrates the bottom of the mantle, allowing more heat to cross the boundary. There is also a higher variability in the CMB heat flow after the layer break-up, as the filtering effects of the thermal diffusion in the basal layer are removed. Also, convection in the mantle is affected, and it can be observed that intense avalanches occur, as evidenced by spikes in the heat flow at the surface and at 660-km phase depth. These spikes occur after the layer is de-stabilized, reflecting the increased heat transport at the CMB, suddenly received from the core,

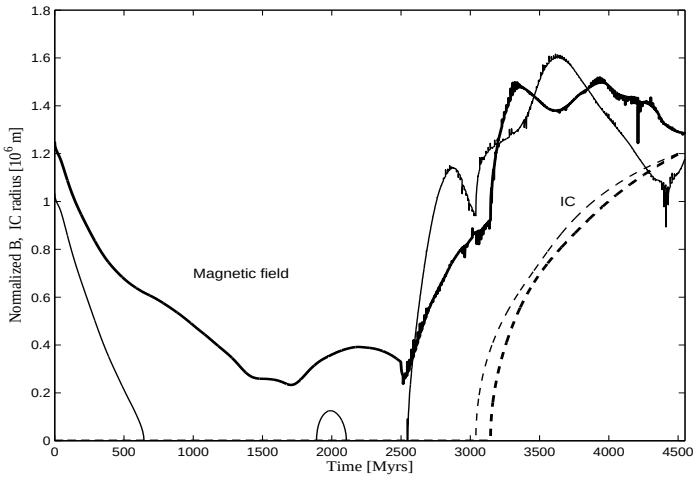

Figure 4.7: Time evolution of the modeled magnetic field and growth of the inner core for a stagnant layer in D″that breaks up after 2.5 Gyr of evolution T3 and T4). Magnetic field - solid lines. IC radius - dash lines. Thicker profiles represent a depleted D″layer (T3), thinner lines represent a D″layer enriched in internal heating, with 1 TW final rate (T4).

which is decreasing the viscosity in the lower mantle. The time lag between the layer rupture and the heat flow spikes is roughly 0.5 Gyr, probably reflecting the characteristic timescale of mantle overturn combined with phase boundary effects. This result is consistent with the paper by *Condie* [2000], who suggests that the change in pattern of mantle convection, from layered to whole-mantle convection, would trigger a mantle superevent responsible for increased crustal production and formation of supercontinents.

Additionally, the results show that the events at the 660-km phase transition are more intense for the cases when the layer that breaks-up is enriched in radioactive heating (*i.e.*, T2 and T4), and it is expected that this phenomenon will be even stronger for cases with higher additional internal heating ($>$ 1 TW, not studied here). The surface heat flows at the end of the simulations tend to be higher for the case of layer break-up at 2.5 Gyr (T3 and T4), compared to the cases with break-up at 2.0 Gyr (T1 and T2). This could be a consequence of the fact that the mantle cools more efficiently for a longer period of time in the latter calculations.

In contrast with cases with a stagnant layer throughout the Earth's lifetime, for the cases where the stagnant layer is entrained in mantle convection, the age of the inner core decreases significantly. The inner core solidification is delayed for about 0.5 Gyr in the case of a transition at 2.5 Gyr (cases

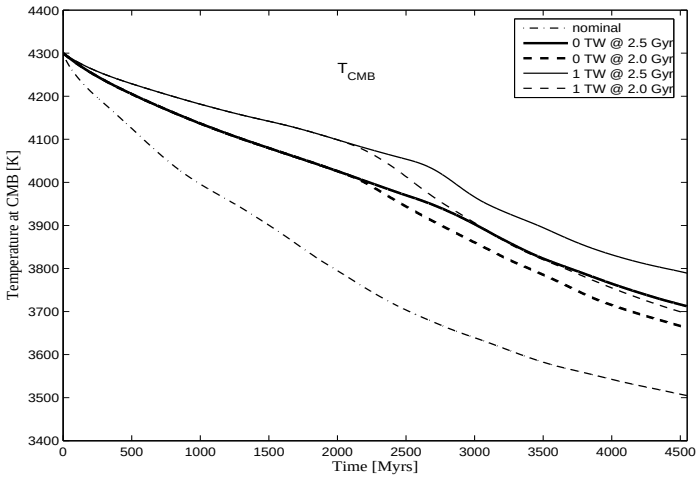

Figure 4.8: Summary plot for evolution of CMB temperatures for the nominal case B0 and T series, representing transition from stagnant to convective regime in D″.

T3 and T4 and Figure 4.7) and by 1 Gyr for the case with a transition at 2.0 Gyr (cases T1 and T2 and Figure 4.5). This is a direct consequence of the efficiency with which heat is removed from the core. The sooner the mantle becomes wholly-convective, the less time is required to grow an inner core the size of the present-day radius. It can be observed from the plots that the earlier the layer is entrained in whole mantle convection, the younger the inner core becomes. The simulations do not account for the possibility of an inner core that starts to freeze prior to the break-up of the layer, however, in none of these simulations is nucleation required to occur before break-up, due to the mechanism explained above.

At the time of the layer break-up, a sudden increase in magnetic field intensity can be observed for the cases with un-interrupted magnetic field (T1 and T3). A similar effect was seen in the model of *Stegman et al.* [2003], who suggest that a transient increase in core heat flux after an overturn of an initially stratified lunar mantle might explain the short existence of an early lunar dynamo. For the cases where there is no magnetic field prior to the layer break-up, a complete regeneration of the magnetic field is observed (T2 and T4). These effects are due to the increase of the CMB heat flow, which triggers a re-vitalization of the magnetic field by increasing the contribution of the core secular cooling to the entropy of ohmic dissipation. This is an interesting observation, as the magnetic field re-activates prior to the inner core inception, showing that there are possible

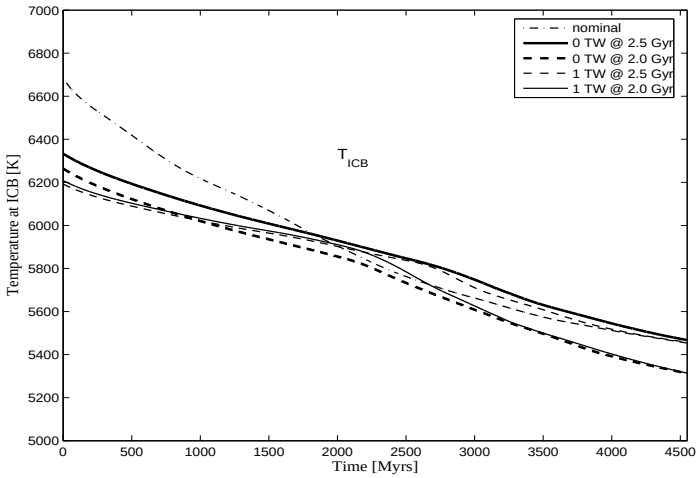

Figure 4.9: Summary plot for evolution of ICB temperatures for the nominal case B0 and T series representing transition from stagnant to convective regime in D″

scenarios where the resurgence of the magnetic field is not necessarily related to the supplementary contribution of latent heating and potential energy release.

A second, sudden increase in the magnetic field intensity can be observed at the time of the onset of the IC solidification, due to the additional energy sources that enter the system (latent heating and release of gravitational potential). This effect is observed in all of the simulations performed without a stagnant layer at the base of the mantle. For the cases with a stagnant layer, this effect is diminished by the low-pass filter action of the diffusive process. The magnetic phenomena can be observed happening in the core almost concomitantly with the layer break-up or beginning of inner core freezing, owing to the very short characteristic time scales in the core. The energy required to maintain an active dynamo for the cases with a transition from stagnant layer to mantle convection in D″, is significantly increased, as can be seen from Table 4.2. The highly dissipative dynamo could be explained by the fact that after the layer break-up the mantle becomes more active and therefore the heat flux across CMB is increased and this leads to a more dissipative regime in the core.

I note that for the case with 1TW additional internal heating in the layer, the 'quiet' period, with no magnetic field generation, is increased from $\sim$ 1 Gyr for the stagnant case to more than 1.5 Gyr when the layer breaks up. This is due to the steeper adiabat (e.g., $\Gamma = 1.44$ for break-up

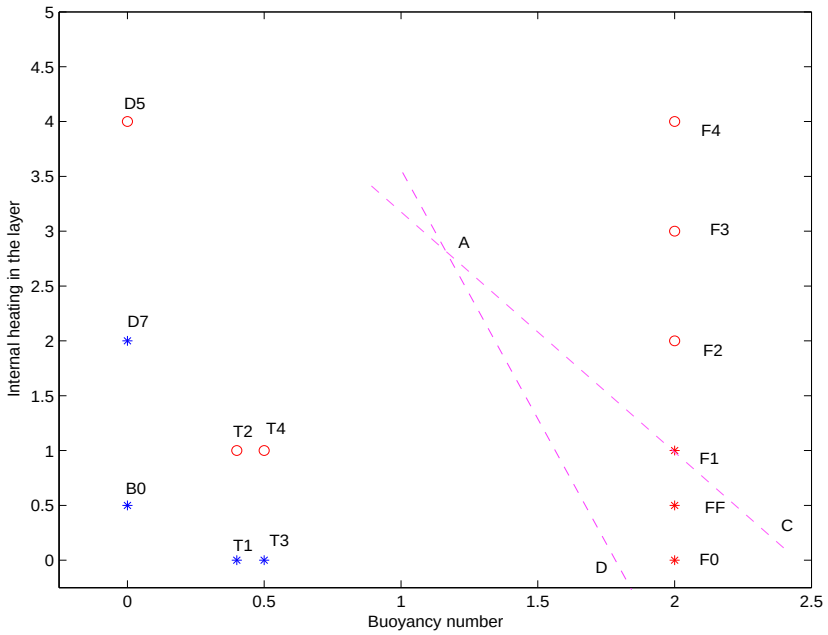

Figure 4.10: Geodynamo regime diagram as a function of buoyancy number and internal heating in the core. Blue color indicates a final CMB temperature lower than $\sim$ 3800 K. Red color indicates a final CMB temperature in excess of $\sim$ 3800 K. Stars indicate a quasi-continuous magnetic field generation, whereas open circles indicate an interrupted magnetic field generation. A continuous magnetic field and high CMB temperatures are predicted for regimes delineated by ADC.

at 2 Gyr, as opposed to $\Gamma = 1.38$ for the stagnant case) used to constrain the growth of the inner core, which causes a higher entropy of the heat conducted down the core adiabat, hence decreasing the entropy available for Ohmic dissipation.

Figures 4.8 and 4.9 display the final temperatures at the CMB and ICB for the transition cases, along with the nominal case B0, for comparison. The final temperatures at the CMB decrease as the layer breaks up earlier, because the convection regime is more efficient in transporting heat from the core to the surface. Additionally, the final CMB temperature decreases if less internal heating is present in the layer. The cooling rate at the CMB horizon for the cases with a layer break-up is very close to that for the cases with whole-mantle convection, as shown from Table 4.2. The initial temperatures at the centre of the Earth, required to end up with $\sim$ 5700 K at the ICB and a inner core radius of the present-day value, decrease significantly from the nominal case to the case with additional internal heating in the layer, showing that the presence of a conductive

layer has a 'blanketing" effect on the core cooling.

Figure 4.10 shows the dynamo regime diagram for the cases that have been studied in this chapter, in the Buoyancy number-internal heating in the dense layer parameter space. Although an exhaustive study was not performed, it can be seen from the regime diagram that a high modern-day CMB temperature and a quasi-continuous magnetic field is only achieved for a layer that remains un-entrained in the mantle flow for the most part of the Earth history. If the layer is not stagnant over the Earth's lifetime, due to instabilities which may entrain the layer in mantle convection, a more active mantle will render final CMB temperatures which are less than 4000 K, with much younger inner cores and models of magnetic field that have survived for around 3.5 Gyr. It can also be seen that the internal heating in the layer must not exceed 1 TW final rate. The ADC region delineated in the regime diagram is a prediction of the conditions that could lead to a successful magnetic history and a high final CMB temperature. Namely, from the regime diagram we may envisage a scenario of a layer that breaks very late in the Earth's history, such that the temperature at the CMB doesn't drop too much due to vigorous convection and for which the magnetic field will not be interrupted as the inner core may start initiating soon after the layer break-up. In addition, the persistence of a stagnant layer over most of the geological time would not conflict with seismological observations, as these only give us a snapshot of the present mantle structure. However, the predicted successful regime (ADC area) shows that the amount of internal heating in the layer is still low compared to the global mass balance requirements [*e.g., Boyet and Carlson*, 2005].

From this analysis, it can be concluded that for maintaining modern core temperatures around 4000 K and an almost continuous magnetic field the long-standing and thermally conductive layer at the base of D″ appears to be a successful scenario.

Run	Mechanism in D″	$\mathcal{H}$ in D″ (final rate) [TW]	T^0_{cmb} [K]	$T^{4.55}_{cmb}$ [K]	Γ	Grüneisen (γ)	Thermal exp. (α_c) [10^{-5} K^{-}1]
B0	mobile	0.5	4300	3505	1.556	1.438	1.100
D7	mobile	2.0	4300	3583	1.524	1.398	1.070
D5	mobile	4.0	4300	3676	1.483	1.429	1.095
F0	stagnant	0.0	4300	3834	1.424	1.403	1.074
FF	stagnant	0.5	4300	3900	1.401	1.402	1.073
F1	stagnant	1.0	4300	3946	1.384	1.393	1.067
F2	stagnant	2.0	4300	4030	1.354	1.361	1.049
F3	stagnant	3.0	4340	4153	1.320	1.354	0.991
F4	stagnant	4.0	4510	4355	1.264	1.295	0.889
T1	trans@2.0	0.0	4300	3662	1.491	1.399	1.0716
T2	trans@2.0	1.0	4300	3696	1.477	1.4159	1.084
T3	trans@2.5	0.0	4300	3723	1.473	1.352	1.035
T4	trans@2.5	1.0	4300	3790	1.441	1.399	1.07

Table 4.1: Summary of the thermal parameters of the core. Comparison between results and parameters for purely thermal conduction in D″ (F cases), whole-mantle convective regime (B and D cases) and mixed heat transport, with transition from purely thermal conduction to whole-mantle convection (T cases). The nominal run is represented by B0. Superscripts ^{0} and $^{4.55}$ refer to the beginning and the end of the simulation (starting from 4.55 Gyr ago to present).

Run	Cooling rate @ CMB [K Gyr^{-1}]	Age of IC [Gyr]	$Q_{cmb}^{4.55}$ [TW]	Total dissipation [J]	Onset of modern **B** [Gyr]	Duration of **B** [Gyr]
B0	175	1.756	5.07	1.45×10^{29}	0	4.550
D7	158	1.884	5.88	1.22×10^{29}	0	4.550
D5	137	1.679	8.37	9.52×10^{28}	2.131	3.821
F0	102	2.323	4.84	6.22×10^{28}	0	4.550
FF	89	2.682	4.35	5.16×10^{28}	1.658	4.139
F1	78	2.742	3.73	4.43×10^{28}	1.808	3.534
F2	59	3.145	3.58	3.95×10^{28}	1.676	3.105
F3	42	4.272	3.49	2.71×10^{28}	1.683	2.987
F4	34	4.550	3.07	2.64×10^{28}	1.744	2.961
T1	140	1.305	6.72	2.76×10^{29}	0	4.550
T2	133	1.317	6.70	2.75×10^{29}	1.997	3.050
T3	128	1.410	6.29	2.26×10^{29}	0	4.550
T4	112	1.515	5.71	1.93×10^{29}	2.542	2.642

Table 4.2: Summary of core energetics and magnetic field evolution. Comparison for results and parameters for purely thermal conduction in D$''$ (F cases), whole-mantle convective regime (B and D cases) and mixed heat transport, with transition from purely thermal conduction to whole-mantle convection (T cases). The nominal run is represented by B0. Superscripts ^{0} and $^{4.55}$ refer to the beginning and the end of the simulation (starting from 4.55 Gyr ago to present).

Chapter 5

Summary of Results and Discussion

The aim of this chapter is to summarize the various scenarios that were considered for the thermal and magnetic history of the Earth, implementing new geochemical models, related to the lowermost mantle and the composition of the core. The Earth's core is a heat reservoir cooling at a rate controlled by the overlying mantle. Understanding the energy budget of both the core and the mantle and studying the contributing factors is important for several reasons, of which some are enumerated here. First, the nature of heat transport in the mantle, the vigor of convection, the amount and distribution of internal heating are affecting the thermal history of the mantle, which is responsible for surface processes such as plate tectonics, mountain building and large igneous provinces. The surface heat flow is also strongly affected by the underlying convection in the mantle.

Second, the viability of the magnetic field is determined by the thermal history of the Earth. If the mantle cools the core at a sufficient rate as to create thermal convection in the core, the buoyancy sources may in turn generate a magnetic field. Slowing the rate of the core cooling can allow the core to cool only through thermal conduction, which cannot sustain a dynamo.

Third, it has been shown that implementing present-day constraints on the thermal and magnetic evolution of the core proves a difficult task. The magnetic field has existed for most of the Earth's lifetime, hence the necessity to maintain proper conditions for a working dynamo. Another complication arises from recent studies that require high modern-day CMB temperatures, which unavoidably lead to initial CMB temperatures above the solidus point of lower mantle materials. However, very recently, a scenario was proposed where the mantle starts to crystallize from a basal magma ocean [*Labrosse et al.*, 2007]. It was not possible in this study to take into account for such

a scenario, as a molten state for the mantle would significantly change the physics of the mantle, and these effects are not accounted for in the mantle numerical model.

Finally, understanding the thermal history of the mantle and core and the magnetic field on Earth will help in constructing viable evolution models for other solar system bodies which posses or have once possessed a magnetic field [*e.g., Acuña et al.*, 1999].

The study of the thermal evolution of the Earth has been carried out by coupling a 2D axi-symmetric model for mantle convection with a parameterized model for the Earth's core, by requiring continuity of heat flow at the core mantle boundary, which allows for feed-back between the two models at each time step. The main findings revealed by the entire analysis and the most successful models will be discussed below.

5.1 Onset and continuity of the magnetic field

Among the models presented in this thesis, those that have a continuous magnetic field for the past 3.5 Gyr in agreement with the PSV, or with minor interruptions (which can be resolved within the error margins for various physical parameters of the core), are the following:

- Core potassium. A concentration of 300 ppm of K in the core, resulting in a final rate of internal heating of 2 TW was sufficient to maintain a magnetic field over the age of the Earth (case B2). This model displays a strong, stable magnetic field throughout the geologic time, with small intensity variations. Case B1, with a final rate of 1 TW also yields a continuous magnetic field. This scenario corresponds to a concentration of 150 ppm K in the core, which cannot be ruled out by geochemical constraints [*e.g., Nimmo*, 2007; *Lassiter*, 2006]. However, for this case, the magnetic field displays more pronounced time dependence than for the case B2.

- A soft layer in D$''$ bearing no more than 2-3 TW additional internal heating in D$''$, assuming the presence of U, Th and K radioactive isotopes (*e.g.*, case D7). The magnetic field intensity for this case displays high variability compared to the case B2. Model D5, consistent with

the geochemical model of *Tolstikhin and Hofmann* [2005] is only marginally included in this category, because it requires tuning in parameter space (*e.g.*, lower thermal conductivity). In addition, short-term fluctuations in the modeled field intensity are significant (may vary by a factor of 3). Higher concentrations of radioactive elements render models where the magnetic field cannot be continuously sustained (series D models).

- A stagnant, 'blanketing' layer in D″, provided it bears only reduced amounts of additional internal heating (*e.g.*, case F1). The layer may also be depleted in radioactive elements or have the same concentration as the lower mantle background (F0 or FF). The stagnant layer (in D″) scenario brings a new feature in the magnetic evolution, in that the diffusive process in the lowermost mantle imposes a reduced variability of the magnetic field intensity. Another distinctive feature observed in these models is that a transient field is present for about 0.5 - 1 Gyr, followed by an intensity 'low' or 'quiet' period, and lastly, a modern, stronger field is re-activated. This evolution pattern is however decoupled form the onset of the IC nucleation, which happens very early in the Earth's history.

- A stagnant layer which becomes entrained in convection. Cases T1 and T3, where the stagnant basal layer is allowed to enter convection after 2.0 or 2.5 Gyr are also displaying a continuous magnetic field throughout time. The presence of additional heating in such a mixed scenario (T2 and T4) is unlikely. The CMB cooling history and the constraints imposed by growing a correct size of the modern-day IC require a higher value for the adiabatic parameter Γ than for the cases without internal heating. This increases the value of the adiabatic entropy term, and therefore the magnetic history for cases that allow the presence of additional heating in the layer, renders larger gaps in the magnetic field.

- The nominal case. Model B0, which has been considered the reference case, is also able to produce a continuous magnetic field. The modeled field displays large fluctuations in the field intensity.

5.2 Trends in modeled magnetic field intensity

Most of the models of magnetic field intensity presented in this thesis are highly time dependent. These fluctuations may be superimposed on a declining, increasing or almost steady trends. In addition, an interesting remark regarding big swings in modeled field intensity is worth noting. The classical view expressed in many studies [*e.g., Stevenson et al.*, 1983; *Tarduno et al.*, 2006] is that the onset of inner core solidification triggers a sudden increase of the magnetic field intensity, due to the energy terms released by the IC freezing. This is often seen in the models presented in the thesis. Moreover, there seem to be other causes that trigger significant and sudden magnetic field intensity swings, demonstrating that a favorable entropy production for magnetic field generation can be attained through other mechanisms as well. The summarizing remarks on the trends in magnetic field are listed below.

- Declining intensity trend, followed by increasing trend. This feature is encountered in most of the models, including B0, D5, D6, F series and T series. The initial declining trend is reflecting a dynamo that is sustained from secular cooling alone, which diminishes in time, to the point that the magnetic field can disappear. This is consistent with evidence in favor of low intensity during the Precambrian [*e.g., Macouin et al.*, 2003; *Valet*, 2003]. Once the available entropy for the dynamo overcomes the adiabatic sink (most of the times due to entropy produced by compositional buoyancy), the magnetic field displays a steady increase in intensity, yielding the strongest magnetic field in modern times in most cases. Undoubtedly, this evolution pattern is the most often seen in models of magnetic field evolution based on theoretical studies of core energetics [*e.g., Nimmo*, 2007; *Davies*, 2007; *Labrosse*, 2003; *Stevenson et al.*, 1983].

- Steady trends. A stable and robust geodynamo action is present throughout the entire evolution for cases B2, B4 and C series. For these cases, there is significant entropy produced by the buoyancy generated by either radioactive heating in the core (B2, B4), or rapid secular cooling of the core due to high initial temperatures (C0, C6), which render a strong dynamo

action at all times; in addition, there is a smaller jump when the IC starts to freeze, since the latent heat and gravitational energy decrease the secular cooling.

- Intensity swings due to the IC nucleation. The increase in magnetic field intensity at the moment of the onset of IC freezing is observable in the nominal model B0, as well as in all of the D series and most of the F series and is less noticeable in T models. This can be related to the additional compositional buoyancy that is generated with the IC solidification, which has a positive effect on magnetic field generation. For the cases where there is significant entropy produced by the buoyancy generated by other sources as explained above (B2, B4, C0, C6), the effect of IC solidification is quite obscure, and cannot be identified in the evolution of model magnetic field, unless additional information is available.

- Intensity swings due to changes in the lowermost mantle thermal regime. When a stagnant layer becomes entrained in whole mantle convection (T series) and convection is allowed to penetrate to the bottom of the mantle, there is a sudden increase in the efficiency with which the mantle removes heat from the core. This sudden pattern change is noted in the magnetic field and with some delay, in the heat flows at the surface and 660-km depth. Studies of *Davaille and Arndt* [2007] and *Montague and Kellogg* [2000] have discussed the implications on mantle convection for such scenarios, but did not extend their analysis on the on magnetic field evolution.

- Intensity swings due to intense mantle events at the surface and 660-km depth. This is another novel feature that has not been previously discussed, except in *Costin and Butler* [2006]. This situation is illustrated by models D2, D5 and possibly D4. The revival of the magnetic field, often of short duration, is solely due to the increase in CMB flow as a consequence of peaks in 660-km depth and surface heat flows, which enable the mantle to episodically increase the amount of heat that it is able remove from the core. There is usually a time lag of around 50-60 Myr between the two events, when the descending cold plume is felt at the CMB. Increased heat flow at the CMB produces more thermal buoyancy in the core, which creates available entropy for the dynamo.

5.3 Age of the inner core

The age of the inner core is a critical parameter for constructing thermal and magnetic evolution models. Some attractive, but highly contentious suggestions have proposed observational constraints for the age of the inner core [*e.g., Brandon et al.*, 2003]. These models predict that the IC formation began ~ 3.5 Gyr ago. The geochemical arguments for these models have been strongly contested [*e.g., Luguet et al.*, 2008]. Nonetheless, the idea of obtaining constraints on the IC age from geological observations, which can otherwise be addressed only by theoretical modeling, is intriguing [*Nimmo*, 2007]. So far, the great majority of the theoretical models for a core that is radionuclide-free, have predicted an age of the IC anywhere from 0.3 to 2.0 Gyr. An increased age of the inner core is obtained by *Gubbins et al.* [2004] when using internal heating in the core, with a concentration of 400 ppm of ^{40}K. *Lassiter* [2006] and *Davies* [2007] obtain an age for the IC that exceeds 2.5 Gy, using various schemes for CMB heat flow and boundary layer parameterization.

The models analyzed in this study predict the IC age as a corollary to the constraints imposed on growing an inner core that ends up with a correct radius. In turn, this affects the slope of the adiabatic temperature increase and consequently the moment in time when the adiabatic temperature equals the solidification temperature. Therefore, the age predicted from the models covers a wide range, from ~ 1.2 billion-year old to virtually the age of the Earth. An interesting remark will be noted for the cases with old inner cores. Due to the shallow adiabat required to start freezing an inner core early, the efficiency of producing dynamo action is also reduced, as there is only a small temperature difference between different horizons in the outer core. As such, the models have yielded scenarios where the IC starts to grow, but the dynamo is not operational. In the previous paragraph we have seen the magnetic field re-instated without the onset of the inner core; from this observation, inner cores without magnetic field can be envisaged.

Based on the age of the IC, the models are grouped as follows:

- Young inner core (< 2.5 Gyr). The models with young inner cores include the nominal case B0, the B series, C series and T series. The young IC age predicted from these models is

consistent with previous analyses [*Labrosse et al*, 2001; *Nimmo et al.*, 2004; *Aubert*,2005]. All of these cases are characterized by a fast cooling of the core, which requires a short time to grow an IC of the size inferred from seismological observations.

- An IC older than $\sim$ 2.5 Gyr. An older age for the inner core is achieved in most of the D series and all of the F series. These models contain additional internal heating at the base of the mantle, in a mobile or stagnant layer. These scenarios were constructed based on the new hypotheses of the existence of an early isolated reservoir, enriched in incompatible elements. This formulation for the thermal history of the mantle has been previously envisaged by *Buffett* [2002], but no detailed analysis has been previously carried forward. Therefore, the new formulation represents a starting point for more refined models. The increased age of the inner core is due to the 'blanketing' effect of a hot layer at the base of the mantle, which only allows low rates of core cooling. Consequently, a modern-sized inner core needs a longer time to crystallize. These models require the IC to start solidifying in Archean or early Proterozoic time, and are consistent with some suggestions from paleointensity data [*e.g., Tarduno et al.*, 2006; *Yoshihara and Hamano*, 2000], and with theoretical models of *Davies* [2007] and *Lassiter* [2006] and are reminiscent of the geochemical models which predict old inner cores. Analytical models that do not include the effects of additional internal heating at the base of the mantle [*e.g., Labrosse*, 2003; *Roberts et al*, 2003; *Nimmo et al.*, 2004] predict much younger inner cores. It is also to be noted that for the sake of reducing the CMB heat flow over geological time and thus obtaining an old inner core, a stagnant layer, with no additional internal heating, or even one depleted in internal heating (FF and F0 cases), have sufficed.

5.4 Modern-day CMB temperature and CMB heat flow.

The final temperature at the CMB is an important parameter, and the understanding of the value of the modern-day CMB temperature has changed in time. In view of recent calculations, the predicted of modern-day temperature at the CMB horizon, obtained by extrapolating the melting temperature

at the ICB, is around 4100 K [*e.g., Alfè et al.*, 2007]. Such a high final temperature is hard to achieve in thermal models, in the context of starting with a mantle temperature near or at the solidus point. This can be seen from the nominal model, which ended up with a CMB temperature of 3505 K. Most of the B, C, D and F series models presented have CMB final temperatures around 4000 K, in agreement with recent calculations, as seeking high final temperatures was one of the goals in this study. The mechanisms that have rendered final CMB temperatures around 4000 K (starting from the solidus temperature for the mantle) include the presence of core potassium (B series), or additional internal heating in the basal layer in excess of 4 TW (D series), or a stagnant layer in D″(F series). Cases where the stagnant layer becomes entrained in convection render final temperatures around 3700 to 3800 K, still higher than predictions from the nominal case.

Modern-day CMB heat flow in the models presented in this study ranges from ~ 4 TW to ~ 10 TW, in agreement with the current estimates which suggest a value of 10 ± 4 TW [*e.g., Nimmo*, 2007]. The CMB heat flow shows some degree of variability in most models presented in this thesis. Generally, the heat flow at the CMB follows the same trends with the modeled heat flow at the surface and at 660-km depth. Thermal models that account for a stagnant layer on top of the liquid core, display reduced fluctuations, due to the diffusive processes in the D″ layer which tend to smooth out the effects of the phase boundary and surface heat flow variations.

Models that have a significant additional amount of radioactive elements at the base of the mantle (exceeding 4 TW final rate) show a reversed direction for CMB heat flow at the beginning of the simulations, which leads to core heating at early times (D1, D2, D4, F4). Models that contain a stagnant layer in D″ end up with the lowest values for CMB heat flow, because the amount of heat extracted by the mantle is limited by the thermal conduction in the layer. The analysis shows that the lower bound for modern-day CMB heat flow which renders a continuous magnetic field throughout the Earth's life time is roughly 4 TW.

5.5 Mantle evolution and present-day surface heat flow

Among the simulations, few models end up with the heat flow suggested by observations [*e.g.,*

Pollack, 1993]. Modeling has suggested that obtaining the correct present-day value is a mere coincidence and is probably strongly dependent on the initial temperature distribution, which is a free parameter. Hence, the modern-day surface heat flow cannot be in itself a viable criterion in deciding the success of a model. The surface heat flow obtained from the simulations shows a long-term variability, displaying around 5 to 6 spikes in the heat flow over the entire geological time. The duration of these spikes is short, of order 100 Myr or less. These spikes correspond to mantle overturns, when the upper mantle is replaced by hot material from the lower mantle. Simultaneously, the lower mantle is replaced by the cool material from the upper mantle. The average period of time between two spikes is around 600 to 700 Myr, however the frequency of overturns decreases towards the end of the evolution, due to the decline of radioactive heating in the mantle. The mantle evolution from the simulations is consistent with suggestions that crustal production and continental growth at 2.7, 1.9, and 1.2 Gyr ago are caused by short (70 to 80 Myr) superevents in the mantle [*e.g., Condie*, 1998; 2000]. Simulations show that if a spike in the heat flow occurs in the last billion years or so, the surface heat flow at the end of the simulation is increased.

5.6 Preferred scenarios

From the analysis of all the simulations performed in this study, a number of cases stand out as possible viable scenarios for the evolution of the Earth, consistent with the criteria for a successful model, *i.e.*, correct radius of the inner core, a magnetic field operating for at least the past 3.5 Gyr, that has not fluctuated in intensity more than by a factor of 5 [*Valet*, 2003], a final CMB temperature around 4000 K, and desirably, a mantle contribution to the surface heat flow at present times around 36 TW [*e.g., Pollack et al.*, 1993]. The preferred scenarios include: a scenario with radioactive potassium in the core [*e.g., Murthy et al.*, 2003] (*e.g.,* B2, with 300 ppm or B1, with 150 ppm); a scenario for which the initial core temperature is in excess of the solidus point for mantle silicates at CMB pressures (*e.g.*, C0); a scenario with an early-isolated, incompatible-element enriched layer in D$''$ [*e.g., Boyet and Carlson*, 2005], mobile or stagnant, bearing reduced

amounts of additional internal heating, with trade-off between the mobility of the layer and the amount of additional internal heating (*e.g.* D7 or F1); lastly, a dense layer in D″, as a possible outcome of iron-enrichment, that has been immobile over most of the Earth's lifetime (*e.g.*, FF).

Each of these scenarios are attractive from the standpoint of the success of thermal and magnetic history modeling. Additionally, scenarios D7 or F1 could alleviate the geochemical paradox and hence bring an agreement between geochemical requirements for an apparently isolated mantle reservoir and geophysical evidence for mantle convection [*e.g., Tolstikhin and Hofmann*, 2005; *Lassiter*, 2006]; a solution to the geochemical paradox could also be resolved by scenario C0, if accounting for the possibility that incompatible-elements have been sequestered in the magma ocean at the bottom of the mantle [*e.g., Labrosse et al.*, 2007]. Scenario FF does not contain any enhancement in heat-producing elements in the immobile layer, rather it emulates a denser layer, due to iron-enrichment [*e.g., Mao et al.*, 2006], that has persisted over much of the geological time.

All of the scenarios brought forth contain implementations of recent geochemical and dynamical suggestions, and thus, the future will reveal if they continue to stand up to scrutiny. Further analyses of the Earth's thermal and magnetic evolution will benefit from advancements in various disciplines. There are still uncertainties in the thermal parameters of the core such as thermal expansivity, heat capacity or thermal conductivity. Improving the knowledge of these parameters will help future models to better constrain the core thermal evolution and implicitly the age of the inner core. The melting behavior of the iron-light element system is not yet sufficiently well understood, as well as there are still few constraints on the light element core composition. New constraints on the light element in the core could possibly lead to binary, tertiary or quaternary systems, which would affect the melting curve of the core alloy or the density contrast across the ICB [*e.g., Vočadlo et al.*, 2007]. These advancements from mineral physics could help constrain the temperature at the inner core boundary and implicitly the temperature at the CMB. Likewise, a better calibration of the heat flow at the CMB becomes crucial in in determining the age of the inner core. Estimates for this quantity vary by at least a factor of 2, and its evolution in time remains unknown [*e.g., Nimmo*, 2007].

All of the above could provide better estimates of the energy flow required to maintain a geodynamo. Improvements are also expected in convection modeling and in the imaging resolution of the D″ layer, which could bring new evidence of the dynamics of the lowermost mantle. Evidence of the presence of heat producing elements in the core and the distribution of the internal heating throughout the mantle, radially and laterally, could be expected from geo-neutrino detection in future experiments [*e.g., McDonough*, 2007]. Lastly, modeling the magnetic evolution could benefit from more secure evidence of the strength of the magnetic field throughout Earth's history [*Davies*, 2007], for instance, if constraints on the field intensity will be obtained from the amount of cosmonuclides sequestered in the Earth's rocks [*e.g., Valet*, 2003].

Taking into account all constraints known to date, the most successful scenario for thermal and magnetic evolution is represented by a long-standing, $\sim 5\%$ denser layer in the lowermost 200 km of the mantle, which may be enriched in incompatible-elements, but only slightly enriched in the heat-producing elements U, Th and K (at most 1 TW final rate, representing $\sim 5\%$ in excess of the BSE). This scenario yields a quasi-continuous magnetic field, generated by a moderately-dissipative dynamo, which was functional for at least 3.5 Gyr. The modeled magnetic field for such a scenario has less short-term fluctuations, but its intensity would vary on a billion-year timescale by a factor of 4.

The initial CMB temperature is at the solidus point for the lower mantle silicates, the core is cooling at the rate of 141 K/Gyr, and the predicted modern-day CMB temperature is 3946 K. As a consequence of the reduced heat flow at the CMB, the inner core has started to solidify after 1.8 Gyr of evolution (Proterozoic) and has grown to the present-day size of 1220 km with a rate of 270 km/Gyr.

This scenario is attractive from the geochemical, paleomagnetic and high pressure mineral physics perspectives and does not rely on still debated assumptions, *i.e.*, core potassium or extensive lower mantle melting in the distant past. The increment of the adiabatic temperature, constrained by the cooling history for this model (*i.e.*, $\Gamma = 1.384$), yields a thermal expansivity value of $\alpha_c = 1.067 \times 10^{-5}$ K^{-1}, and a value for the Grüneisen parameter of 1.393, in excellent

agreement with the values employed in other studies.

5.7 Relevance of the project

The dissertation has presented an analysis for the thermal and magnetic evolution of the Earth's core and mantle, by implementing recent results from experimental and theoretical high-pressure mineral physics, rare gases and Sm-Nd systematics, and geodynamics. Therefore, most of the scenarios analyzed in this paper have not been evaluated in previous published work.

The study has employed a fully-dynamical model for the mantle convection, which is closer to the real Earth, but has been less utilized in other studies, due to the time required for computations. The analysis of the conditions that can maintain an active dynamo has been performed in a more detailed and systematic fashion than in other studies. As a consequence of using numerical simulations, the models take into account the time dependance of the CMB heat flow and the time evolution of core temperatures at various horizons, which determine the efficiency factors that govern the entropy production in the core.

The project proposes a new approach for constraining the rate of growth for the inner core, such that the models achieve the correct size of the inner core each time, and hence, the analysis of the effects of the IC growth on magnetic field generation can be carried out more readily. The models studied in this thesis reveal new mechanisms that affect the intensity of the core magnetic field (besides the IC nucleation), thus suggesting a wider range of interpretations of the PSV data. The thesis also brings to attention alternate scenarios for the Earth evolution, which better meet the constraints known to date (*e.g.*, present-day CMB temperatures and magnetic field history).

References

[1] Acuña, M.H., Connerney, J.E.P., Ness, N.F., Lin, R.P., Mitchell, D., Carlson, C.W., McFadden, J., Anderson, K.A., Reme, H., Mazelle, C., Vignes, D., Wasilewski, P., Cloutier, P., 1999. Global distribution of crustal magnetization discovered by the Mars Global Surveyor MAG/ER experiment, *Science*, *284*, 790-793.

[2] Alfè, D., 2009. Temperature of the inner-core boundary of the Earth: Melting of iron at high pressure from first-principles coexistence simulations, *Phys. Rev. B*, *79*, doi:060101.

[3] Alfè, D., Gillan, M.J., Price, G.D., 2007. Temperature and composition of the Earth's core, *Contemporary Physics*, *48*, 63-80.

[4] Anderson, D.L., 2005. Self-gravity, self-consistency, and self-organization in geodynamics and geochemistry, in van der Hilst, R.D., Bass, J.D., Matas, J., Trampert, J., Editors, *Earth's Deep Mantle: Structure, Composition and Evolution*, 165-186.

[5] Anderson, O.L., 2002. The power balance at the core-mantle boundary, *Phys. Earth Planet. Int.*, *131*, 1-17.

[6] Atreya, S.K., Mahaffy, P.R., Wong, A.S., 2007. Methane and related trace species on Mars: Origin, loss, implications for life, and habitability, *Planet. Space Science*, *55*, 358-369.

[7] Aubert, J, 2005. Steady zonal flows in spherical shell dynamos, *Jour. Fluid Mech.*, *542*, 53-67.

[8] Aurnou J., Andreadis S., Zhu L.X., Olson P., 2003. Experiments on convection in Earth's core tangent cylinder, *Earth Planet. Sci. Lett.*, *212*, 119-134.

[9] Auzende, A.L., Badro, J., Ryerson, F.J., Weber, P.K., Fallon, S.J., Addad, A., Siebert. J., Fiquet, G., 2008. Element partitioning between magnesium silicate perovskite and ferropericlase: New insights into bulk lower-mantle geochemistry, *Earth Planet. Sci. Lett.*, *269*, 164-174.

[10] Badro J.,Fiquet G., Guyot F., 2005. Thermochemical State of the Lower Mantle: New Insights from Mineral Physics, in van der Hilst, R.D., Bass, J.D., Matas, J., Trampert, J., Editors, *Earth's Deep Mantle: Structure, Composition and Evolution*, 241-260.

[11] Badro J. , Rueff J-P. , Vank, G. , Monaco G. , Fiquet G., Guyot F., 2004. Electronic Transitions in Perovskite: Possible Nonconvecting Layers in the Lower Mantle, *Science*, *305*, 383-386.

[12] Badro, J., Fiquet, G., Guyot, F., Rueff, J.P., Struzhkin, V.V., Vanko, G., Monaco, G., 2003. Iron partitioning in Earth's mantle: Toward a deep lower mantle discontinuity, *Science*, *300*, 789-791.

[13] Boehler, R., 2000. High-pressure experiments and the phase diagram of mantle and core materials, *Rev. Geophys.*, *38*, 221-245.

[14] Boehler, R., Chopelas A., Zerr, A., 1995. Temperature and chemistry of the core-mantle boundary, *Chemical Geology, 120*, 199-205.

[15] Boyet M., Carlson, R.W., 2005. ^{142}Nd Evidence for early ($>$ 4.53 Ga) Global Differentiation of the Sillicate Earth, *Science*, *309*, 576-581.

[16] Braginsky S.I., Roberts, P.H., 1995. Equations governing convection in Earth's core and the geodyanmo, *Geophysical and Astrophysical Fluid Dynamics*, *79*, 1-97.

[17] Braginski, S.I., 1991. Towards a realistic theory of the geodynamo, *Geophys. astrophys. Fluid Dynamics*, *60*, 89-134.

[18] Brandon, A.D., Walker, R.J., Puchtel, I.S., Becker, H., Humayun M., Revillon, S., 2003. ^{186}Os-^{187}Os systematics of the Gorgona Island komatiites: implication for early growth of the inner core, *Earth Planet. Sci. Lett.*, *206*, 411-426.

[19] Brandon A.D., Walker, R.J., Morgan, J.W., Norman, M.D., Prichard, H.M., 1998. Coupled Os-186 and Os-187 evidence for core-mantle interaction, *Science*, 280, 1570-1573.

[20] Breuer, D., Spohn, T., 2006. Viscosity of the Martian mantle and its initial temperature: Constraints from crust formation history and the evolution of the magnetic field, *Phys. Earth Planet. Int.*, *52*, 153-169.

[21] Breuer, D., Spohn, T., 1993. Cooling of the Earth, Urey ratios, and the problem of potassium in the core, *Geophys. Res. Lett.*, *20*, 1655 -1658.

[22] Brunet, D., Machetel, P., 1998. Large scale tectonic features induced by mantle avalanches with phase, temperature, and pressure lateral variations of viscosity, *J. Geophys. Res.*, *103*, 4929-4945.

[23] Buffett, B.A., 2007. Core-Mantle Interactions, in *Treatise on Geophysics: Core Dynamics*, Vol. 8, Schubert, G., Editor-in-chief, Olson P., Editor, Elsevier, Oxford. 345-358.

[24] Buffett, B.A., 2002. Estimates of heat flow in the deep mantle based on the power requirements for the geodynamo, *Geophys. Res. Lett.*, *29*, (No. 12), 7.

[25] Buffett, B.A., Garnero, E.J., Jeanloz, R., 2000. Sediments at the top of Earth's core, *Science*, *290*, 1338-1342.

[26] Buffett, B.A., Huppert, H.E., Lister, J.E., Woods, A.W., 1996. On the thermal evolution of the Earth's core, *J. Geophys. Res.*, *101*, 7989-8006.

[27] Buffett, B.A., Huppert, H.E., Lister, J.E., 1992. Analytical model for solidification of the Earth's core, *Nature*, *356*, 329-331. 101, 7989-8006.

[28] Butler, S.L., Peltier, W.R., Costin, S.O., 2005. Numerical models of the Earth's thermal history: Effects of inner-core solidification and core potassium, *Phys. Earth Planet. Int.*, *152*, 22-42.

[29] Butler, S.L., Peltier, W.R., 2002. Thermal evolution of Earth: Models with time-dependent layering of mantle convection which satisfy the Urey ratio constraint, *J. Geophys. Res.*, *107*, B62109.

[30] Butler, S.L., Peltier, W.R., 2000. On scaling relations in time-dependent mantle convection and the heat transfer constraint on layering, *J. Geophys. Res.*, *105*, 3175-3208.

[31] Chabot, N.L., Drake, M.J., 1999. Potassium solubility in metal: The effects of composition at 15 kbar and 1900 C on partitioning between iron alloys and silicate melts, *Earth Planet. Sci. Lett.172*, 323-335.

[32] Christensen, U., Tilgner, A., 2004. Power requirements of the geodynamo from ohmic losses in numerical and laboratory dynamos, *Nature*, *429*, 169-171.

[33] Christensen, U. R., Hofmann, A.W., 1994. Segregation of subducted oceanic crust in the convecting mantle, *J. Geophys. Res.*, *99*, 19,867-19,884.

[34] Coltice, N, Richard, Y., 1999. Geochemical observations and one layer mantle convection, *Earth Planet. Sci. Lett.*, *174*, 125-137.

[35] Condie, K.C., 2000. Episodic continental growth models: afterthoughts and extensions, *Tectonophysics, 322*, 153-162.

[36] Condie, K.C., 1998. Episodic continental growth and supercontinents: a mantle avalanche connection?, *Earth Planet. Sci. Lett.*, *163*, 97-108.

[37] Corgne, A., Keshav, S., Fei, Y.W., McDonough, W.F., 2007. How much potassium is in the Earth's core? New insights from partitioning experiments, *Earth Planet. Sci. Lett.*, *256*, 567-576.

[38] Costin, S.O., Butler, S.L., 2006. Modelling the effects of internal heating in the core and lowermost mantle on the Earth's magnetic history, *Phys. Earth Planet. Int.*, *157*, 55-71.

[39] Costin, S.O., Buffett, B.A., 2004. Preferred reversal paths caused by a heterogeneuos conducting layer at the base of the mantle, *J. Geophys. Res.*, *109*, Art. No. B06101.

[40] Courtillot, V., Gallet, Y., Le Mouël, J.-L., Fluteau, F.,, Genevey, A., 2007. Are there connections between the Earth's magnetic field and climate?, *Earth Planet. Sci. Lett.*, *253*, 328-339.

[41] Davaille, A., Arndt, N., 2007. When hot thermochemical instabilities trigger subduction and continental growth: the episodic Earth history, *Geophys. Res. Abstracts*, Abstract EGU2007-A-05927.

[42] Davaille, A., Le Bars, M., Carbonne, C., 2003. Thermal convection in a heterogeneous mantle, *C.R. Geoscience*, *335*, 141-156.

[43] Davaille, A., 1999. Two-layer thermal convection in miscible viscous fluid, *J. Fluid. Mech., 379*, 223-253.

[44] Davies, G.F., 2007. Mantle regulation of core cooling: A geodynamo without core radioactivity?, *Phys. Earth Planet. Int.*, *160*, 215-229.

[45] Davies, G.F., 1980. Thermal histories of convective Earth models and constraints on radiogenic heat production in the Earth, *J. Geophys. Res.*, *85*, 2517-2530.

[46] Dubrovinsky L., Dubrovinskaia, N., Langenhorst, F., Dobson, D., Rubie, D., Gessman, C., Abrikosov, I.A., Johansson, B., Baykov, V.I., Vitos, L., Le Bihan, T., Crichton, W.A., Dmitriev V., Weber, H.-P., 2003. Iron-silica interaction at extreme conditions and the electrically conducting layer at the base of Earth's mantle, *Nature*, 422, 58-61.

[47] Eaton, D.W., Kendall, J.M., 2006. Improving seismic resolution of outermost core structure by multichannel analysis and deconvolution of broadband SmKS phases, *Phys. Earth Planet. Inter., 155*, 104119.

[48] Garnero, E.J., Helmberger, D.V., 1995. A very slow basal layer underlying large-scale low-velocity anomalies in the lower mantle beneath the Pacific - evidence from core phases, *Phys. Earth Planet. Int.*, *91*, 161-176.

[49] Goncharov, A.F., Struzhkin, V.V., Jacobsen, S.D., 2006. Reduced radiative conductivity of the low-spin (Mg, Fe)O in the lower mantle, *Science*, *312*, 1205-1208.

[50] Gessmann, C.K., Wood, B.J., 2002. Potassium in the Earth's core?, *Earth Planet. Sci. Lett.200*, 63-78.

[51] Glatzmaier, G.A., Coe, R.S., Hongre, L., Roberts, P.H., 1999. The role of the Earths mantle in controlling the frequency of geomagnetic reversals, *Nature*, *401*, 885890.

[52] Glatzmaier, G.A., Roberts, P.H., 1995. A 3-dimensional self-consistent computer-simulation of a geomagnetic-field reversal, *Nature*, *337*, 203-209.

[53] Grigné, C., Labrosse, S., Tackley, P., 2007. Convenction under a lid of finite conductivity in a wide aspect ratio models: Effects of continents on the wavelength of mantle flow, *J. Geophys. Res.*, *112*, B08403.

[54] Gubbins, D., Alfé, D., Masters, G., Price, D.G., Gillan, M.J. 2004. Gross thermodynamics of two-component core convection, *Geophys. J. Int.*, *157*, 1407-1414.

[55] Gubbins, D., Alfé, D., Masters, G., Price, D.G., Gillan, M.J., 2003. Can the Earth's dynamo run on heat alone?, *Geophys. J. Int.*, 155, 609-622.

[56] Gubbins, D., 1982. Magnetic messages from the Earth's core, *Nature*, *295*, 15-16.

[57] Gubbins, D., Masters, T.G., Jacobs, J.A., 1979. Thermal evolution of the Earth's core, *Geophys. J. R. Astron. Soc., 59*, 5799.

[58] Griffiths, D.J., 1999. *Introduction to Electrodynamics*, Prentice Hall, N.J.

[59] Hale, C.J., Dunlop, D. J., 1984. Evidence for an early Archean geomagnetic field; A paleomagnetic study of the Komati Formation, Barberton Greenstone Belt, South Africa, *Geophys. Res. Lett.*, *11*, 97-100.

[60] Hale, C.J., 1987. The intensity of the geomagnetic field at 3.5 Ga: paleointensity results from the Komati Fomation, Barberton Mountain land, South Africa, *Earth Planet. Sci. Lett.*, *86*, 354-364.

[61] Hansen, U., Yuen, D.A., 1988. Numerical simulations of thermal-chemical instabilities at the core mantle boundary, *Nature*, *334*, 237-240.

[62] Hart, S., Zindler, A., 1986. In search of a bulk-earth composition, *Chem. Geol.*, *57*, 247-267.

[63] Heimpel, M.H., Aurnou, J.M., Al-Shamali, F.M., Gomez Perez, N., 2005. A numerical study of dynamo action as a function of spherical shell geometry, *Earth Planet. Sci. Lett.*, *236*, 542-557.

[64] Helffrich, G., Kaneshima, S., 2004. Seismological constraints on core composition from FeOS liquid immiscibility, *Science, 306*, 22392242.

[65] Hernlund, W., Thomas, C., Tackley, P.J., 2005. A doubling of post-perovskite phase boundary and structure of the Earth's lowermost mantle, *Nature*, *434*, 882-886.

[66] Holzapfel, C., Rubie, D.C., Frost, D.J., Langenhorst, F., 2005. Fe-Mg interdiffusion in (Mg,Fe)SiO3 perovskite and lower mantle reequilibration, *Science*, *309*, 1707-1710.

[67] Humayun, M., Qin, L., Norman, M.D., 2004. Geochemical Evidence for excess iron in the mantle beneath Hawaii, *Science*, *306*, 91-94.

[68] Jackson, I., 1998. The Earth's Mantle: Composition, Structure and Evolution, Cambridge University Press, Cambridge, U.K.

[69] Jarvis, G.T., McKenzie, D.P., 1980. Convection in a compressible fluid, *J. Fluid Mech., 96*, 515-583.

[70] Jaupart, C., Molnar, P., Cottrell, E., 2007. Instability of a chemically dense layer heated from below and overlain by a deep less viscous fluid, *J. Fluid. Mech., 572*, 433-469.

[71] Jellinek, A.M., Manga, M., 2004. Links between long-lived hot spots, mantle plumes, D$''$, and plate tectonics, *Rev. Geophys.*, *42*, RG3002.

[72] Jellinek, A.M., Manga, M., 2002. The influence of a chemical boundary layer on the fixity, spacing and lifetime of mantle plumes, *Nature*, *418*, 760-763.

[73] Kavner, A., Walker, D., 2006. Core/mantle-like interactions in an electric field, *Earth Planet. Sci. Lett.*, *248*, 316-329.

[74] Keppler, H., Smyth J.R., 2005. Optical and near infrared spectra of ringwoodite to 21.5 GPa: Implications for radiative heat transport in the mantle, *American Mineralogist*, *90*, 1209-1212.

[75] Knittle, E., Jeanloz, R., 1991. The Earth's core-mantle boundary: Results of experiments at high pressures and temperatures, *Science*, 251, 1438-1443.

[76] Korenaga, J., 2008. Urey ratio and the structure and evolution of Earth's mantle, *Rev. Geophys., 46*, RG2007.

[77] Kuang, W., Chao, B.F., 2003. Geodymano modelling and core-mantle interactions, in *Earth's Core: Dynamics, Structure, Rotation*, AGU Geodymanics Series, V. Dehant, K.C. Creager, S. Karato and S. Zatman - editors, *31*, 193-212.

[78] Labrosse, S., Hernlund, J. W., Coltice, N., 2007. A crystallizing dense magma ocean at the base of the Earth's mantle, *Nature*, 450, 866-869.

[79] Labrosse, S., Macouin, M., 2003. The inner core and the geodynamo, *C.R. Geosciences*, 335, 37-50.

[80] Labrosse S., 2003. Thermal and magnetic evolution of the Earth's core, *Phys. Earth Planet. Int.*, *140*, 127-143.

[81] Labrosse S., J.P. Poirier, Le Mouël, J.-L., 2001. The age of the inner core, *Earth Planet. Sci. Lett.*, *190*, 111-123.

[82] Laio, A., Bernard, S., Chiarotti, G.L., Scandolo, S., Tosatti, E., 2000. Physics of iron at Earth's core conditions, *Science*, *287*, 1027-1030.

[83] Lammer, H., Kasting J.F., Chassefiere, E., Johnson, R.E., , Kulikov, Y.N., and Tian, F., 2008. Atmospheric Escape and Evolution of Terrestrial Planets and Satellites, *Space Science Reviews*, *139*, 399-436.

[84] Lassiter, J.C., 2006. Constraints on the coupled thermal evolution of the Earth's core and mantle, the age of the inner core, and the origin of the (OS)-O-186/(OS)-O-188 "core signal" in plume-derived lavas, *Earth Planet. Sci. Lett.*, *250*, 306-317.

[85] Lassiter, J.C., 2004. Role of recycled oceanic cruat in the potassium and argon budget of the Earth: Toward a resolutin of the 'missing' argon problem, *Geochemistry Geophysics Geosystems*, 5, Q11012.

[86] Lay, T., Garnero, E.J., Williams, Q., 2004. Partial melting in a thermo-chemical boundary layer at the base of the mantle, *Phys. Earth Planet. Int.*, *146*, 441-467.

[87] Lay, T., Garnero, E.J., 2004. Coremantle boundary structures and processes. In: R.S.J. Sparks and C.J. Hawkesworth, Editors, The State of the Planet: Frontiers and Challenges in Geophysics, *Geophys. Monogr.*, *150*, American Geophysical Union, Washington, DC, 2541.

[88] Lee K., Jeanloz, R., 2003. High-pressure alloying of potassium and iron: Radioactivity in the Earth's core?, *Geophys. Res. Lett.*, *30* (23), Art. no. 2212.

[89] Lin, J.F., Tsuchiya, T., 2008. Spin transition of iron in the Earth's lower mantle, *Phys. Earth Planet. Int.*, *170*, 248-259.

[90] Lin, J.F., Struzhkin, V.V., Jacobsen, S.D., Hu M.Y., Chow, P., Kung, J., Liu, H.Z., Mao, H.K., Hemley, R.J., 2005. Spin transition of iron in magnesiowüstite in the Earth's lower mantle, *Nature*, *436*, 377-380.

[91] Lister, J.R., Buffett, B.A., 1998. Stratification of the outer core at the core-mantle boundary, *Phys. Earth Planet. Int.*, *105*, 5-19.

[92] Lister, J.R., Buffett, B.A., 1995. The strength and efficiency of thermal and compositional convection in the geodynamo, *Phys. Earth Planet. Int.*, *91*, 17-30.

[93] Loper, D.E., 1991. The nature and consequences of the thermal interactions twixt core and mantle, *J. Geomag Geoelectr*, 43, 79-91.

[94] Lubetskaya, T., Korenaga, J., 2007. Chemical composition of Earth's primitive mantle and its variance: 2. Implications for global geodynamics, *J. Geophys. Res.*, *112*, Art. No. B03212.

[95] Luguet, A., Pearson, D.G., Nowell, G.M., Dreher, S.T., Coggon, J.A., Spetsius Z.V., Parman, S.W., 2008. Enriched Pt-Re-Os isotopes systematics explained by metasomatic sulfides, *Nature*, *319*, 453-456.

[96] Ma, Y.Z., Somayazulu, M., Shen, G.Y., Mao, H.K., Shu, J.F., Hemley, R.J., 2004. In situ X-ray diffraction studies of iron to Earth-core conditions, *Phys. Earth Planet. Int.*, *143*, 455-467.

[97] Macouin, M., Valet, J.-P., Besse, J., 2004. Long term evolution of the geomagnetic dipole moment, *Phys. Earth Planet. Int.*, *147*, 239-246.

[98] Macouin, M., Valet, J.-P., Besse, J., Bichan, K., Ernst, R., LeGoff, M., Scharer, U., 2003. Low paleointensities recorded in 1 to 2.4 Ga old Proterozoic dykes, Superior Province, Canada, *Earth Planet. Sci. Lett.*, *213*, 79-95.

[99] Mao, W.L., Mao, H.K., Sturhan, W., Zhao, J., Prakapenka,V.B., Meng, Y., Shu, J., Fei, Y., Hemley, R., 2006. Iron-rich post-perovskite and the origin of ultra-low velocity zones, *Science*, *312*, 564-565.

[100] Mao, W.L., Meng, Y., Shen,G., Prakapenka,V.B., Campbell, A.J., Heinz, D.J., Shu, J., Caracas, R., Cohen, R.E., Fei, Y., Hemley R.J., Mao, H.K., 2005. Iron-rich silicate in the Earth's D″ layer, *Proc. natl. Acad. Sci. USA , 102*, 9751-9753.

[101] Mao, W.L., Shen, G.Y., Prakapenka, V.B., Meng, Y., Campbell, A.J., Heinz, D.L., Shu, J.F., Hemley, R.J., Mao, H.K., 2004. Ferromagnesian postperovskite silicates in the D″layer of the Earth, *Proc. natl. Acad. Sci. USA , 101*, 15867-15869.

[102] Masters, G., 2008. On the possible (1D) seismological signature of the spin crossover in ferropericlase, American Geophysical Union, Fall Meeting 2008, abstract MR23A-04.

[103] Matsui, H., Buffett, B.A., 2005. Sub-grid scale model for convection-driven dynamos in a rotating plane layer, *Phys. Earth Planet. Int.*, *153*, 108-123.

[104] Matyska, C., Yuen, D.A., 2005. The importance of radiative heat transfer on superplumes in the lower mantle with the new post-perovskite phase change, *Earth Planet. Sci. Lett.*, *234*, 71-81.

[105] McDonough, W.F., 2007. Mapping the Earth's engine, *Science*, *317*, 1177-1178.

[106] McDonough, W.F., 2004. Compositional Model for the Earth's Core, in *Treatise on Geochemistry: The Mantle and Core*, Vol. 2, R.W. Carlson, H.D. Holland and K.K. Turekian editors , Elsevier, Oxford. 547-569

[107] McDonough, W.F., S.S. Sun, 1995. The composition of the Earth, *Chem. Geol.*, *120*, 223-253.

[108] McElhinny, M.W., Senanayake, W.E., 1980. Paleomagnetic evidence for the existence of the geomagnetic field 3.5 Ga ago, *J. Geophys. Res.*, 85, 3523-3528.

[109] McKenzie, D.P., Roberts, J.M., Weiss, N.O., 1974. Convection in the Earth's mantle - towards a numerical-simulation, *Jour. Fluid Mech., 62*, 465-538.

[110] McNamara, A.K., Zhong, S., 2004. Thermochemical structures within a spherical mantle: Superplumes or piles? *J. Geophys. Res.*, *109*, B07402, doi: 10.1029/2003JB002847.

[111] Montague, N.L., Kellogg, L., 2000. Numerical models of a dense layer at the base of the mantle and implications for the geodynamics of D″, *J. Geophys. Res.*, *105*, 11,101-11,114.

[112] Murthy, V.M., van Westrenen W., Fei, Y.W., 2003. Experimental evidence that potassium is a substantial radioactive heat source in planetary cores, *Nature*, *423*, 163-165.

[113] Nakagawa, T., Tackley, P.J., 2005. Deep mantle heat flow and thermal evolution of the Earth's core in thermochemical multiphase models of mantle convection, *Geochem. Geophys. Geosyst.*, *6*, doi:10.1029/2005GC000967.

[114] Nakagawa, T., Tackley P.J., 2004. Effects of thermo-chemical mantle convection on the thermal evolution of the Earth's core, *Earth Planet. Sci. Lett.*, *220*, 107-119.

[115] Naliboff, J.B., Kellogg, L.H., 2007. Can large increases in viscosity and thermal conductivity preserve large-scale heterogeneity in the mantle?, *Phys. Earth Planet. Int.*, *161*, 86-102.

[116] Nimmo, F., 2007. Energetics of the Core, in *Treatise on Geophysics: Core Dynamics*, Vol. 8, Schubert, G., Editor-in-chief, Olson P., Editor, Elsevier, Oxford. 31-65.

[117] Nimmo, F., G.D. Price, J. Brodholt, D. Gubbins, 2004. The influence of patassium on core and geodynamo evolution, *Geophys. Jour. Int.*, *156*, 363-376.

[118] Nimmo, F., 2002. Why does Venus lack a magnetic field?, *Geology*, *30*, 987-990.

[119] Olson, P., Christensen, U.R., 2002. The time-averaged magnetic field in numerical dynamos with non-uniform boundary heat flow, *Geophys. Journ. Int.*, *151*, 809-823.

[120] Olson, P., Aurnou, J., 1999. A polar vortex in the Earth's core, *Nature*, *402*, 170-173.

[121] Ozawa, H., Hirose, K., 2006. Is the Bottom of the Mantle Iron-enriched?, *Eos Trans. AGU*, 87(52), Fall Meet. Suppl., Abstract U34A-04.

[122] Ozawa, H., Hirose, K., Mitome, M., Bando, Y., Sata, N., Ohishi, Y., 2008. Chemical equilibrium between ferropericlase and molten iron to 134 GPa and implications for iron content at the bottom of the mantle, *Geophys. Res. Lett.*, *35*, Art. L05308.

[123] Ozima, M., Seki K., Terada, N., Miura, Y.N., Podosek, F.A., Shinagawa, H., 2005. Terrestrial nitrogen and noble gases in lunar soils, *Nature*, *436*, 655-659.

[124] Peltier, W.R., X. Jiang, 1996. Mantle viscosity from the simultaneous inversion of multiple data sets pertaining to postglacial rebound, *Geophys. Res. Lett.*, *23*, 503-506.

[125] Pollack, H.N., S.J. Hunter, Johnson, J.R., 1993. Heat flow from the Earth's interior: Analysis of the global data set, *Rev. Geophys.*, *31*, 267-280.

[126] Prévot, M., Derder, M.E., McWilliams M., Thompson, J., 1990. Intensity of the Earth's magnetic field: evidence for a Mesosoic dipole low, *Earth Planet. Sci. Lett.*, *97*, 129-139.

[127] Richter, F.M., 1978. Mantle convection models, *An. Rev. Earth Planet. Sci., 6*, 9-19.

[128] Roberts, P.H., Jones, C.A., Calderwood, A., R., 2003. Energy fluxes and Ohmic dissipation in the earth's core, in *Earth's Core and Lower Mantle*, Jones, C.A., Soward, A.M., Zhang, K., editors. London, New York, Taylor and Francis.

[129] Russell, S. A., Lay, T., Garnero, E.J., 1998. Seismic evidence for the small-scale dynamics in the lowermost mantle at the root of the Hawaiian spot, *Nature*, *396*, 255-258.

[130] Sakai, T., Kondo, T., Kobayashi, Y.,Ohtani, E., Masaaki, M., Yoo, J.-H., Nagase, T., 2006. Fe-Mg partitioning between post-perovskite and magnesiowustite, *Geochem. and Cosmochem. Acta*, *70*, A552-A633.

[131] Schubert, G., Turcotte, D. L., Olson, P., 2001. *Mantle Convection in the Earth and Planets*, Cambridge University Press, Cambridge, UK.

[132] Schubert, G., Stevenson, D.J., Cassen, P., 1980. Whole planet cooling and the radiogenic heat source of the Earth and Moon, *J. Geophys. Res.*, *85*, 2531-2538.

[133] Selkin, P.A., Tauxe, L., 2000. Long-term variations in palaeointensity, *Phil. Trans. of the Royal Society of London*, *358*, 1065-1088.

[134] Sharpe, H., Peltier, W.R., 1978. Parameterized mantle convenction and the Earth's thermal history, *Geophys. Res. Lett.*, *5*, 737-740

[135] Sleep, N.H., 1988. Gradual entrainment of a chemical layer at the base of the mantle by overlying convection, *Geophys. J.*, *95*, 437-447.

[136] Smirnov, A.V., Tarduño, J.A., Pisaken, B.N., 2003. Paleointensity of the early geodynamo (2.45 Ga) as recorded in Karelia: A single-crystal approach, *Geology*, *31*, 415-418.

[137] Solheim, L., W.R. Peltier, 1994a. Avalanche effects in phase transition modulated thermal convection: A model of the Earth's mantle, *J. Geophys. Res.*, *99*, 6997-7018.

[138] Solheim, L., W.R. Peltier, 1994b. Phase boundary deflections at 660 km depth and episodically layered isochemical convection in the mantle, *J. Geophys. Res.*, *99*, 15861-15875.

[139] Speziale, S., Milner A., Lee V.E., Clark S.M., Pasternak, M.P., Jeanloz, R., 2005. Iron spin transition in Earth's mantle, *Proc. natl. Acad. Sci. USA*, *102*, 17918-17922.

[140] Stacey, F.D, 1992. Physics of the Earth, 3^{rd} ed. Brookfield Press, Brisbane, Australia.

[141] Stanley, S., Elkins-Tanton, L., Zuber, M.T., Parmentier, E.M., 2008. Mars' paleomagnetic field as the result of a single-hemisphere dynamo, *Science*, *321*, 1822-1825.

[142] Steinle-Neumann, G., Stixrude, L., Cohen, R.E., Gulseren, O., 2001. Elasticity of iron at the temperature of the Earth's inner core, *Nature*, 413 (6851): 57-60.

[143] Steinbach, V., Yuen, D.A., Zhao, W., 1993. Instabilities from phase transitions and the timescales of mantle thermal evolution, *Geophys. Res. Lett.*, *20*, 1119-1122.

[144] Stegman, D.R., Jellinek, A.M., Zatman, S.A., Baumgardner J.R., Richards M.A., 2003. An early lunar core dynamo driven by thermochemical mantle convection, *Nature*, *421*, 143-146.

[145] Stevenson, D.J., Spohn T., Schubert, G., 1983. Magnetism and thermal evolution of terrestrial planets, *Icarus 54*, 466-489.

[146] Tackley, P.J., Xie, S.X., 2002. The thermochemical structure and evolution of Earth's mantle: constraints and numerical models, *Phil. Trans. Royal Society of London*, *360*, 2593-2609.

[147] Tackley, P.J., 1998. Three-dimensional simulations of mantle convection with a thermochemical basal boundary layer: D$''$?, in *The Core-Mantle Boundary Region*, vol.28, M. Gurnis et al., editors, AGU, Washigton, DC, 231-254.

[148] Tackley, P.J., Stevenson D.J., Glatzmaier, G.A., Schubert, G., 1993. Effects of an endothermic phase transition at 670 km depth in a spherical model of convection in the Earth's mantle, *Nature*, *361*, 699-704.

[149] Tanaka, S., 2007. Possibility of a low P-wave velocity layer in the outermost core from global *SmKS* waveforms, *Earth Planet. Sci. Lett.*, *259*, 486-499.

[150] Tanaka, H., Kono, M., Uchimura, H., 1995. Some global features of palaeointensity in the geological time, *Geophys. J. Int.*, *120*, 97-102.

[151] Tarduno, J.A., Cottrell R.D., Watkeys, M.K., Bauch, D., 2007. Geomagnetic field strength 3.2 billion years ago recorded by single silicate crystals, *Nature*, *446*, 657-660.

[152] Tarduno, J.A., Cottrell R.D., Smirnov A.V., 2006. The paleomagnetism of single silicate crystals: Recording geomagnetic field strength during mixed polarity intervals, superchrons, and inner core growth, *Rev. Geophys.*, *44*, Art. RG1002.

[153] Tateno, S., Hirose, K., Nagayoshi, S., Yasuo, O., 2007. Solubility of FeO in (Mg, Fe)SiO_3 perovskite and the post-perovskite phase transition, *Phys. Earth Planet. Int.*, *160*, 319-325.

[154] Tolstikhin, I., Kramers, J.D., Hofmann, A.W., 2006. A chemical Earth model with whole mantle convection: The importance of a core-mantle boundary layer (D″) and its early formation, *Chemical Geology*, *226*, 79-99.

[155] Tolstikhin, I., Hofmann, A.W., 2005. Early crust on top of the Earth's core, *Phys. Earth Planet. Int.*, *148*, 109-130.

[156] Tromp, J., 2001. Inner-core anisotropy and rotation, in *Annual Review of Earth and Planetary Sciences*, *29*, 47-69.

[157] Turcotte, D.L, Schubert, G., 2002. *Geodynamics*, 2nd edition, Cambridge University Press, Cambridge, U.K.

[158] Valet, J.P., 2003. Time variations in geomagnetic intensity, *Reviews of Geophysics, 41*, 1004.

[159] van der Hilst, R.D., de Hoop, M.V., Wang, P., Shim, S.-H., Ma, P., Tenorio, L., 2007. Seismostratigraphy and Thermal Structure of Earth's Core-Mantle Boundary Region, *Science*, *315*, 1813-1817.

[160] Vočadlo, L., 2007. Mineralogy of the Earth - The Earth's core: Iron and Iron Alloys, in *Treatise on Geophysics: Mineral Physics*, Vol. 2, Schubert, G., Editor-in-chief, Price, D., Editor, Elsevier, Oxford. 91-120.

[161] Vočadlo, L., Alfè, D., Gillan, M.J., Price, G.D., 2003. The properties of iron under core conditions from first principles calculations, *Phys. Earth Planet. Int.*, *140*, 101-125.

[162] Walker, R.J., Morgan, J.W., and Horan, M.F., 1995. Os-187 enrichement is some plumes - Evidence for core-mantle interation, *Science*, *269*, 819-822.

[163] Whaler, K.A., 1980. Does the whole Earth's core convect? *Nature*, *287*,528-530.

[164] Williams, Q., 1998. The temperature contrast across D″, in *The Core-Mantle Boundary Region*, vol.28, M. Gurnis et al., editors, AGU, Washigton, DC, 73-81.

[165] Williams, Q., Garnero, E.J., 1996. Seisminc evidence for partial melt at the base of the Earth's mantle, *Science*, *273*, 1528-1530.

[166] Yoshihara, A., Hamano, Y., 2004. Paleomagnetic constraints on the Archean geomagnetic field intensity obtained from komatiites of the Barberton and Belingwe greenstone belts, South Africa and Zimbabwe, *Precambrian Research*, *131*, 112-142.

[167] Yoshihara, A., Hamano, Y., 2000. Intensity of the Earth's magnetic field in late Archean obtained from dibase dykes of the Slave province, Canada, *Phys. Earth Planet. Int.*, *117*, 295-307.

[168] Zhang, K.K., Schubert, G., 2000. Teleconvection: Remotely driven thermal convection in rotating stratified spherical layers, *Science*, *290*, 1944-1947.